Next Generation Multibeam Satellite Systems

By

Vahid Joroughi

Submitted to the Universitat Politecnica de Catalunya (UPC)

in partial fulfillment of the requirements for the degree of

DOCTOR OF PHILOSOPHY

Barcelona, December 2015

Advised by

Prof. Ana Isabel Perez Neira

Supervised by

Dr. Miguel Angel Vazquez
Dr. Bertrand Devillers

PhD program on Satellite communications in the signal theory and communication department (TSC)

تقدیم به مادر و روح پدر عزیزم که وجودم جز هدیه وجودشان نیست

تقدیم به همسر مهربانم

که مسیح وار با صبرش در تمام لحظات رفیق راه بود

تقدیم به خانواده ام که محبتشان هرگز فروکش نکرد

و آموزگارانی که برایم زندگی ، بودن و انسان بودن را معنا کردند

حال این برگ سبزیست تحفه درویش تقدیم به آنان....

II

III

Abstract

Satellite communications will play a central role towards fulfilling next generation 5G communication requirements. As a matter of fact, anytime-anywhere connectivity cannot be conceived without the presence of the satellite segment. Indeed, the satellite industry is not only targeting areas without backbone connectivity (maritime, aeronautic, rural,) but also high dense populated scenarios with an existing communication infrastructure where the satellite will become an essential element to decongest the terrestrial wireless network.

In order to deliver broadband interactive data traffic, satellite payloads are currently implementing a multibeam radiation pattern. The use of a multibeam architecture brings several advantages in front of a single global beam transmission. First, since an array fed reflector is employed, the antenna gain to noise ratio can be increased leading to high gain of the achievable throughput. Second, different symbols can be simultaneously sent to geographically separated areas, allowing a spatially multiplexed communication. Last but not least, the available bandwidth can be reused in sufficiently separated beams, leading to an increase of the user bandwidth yet maintaining a low multiuser interference.

Nevertheless, whenever the system designers target the terabit satellite system (i.e. a satellite system offering a terabit per second capacity), the aforementioned multibeam architecture shall be reconsidered. Precisely, full frequency reuse among beams becomes mandatory in order to support the terabit capacity as larger available user bandwidth is required. As a consequence, interference mitigation techniques need to be implemented either at the user terminal (multiuser detection) or in the transmitter (precoding).

This thesis deals with the problem of precoding and linear filtering receiving methods for multibeam satellite systems when full frequency reuse is considered (i.e. all beams share the available spectrum). Concretely, we consider the particular restrictions of satellite communications which, in contrast to terrestrial communication systems, suffer from additional drawbacks.

First, the feeder link (i. e. the bidirectional communication link between the satellite and the internet backhaul connection) must aggregate the overall data traffic leading to a very large capacity requirement. This required data rate is even increased whenever linear filtering at the return link and precoding in the forward link are deployed. This is because the feed signals, which are larger than the number of beams, shall be computed on ground. In order to solve this problem, we propose an hybrid architecture where the satellite payload is equipped with a fixed processing. This on board processing linearly

transforms the user signals into the feed signal domain in order to keep the feeder link rate requirement low. A robust worst case minimum mean square error scheme is proposed and two approximate solutions are obtained by means of considering a classical robust design and a novel first perturbation model. The on board processing results to be the same for both return and forward links, leading to a large reduction of the payload complexity, mass and cost.

Second, as the data traffic can be generated by different Earth stations (gateways), the precoding method shall be designed accordingly. Concretely, in contrast to single gateway transmission where it is assumed the presence of a central computing center taht computes the overall precoding matrix, in the multiple gateway architecture each gateway only have access to a certain part of the channel state information and the symbols to be transmitted. This entails several challenges: i) even though the overall channel knowledge is shared among the gateways, the precoding matrix must be independently computed at each of them. ii) the complete channel state information sharing is an unrealistic assumption and, in general, the system designer only has access to a certain part of the overall channel knowledge. iii) considering that the payload must receive the different feeder links, certain inter-feeder link interference may appear due to system uncalibrations leading to a large reduction of the achievable data rates. In order to solve these problems, we propose a novel precoding scheme based on a regularized zero forcing deisgn. In addition, bearing in mind that the inter-gateway communication shall be kept low, we propose a low complex cooperative method which provides data rates similar to the full sharing case. iv) the impact of the inter-feeder link interference is analyzed.

Finally, apart from the disadvantages that results from increasing the number of beams there is an important phenomena that currently needs to be treated: the fact that a single codeword is embedded the information of multiple users in each beam. This leads to the difficult so-called multigroup multicast model, whose optimization requires computationally complex operations. In order to solve this problem, first we propose a two-stage precoding design in order to both limit the multibeam interference and to enhance the intra-beam minimum user signal power (i.e. the one that dictates the rate allocation per beam). Second, a robust version of the proposed precoder based on a first perturbation model is presented. This mechanism behaves well when the channel state information is corrupted. Third, we propose a per beam user grouping mechanism so as its robust version in order to increase the precoding gain. Forth, a method for dealing with the multiple gateway architecture is presented that offers high throughputs with a low inter-gateway communication.

The proposed schemes are numerically evaluated considering broadband satellite stan-

dards (Digital Video by Satellite 2 and 2X) and channel models provided by the European Space Agency. Under this context, this thesis provides a close-to-real validation of novel interference mitigation techniques for next generation satellite systems.

Acknowledgments

It was four years ago, but it seems like it was only yesterday that I entered UPC and the Centre Tecnologic de Telecomunicacions de Catalaunya (CTTC). First day, Laura Casaus showed me the different offices and labs introducing me to my future colleagues. I was spending stressful days since I came from a country with different culture, community, environment, ...; and I had doubt that I would be able to communicate with the new society or not. After spending a few days, I found that CTTC has an intimate atmosphere and there is not any reason to be worried. Of course, all this joy is due to the great companions and friends at CTTC. In the following lines, I will try to thank you all; I hope I do not forget anyone.

Foremost, I would like to express my sincere gratitude to Prof. Ana Isabel Perez Neira advisor, Dr. Miguel Angel Vazquez and Dr. Bertrand Devillers supervisors for the continuous support of my PhD study and research, for their patience, motivation, enthusiasm, and immense knowledge. Their guidance helped me in all the time of research and writing of this thesis. I could not have imagined having better advisors and mentors for my PhD study.

Ana has been supportive since the days I began working on UPC; I remember she used to say" No worries about anything and keep working!" to encourage me to stay and study; And during the most difficult times when writing this thesis, she gave me the moral support and the freedom I needed to move on. Besides, Ana is someone you will instantly love and never forget once you meet her. Shes usually patience advisor and one of the smartest people I know. I hope that I could be as lively, enthusiastic, and energetic as Ana and to someday be able to command an audience as well as she can.

Bertrand has supported me not only by providing a research assistantship over almost first year, but also academically and emotionally through the rough road to finish this thesis. Besides, Miquel Angel introduced me into the exciting worlds of convex optimization and linear precoder and detector design and taught me the preciseness and rigor required in all the technical derivations. I also want to appreciate Miquel Angel for being always flexible and comprehensive allowing me to select and study the problems for which I felt more interest. In short, I extremely appreciate Miquel Angels support both in professional and personal terms.

I also want to thank CTTC and Professor Miguel Angel Lagunas for giving me the opportunity to join CTTC, treating me as one more of CTTC PhD students, and letting

VIII

Contents

List of Figures

XIII

XIV

List of Tables

List of Acronyms

AGC . . . . . .   Automatic gain control

AWGN . . . .   Additive white Gaussian noise

CDF . . . . . .   Cumulative distribution function

CSI . . . .   Channel state information

CSIT . . . . . .   Channel state information in transmitting side

dB . . . .   Decibel

dBW . . . . . .   decibel watt

DVB . . . . . .   Digital video broadcasting

EIRP . . . . .   Equivalent isotropically radiated power

ESA . . . . . .   European space agency

GEO . . . . . .   Geosynchronous earth orbit

GHz . . . . . .   Giga hertz

Km . . . .   Kilometer

Mb/s . . . . . .   Mega bit per second

MHZ . . . . . .   Megahertz

MIMO . . . . .   Multi-input-multi-out

MISO . . . . .   Multi-input-single-output

MBIM . . . . .   Multibeam Interference Mitigation

MMSE . . . .   Minimum mean square error

MNO . . . . .   Mobile network operators

MSE . . . . . .   Mean square error

M-ZF . . . . .   Multiple zero forcing

Hz . . . .   Hertz

NGW . . . . .   Next generation waveform

PER . . . . . .   Packet error rate

QoS . . . . . .   Quality of Service

SINR . . . . . Signal to interference plus noise ratio

SMSE . . . . . Sum of mean square error

SNR . . . . . . Signal to noise ratio

SVD . . . . . . Singular value decomposition

R-ZF . . . . . . Regularized zero forcing

TDM . . . . . . Time division multiplexed

MF-TDMA . . Multifrequency TDM access

TDMA . . . . Time division multiplexing access

TV . . . . Television

TWTAs . . . . Traveling wave tube amplifiers

ZF . . . . Zero forcing

Notation

A . . . . Matrix

a . . . . Vector

$(.)^{\circ}$ . . . . Degree indicator

$(.)^{H}$ . . . . Hermitian transpose matrix/vector

$(.)^{T}$ . . . . transpose of matrix/vector

$(.)^{+}$ . . . . . . diagonal (which all diagonal elements are positive) matrix

$\mathbf{I}_N$ . . . . $N \times N$ identity matrix

$\mathbf{0}_{K \times N}$ . . . . . . All-zero matrix of size $K \times N$

$\mathbf{A}_{1:K}$ . . . . . . K first rows of the matrix $\mathbf{A}$ of size $N \times N$ with $K \leq N$

$(\mathbf{X})_{ij}$ . . . . . . (ith, jth) element of matrix $\mathbf{X}$

$\mathbf{a} \prec \mathbf{b}$ . . . . . . vector $\mathbf{a}$ majorizes vector $\mathbf{b}$

$\mathbf{A} \leq B$ . . . . . $\mathbf{A} - \mathbf{B} \geq 0$ is semi-definite

$\mathrm{E}\{\pmb{.}\}$ . . . . The expected value operator

$||.||$ . . . . The frobenius norm

$\mathbf{a}_n$ . . . . Zeros vector with an one in the n-th element

$\mathbf{1}$ . . . . Vector of noes

$\mathbf{A}_{c \times d}$ . . . . . . The matrix $\mathbf{A}$ with a number of c rows and d columns

$\mathbb{E}\{ \ . \ |\mathbf{A}\}$ . . . . The conditional expectation given by matrix $\mathbf{A}$

$\Re(.)$ . . . . The real matrix operator

$_{RL}$ . . . . The subscript of the return link

$_{FL}$ . . . . The subscript of the forward link

Colophon

xx

Chapter 1

Introduction

1.1 Motivation

Satellite communication networks can provide global, ubiquitous and multi-point communication (see Figure 1.1). In the lack of terrestrial wireline and wireless, a satellite system can provide a flexible and cost-effective solution for domestic and international networks. In this context, satellite service providers are able to leap across continents and oceans, often linking some of the world's most remote spots, irrespective of the user's geographic location [1].

As a matter of fact, one of the main challenges MNO are facing is the cost of deploying new network infrastructures in both low and high populated areas. In rural or remote areas, there is a scarcity of network infrastructure that requires a big CAPEX for the MNO. The use of satellite backhauling is a virtuous solution that has been considered in research projects such FP7-BATS (http://www.batsproject.eu/). In addition, satellite communications also have a major role to play in designing, developing and expanding a network. With a satellite and Earth stations (gateways), it can be created a network on a permanent or interim basis more rapidly than "laying cable". In this context, an interim station even allows testing a market or provides emergency service prior to a
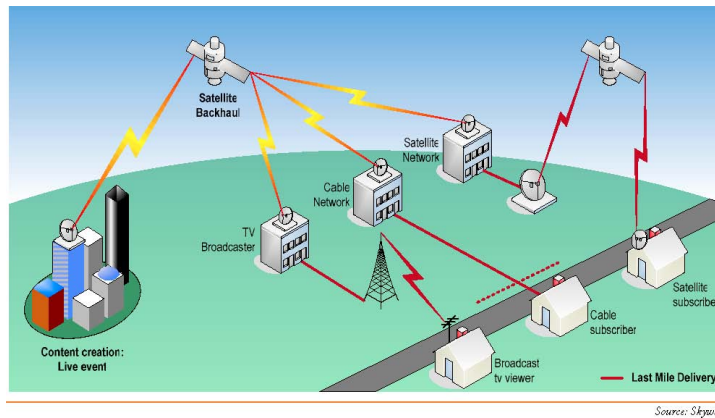
Figure 1.1: Satellite communication network can provide global, ubiquitous and multi-point communication

major infrastructure investment. Moreover, it can rapidly scale and re-provision a satellite based network to meet increasing and changing needs. In recent decades there has
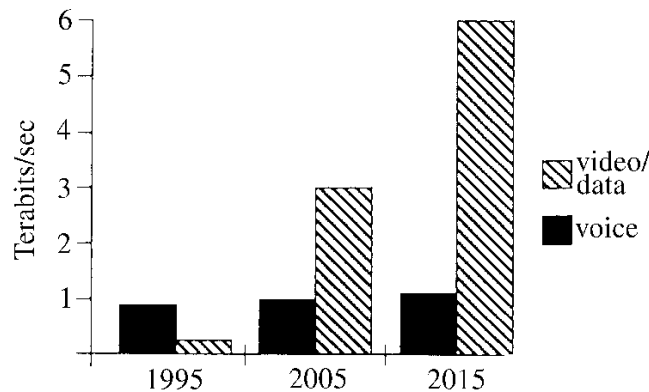
Figure 1.2: The shift from voice to data and video in satellite communication networks [1].

not only been a sudden broadening in the services and applications, but also a shift in the market that brings consumers and business more directly in contact with satellite service providers (see Fig. 1.2). This increasing demand of broadband data services is an opportunity for satellite industries to introduce new services different from the well-known current ones (i.e. TV, emergency communications, ...).

From a system engineering point of view, this requirement for broadband services leads

to the utilization of high frequency bands (e.g. the Ka-band) to increase the overall system bandwidth. As a result, satellite system designers seek for advance signal processing techniques able to accomodate the very large user data rate demands [1, 2].

Considering the success story of MIMO technology in terrestrial applications [1] establishes an intuitive approach to follow this progress. Indeed, it is evident that the advances in MIMO techniques during the past decade shall be mimicked in satellite communication systems so that the satellite service providers are able to serve higher throughput demands with a scalable cost [3]. In this context, multibeam satellite systems naturally fits the idea of multiuser MIMO as spatially separated beams can be jointly processed in order to increase the overall throughput.

Next section provides a brief overview on multibeam satellite systems and, posteriorly, we describe some of the advances of MIMO communications in multibeam satellite systems.

1.2   Multibeam satellite systems

Mimicking the terrestrial cellular networks, satellite systems providing broadband IP services are moving from single beam to multibeam architectures, typically operating in Ka-band. In these systems, the payload is equipped with a multiplicity of feeds so that information is simultaneously sent to different spot beams on ground with a certain frequency reuse pattern. In such a configuration, bandwidth can be efficiently reused in beams sufficiently separated so that the multiuser interference is reduced severely.

The overall multibeam system architecture is depicted in 1.3, where it can be observed that the users both receive and transmit information via the use of the multibeam pattern, which in turn is fed by the feeder link. The available bandwidth in the feeder link must be large enough to support the frequency re-use adopted for the user beams.

---

[1]MIMO technology offers many advantages and degrees-of-freedom, such as: (a) space and multiuser diversity gain (b) spatial multiplexing gain, (c) array and coding gain (d) interference reduction.

The projection of the beam generation process on Earth by the satellite creates a very beneficial multibeam pattern as different information at different rates can be sent by each beam separately, combined with an accurate adaptive coding and modulation technique. However, this multi-spot radiation pattern generates signal interference among adjacent beams. Indeed, as there is no way of having completely isolated spot beam, a carefully planned overlap is indulged between them, leading to a controlled C/I. As it can be observed, a multibeam system includes the following units:

- Ground segment, this unit comprises a gateway process center which allows the satellite to connect with the terrestrial network.

- Space segment, this unit includes a satellite that works by receiving radio signals sent from the gateway and resending the signals back to the coverage area on Earth. In other words, a signal transmitted by gateway is retransmitted by satellite to the another point on the earth surface. This is generally done with an array fed reflector Figure 1.4 show a fed reflector antenna architecture.
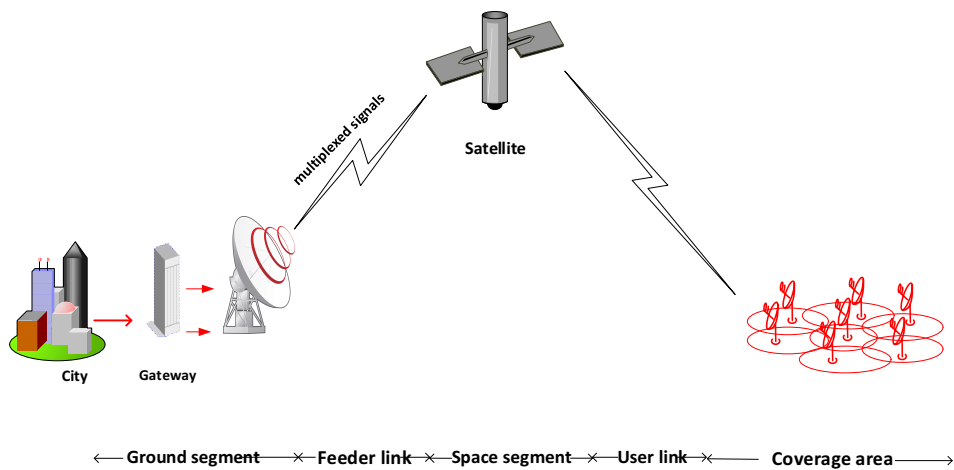
Figure 1.3: A multibeam system architecture.

- User link, the propagation channel between satellite and the coverage area.

- Feeder link, this link transmits the gateway signal streams in a frequency multi-plexed fashion to the satellite. Remarkably, due to high data rate demands the development of feeder link in multibeam systems requires the adoption of noiseless bandwidth resources on this link[2].
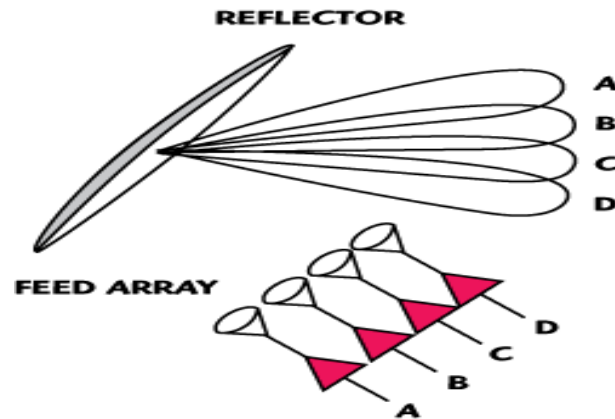
Figure 1.4: A fed reflector antenna architecture.

- Coverage area, this segment includes user terminals that are distributed within a number of beams. These beams allow satellite to target service to a specific area, or to provide different service to different areas (which is covered by a beam).

Remarkably, the transmit signal through a certain beam is partially radiated to the corresponding adjacent beams. Although the received power levels of the adjacent beams are not as large as the intended one, the created interference is not negligible and; therefore, the communication link pairs suffer from a large degradation of the achievable data rates.

In order to cope with the interference, satellite operators and manufactures have proposed to separate the frequency bands of the adjacent beams so that the interference is

---

[2]The quality objective for the feeder link is normally about ten times better than the objective for the user link. This difference results from the relative ease of designing the feeder link for a high data rate compared to the user link where quality is limited by the EIRP that a satellite can provide necessity to use small antennas for user terminals [1].

mitigated at the transmit side by means of frequency selective filters. Generally, the frequency band is divided into 4 sub-bands so that the closer adjacent beams have disjoint frequency bands. Note that the remaining interference due to the frequency reuse is highly eliminated due to the beam radiation pattern. In addition, there might be cases where the available bandwidth is divided into two parts and the satellite system uses both polarization as if they were different frequencies.

Despite this cake-cutting spectrum management sufficiently alleviates the problem of multibeam interference; it precludes the use of all available bandwidth in every beam. Therefore, for achieving a huge leap in offered data rate services, a more efficient use of the spectrum is desirable. This vision has been also promoted in cellular system by shifting the paradigm from single cell to multicell systems.

As a result, appropriate interference mitigation techniques and high frequency reuse is desirable for this scenario. With this, the interference reliever in a communication system sometimes is generally situated in the transmitter rather than in the receiver in order to keep the receiver complexity low as its cost generally determines the overall business profit. Unfortunately, if the transmitter is devoted to mitigate interference, a certain amount of resources must be dedicated to feedback information from the receiver to the transmitter in order to undo the created interference. Moreover, if the feedback information suffers from a degradation (quantization errors, outdated information, transmission errors,), the ability to perform interference mitigation is compromised.

Indeed, deciding whether the interference should be removed either at the transmitter or the receiver in satellite systems needs still a careful study encompassing all the performance metrics and hardware designs. In this thesis we focus on the benefits of precoding techniques as recently results have demonstrated its large potential yet maintaining the receivers complexity low [4].

The implementation of the multibeam radiation pattern can vary depending on the payload computational resources and their flexibility. In the following section different

implementations are listed.

1.2.1   Different multibeam satellite architectures

Recent studies in the multibeam systems have proposed different payload architectures which increase capabilities of managing power and frequency resources among beams. These architectures can be classified as

- **On board processing architecture**: the payload is equipped with a computational unit able to support feed signal processing efficiently. As a matter of fact, the payload designs have been evolving from the bent-pipe concept towards switchboard in the sky. In this novel payload architecture, the received signals from feeder link are routed to user link via a number of on board feeds. This on board processing is applied with operations like digital beamforming, frequency multiplexing and de-multiplexing, interference suppression and signal level control. In such architecture, an imminent gain, achievable without the need for upgrading current satellite technology, can be obtained by exploiting on board multiple carrier operation at the payload and using highly efficient modulation schemes. However, even if on board architecture would provide flexibility in the configuration of the parameters of the carriers waveforms, on board multicarrier joint amplification is a critical operation as it brings severe non-linear distortion effects. This distortion becomes even more severe when high spectrally efficient modulation schemes are used. The inherent non-linearity of the amplifier results in an increased adjacent channel interference and peak to average power ratio that degrades power and spectral efficiencies while offsetting other potential benefits. In Figure 1.5 the on board architecture is depicted.

- **On ground architecture**, to tackle with the aforementioned non-linearity in the on board architecture, the on ground signal processing configuration is proposed.

This is done by shifting on board processing to the gateway which enables efficient joint on board amplification. Moreover, signal processing is realized on ground with all capabilities offered by on ground segment so that it keeps payload complexity low. Consequently, novel advance methods can be implemented considering the available hardware on ground.

Recent on ground signal processing schemes include transmitter techniques as pre-
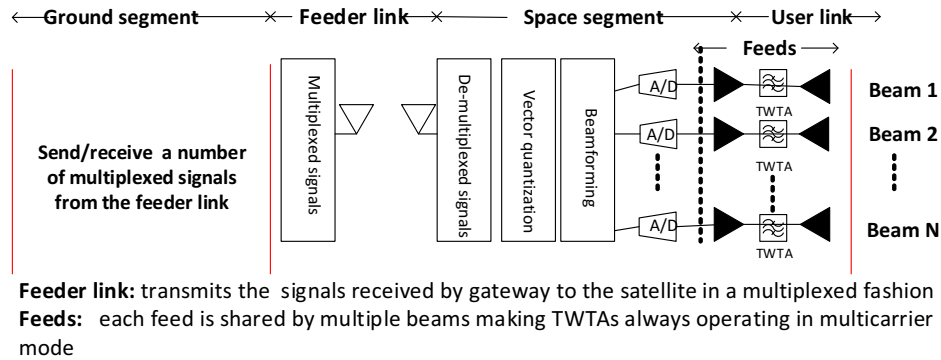
Figure 1.5: On board beamforming architecture.

distortion and receiver techniques as equalization. In fact, both pre-distortion and receive techniques operate the transmitter to pre-compensate the linear and non-linear channel distortion effects and to reduce the resulting receiver interference. However, this scenario required a large amount of feeder link spectral resources and more sophisticated power consuming techniques since the feeder link signals have to be frequency multiplexed both on forward and return links. This will be discussed in the next section.

- **Hybrid space-ground signal processing architecture**, In contrast to space and ground processing, hybrid approach consists in splitting the processing between the satellite and the gateway, aiming to some optimization of the trade-off between performance and payload complexity. The main aim of hybrid solutions is to reduce

the feed signal space to a subspace in order to reduce the feeder link capacity requirements. A schematic representation of the hybrid architecture is given in Fig. 1.6.
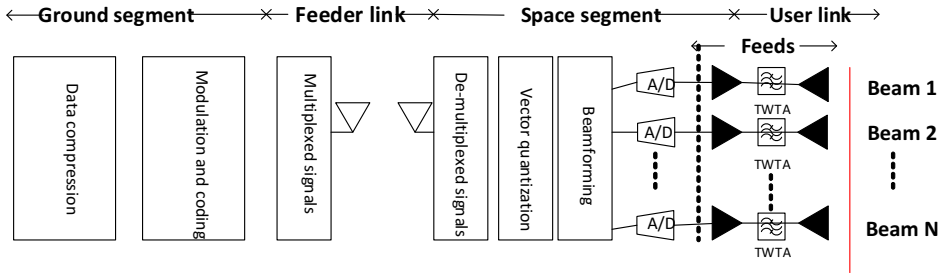
Figure 1.6: Hybrid architecture.

We continue with providing an brief overview on feeder link bandwidth requirement that is an essential parameter in order to develop signal processing architectures in multibeam systems.

1.2.1.1   Feeder link bandwidth requirements

By increasing the demands for using satellite communication systems, the number of beams necessarily must grow. As a consequence, the ground and space units have to employ an excessive communication efforts on the feeder link to exchange all on board feed signals. Indeed, in on ground multibeam architectures the resulting required bandwidth is

$$\mathbf{B}_{\text{feeder-link-on-ground}} = N\mathbf{B}_{\text{user-link}}; \tag{1.1}$$

where N is the number of feed signals, $\mathbf{B}_{\text{user-link}}$ the per-beam bandwidth and $\mathbf{B}_{\text{feeder-link}}$ the feeder link required bandwidth. Considering that the number of feed signals is proportional to (K) and

$$N \geq K \tag{1.2}$$

it is evident that if the user available bandwidth is increased, the feeder link resources must be increased accordingly and; eventually, the feeder link might become the communication bottleneck. It is important to remark that, whenever $N = K$ the payload architecture is coined single-feed-per-beam whereas when $N \geq K$ it is coined multiple-feed-per-beam. This latter approach presents less beamforming scan losses than the single-feed-per-beam architecture and; therefore, it is adequate for continental coverage areas.

Since the feeder link resources are scarce, there might the case where (1.1) bandwidth requirement cannot be supported. In order to solve this problem, there is a vision to move the feeder link from the Ka band to the Q/V band, where there are larger available bandwidths [6]. Unfortunately, in these carrier frequencies the fading is extremely large and more advanced transmitting diversity techniques are needed. In [4] a feeder link compression algorithm was presented so that the payload is equipped with an extra processing stage in order to reconstruct the lossy-compressed signals.

Another option is the use of individual on ground multiple gateway architecture, which might be adequate in order to reduce the feeder link spectral requirements through very directive antennas and also exploits the spatial diversity while sharing all available feeder link spectrum [5], [6]. Under this context, since the feeder link available bandwidth can be reused through the different gateways, the required feeder link bandwidth becomes

$$\mathbf{B}_{\text{feeder-link-MG}} = \frac{N}{G}\mathbf{B}_{\text{user-link}}, \qquad (1.3)$$

where G is the number of gateways. Note that in case of failing one gateway traffic can be rerouted through other gateways to avoid service outage. Nevertheless, the deployment of several gateways increases the cost of the system and; the signal processing must be separated in isolated processing units. This will be addressed in chapter 3.

Another promising solution in front of the aforementioned options is to keep certain

processing in the payload in terms of beam generation process. This is referred to hybrid space-ground processing. In this way, the satellite does not act in transparent mode and it carries out some processing, leading to high reduction of the feeder link bandwidth requirements [9]. Indeed, its role is to achieve a multiple beam type radiation pattern and reduce the amount of bandwidth needed in the feeder link such that the on board beam generation process only requires

$$\mathbf{B}_{\text{feeder-link-on-board}} = K\mathbf{B}_{\text{user}}, \tag{1.4}$$

where K is the number of user terminals.

Finally, an advance architecture will be to consider a combination of both schemes where even if a certain processing is kept at the payload, several gateways are employed so that the feeder link requires

$$\mathbf{B}_{\text{feeder-link-on-board-MG}} = \frac{K}{G}\mathbf{B}_{\text{user}}, \tag{1.5}$$

of bandwidth. As an example, considering that the user bandwidth is 500 MHz in the Ka band, $N = 155$, $K = 100$ and we consider between 6, and 12 gateways, the following table depicts the required bandwidths: Clearly, whenever a larger number of gateways are

On ground	77.5 GHz
On board	50 GHz
On ground with 6 gateways	12.9 GHz
On ground with 12 gateways	6.45 GHz
On board with 6 gateways	8.33 GHz
On board with 12 gateways	4.1 GHz

available, the feeder link bandwidth requirements are reduced. In addition, the on board processing serves as a very important mechanism to reduce the required bandwidth. Note that the aforementioned architectures need to accommodate interference mitigation techniques whose performance might be degraded depending on the used architecture.

This is discussed in the next section.

1.3 Interference mitigation technique in multibeam architecture

In addition to feeder link resources challenge, by growing the number of beams the system performance also becomes limited by the increased level of interference among various beams due to the side lobes of the beam radiation patterns. Therefore, similar to cellular networks in the terrestrial scenario, a frequency diversity among beams could be contributory state to cope with the increased level of interference: typically, beams with adjacent footprint operate on different frequency bands. In this context, the number of colors N_c is the essential parameter which corresponds to the number of disjoint frequency bands employed on the coverage area ($N_c \geq 1$).

In order to increase achievable data rate, another promising technique is to use full frequency reuse pattern ($N_c = 1$) by resorting to extra signal processing, as on ground interference mitigation techniques at gateway [10]. In this way, signals are precoded/detected before being transmitted/received in order to mitigate inter-beam/user interference on ground. Note that, these techniques maintain the user terminal and payload computational complexity low. To this end, more advanced interference mitigation techniques as precoding in the forward link (i.e, the link between gateway and user terminals) and multiuser detection in the return link (i.e, the link between user terminals and gateway) have been considered in studies of the ESA [11, 12].

However, precoding and detecting are sensitive to CSI which is difficult to obtain due to the feedback, estimation and quantization errors. Indeed, with enough channel information at the gateway, precoding and multiuser detection allows to increase multiuser diversity gain.

Let us continue with the CSI procurement. In this context, the natural question is how

to quantize the channel information at the gateway side which makes calculating an exact propagation channel model in multibeam systems compulsory. Next section provides an brief overview on accounting channel model in multibeam systems and, posteriorly, the feedback mechanisms are presented.

1.3.0.2   Channel model in multibeam systems

The characterization of the propagation channel in order to design precoding (or even multi-user detection techniques) is of the highest importance for the system planning. Thus, the research of propagation channel transmission properties and modelling are the significant aspects for engineering exploitation and design of multibeam satellite system [4]. The multibeam propagation channel is modeled based on two characteristics of user terminals which are nowadays driving the commercial development of satellite systems:

- **Fixed satellite systems channel**, operating over frequency bands above 10 GHz (e.g. Ku, Ka) serving fixed satellite terminals in an unobstructed propagation environment.

- **Mobile satellite systems channel**, operating over frequency bands well below 10 GHz (e.g. L, S) serving mobile satellite terminals in propagation environments suffering from different degrees of obstruction (e.g. urban, suburban, rural).

It is important to remark that the difference between the models is in the interpretation of the shadowing mechanism for direct and scattered paths [1].

From theoretical point of view, consider matrix $\mathbf{H}$ denotes the overall $N \times K$ user link channel matrix in the return link where K represents the number of user terminals and N is the number of on board feeds. The i,j, element of $\mathbf{H}$ presents the aggregate gain of the link between the i-th satellite feed and the j-th user (in the j-th beam). This

channel can be decomposed as follows:

$$\mathbf{H} = \mathbf{GD}, \tag{1.6}$$

where:

- $\mathbf{G}$ is a $N \times K$ matrix that models the feed radiation pattern, the on board attenuation, path losses and the receive antenna gain and the noise power. We assume the elements of $\mathbf{G}$ are normalized so that they have unit variance. Its (k, n)-th entry can be described as follows

$$(G)_{k,n} = \frac{G_R a_{kn}}{4\pi \frac{d_k}{\lambda} \sqrt{K_B T_R B_W}} \tag{1.7}$$

  with d_k the distance between the k-th user terminal and the satellite. λ is the carrier wavelength, K_B is the Boltzmann constant, B_W is the carrier bandwidth, G_R^2 the user terminal receive antenna gain, and T_R the receiver noise temperature. The term a_{kn} refers to the gain from the n-th feed to the k-th user. It is important to mention that the $\mathbf{G}$ matrix has been normalized to the receiver noise term. The reader can refer to [14] for a more detailed description of the channel model.

- $\mathbf{D}$ is assumed to be a $K \times K$ diagonal matrix which takes into account the atmospheric fading in the user link, the path loss such that

$$\mathbf{D} = \mathrm{diag}\left(\frac{1}{\sqrt{A_1}}, ..., \frac{1}{\sqrt{A_K}}\right) \tag{1.8}$$

  where A_k denotes the rain attenuation affecting to transmission to user/beam k.

1.3.0.3 Availability of channel knowledge

The degree of CSI varies from no CSI up to full (or perfect) CSI depending on whether exact channel gain values are available at the gateway (and also literally at user ter-

minals) for every channel realization; or only a statistical measure of the channel is available. As stated in 1.3, precoding and multi-user detecting severally rely on the CSI integrity so that the perfect channel knowledge in the gateway provides a specific degree of freedom in order to design these interference mitigation schemes.

Preserving the quality of the estimation carried out by the receiver requires an ideal feedback mechanism which is impossible to implement in real systems. However, as it happens in terrestrial communications, broadband satellite standards are including CSI feedback mechanisms for supporting precoding techniques. This is the case of DVB-S2 and DVB-S2X [8] where for the first time certain feedback technique is offered to the system designer. In the following subsection this mechanism is briefly described.

The measurement and quantizing process of CSI feed back in each gateway is assumed to be continuous and to be reported on the return channels through a signalling table only when significant changes are detected. The maximum delay required for estimation and delivery to the gateway via the interaction channel shall be no more than 500 ms [8, Annex E.4], but this delay should be minimized to maximize capacity gain.

Each user shall estimate and report the channel transfer function to the gateway as a set of complex-valued coefficients. These coefficients should be estimated by a set of 32 orthogonal Wash-Hadamard sequences plus 4 padding symbols. In this context, every feed signal should incorporate a different sequence so that the receiver is able to estimate the channel effect of 31 interfering feed signals. With this, the overall channel matrix cannot be estimated but; however, the closest 31 feed signals are the ones whose largest interference power levels so that the rest can be ignored for precoding purposes. Note that this also reduces the inter-gateway communication overhead.

Under this context, each user can feed back a maximum 7 digits (i.e. maximum 3 digits before decimal point and 4 digits after decimal point) for both amplitude and phase of

each channel element such that

$$(\mathbf{H})_{i,j} = ddd.dddd^{\angle aaa.aaaa}, \tag{1.9}$$

where it is evident that there are 7 bits for the magnitude so as 7 for the phase. Remarkably, this CSI report considers the effects of not only the user channel but also the tentative feeder-link imperfections. This will be justified later on.

As stated before, account for obligating the availability of channel knowledge in the gateway, successful signal modulation can be also an effective element in precoding/detecting outcome (see (b) in subsection 1.3). In this context, next section provides an quick expression about current successful satellite transmission standards.

1.3.0.4 Multibeam satellite transmission standards for fixed satellite services

The signal transmission in multibeam systems (for both two aforementioned fixed and mobile satellite systems) constitutes the main fields of application of a very successful satellite standard, namely the DVB-S2 (also DVB-S2X) standard in the forward link and DVB-RCS2 standard in the return link [8]. It makes use of the latest modulation and coding techniques to deliver performance that approaches the theoretical limit for such systems. Two key features of DVB-S2 and DVB-RCS2 standards in front of previous standards (like DVB-S)are:

- Variable coding and modulation and adaptive coding and modulation modes, which allow optimizing bandwidth utilization by dynamically changing transmission parameters.

- A powerful coding scheme based on a modern low-density parity-check code. For low encoding complexity, the low-density parity-check code chosen have a special structure, also known as Irregular Repeat-Accumulate codes [8].

- The measured DVB-S2 performance gain over DVB-S is around 30% at the same satellite transponder bandwidth and emitted signal power. When the contribution of improvements in video compression is added, an (MPEG-4) HD-TV service can now be delivered in the same bandwidth that supported an early DVB-S based MPEG-2 SD-TV service only a decade before.

1.4   Outline of the dissertation and research contributions

This thesis deals with the problem of finding the interference mitgation techniques that will be able to increase the data rate of future multibeam satellite systems considering the feeder link bandwidth limitations.

The contribution is two fold. First, a novel hybrid space-ground architecture is proposed where an optimal design of on board beam generation process along with typical on ground advance interference mitigation technique is presented. Primarily, we introduce a payload processing which is empirically channel adaptive. Remarkably, channel adaptive characteristic implies that the beam processing mechanism is updated respect to the variation of the channel within each time instant of TDMA scheme.

However, this variation of signal processing scheme in the payload cannot be realistic in the current satellite architecture due to payload signal processing complexity. To cope to this problem, this work posteriorly proposes the on board processing is both: i) to be robust to channel variations; and ii) results the same for both forward and return links. To meet all these requirements a robust MMSE optimization is conceived so that a fixed beam generation can be obtained despite user link channel variation. The benefits of the considered scheme then are evaluated with respect to the current approaches both analytically and numerically. It is important to remark that, a total power optimization among beams is attended.

In addition, we develop the forward link of aforementioned hybrid space-ground archi-

tecture under per-feed power optimization. This is done in order to efficient and more realistic use of payload power resources. In this context, we reformulate the design of on board beam generation process and interference mitigation technique under per-feed power optimization strategy. We analytically show the benefit of the proposed ground and space units design respect to the current scenarios.

Then, in contrast to all limitations offered by even fixed on board segment and avoid payload complexity, we provide a study aiming to design and assessment of the forward link of a multiple gateway multibeam satellite system.

Each gateway includes a linear precoding process such that each precoding is a part
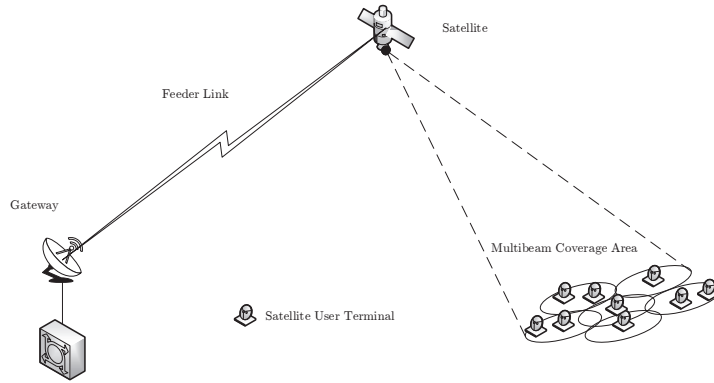
Figure 1.7: The picture depicts the multicast multibeam satellite structure. The gateway delivers certain data to the coverage area by first the feeder link and, posteriorly, the satellite. While the feeder link multiplexes N signals, the satellite that is equipped with an array fed reflector, radiated a total of K signals (one signal per beam). Every radiated signal by the satellite shall be detected by a total number of $Q > 1$ users per beam.

of block precoding technique. Designing the precoding scheme, in contrast to single gateway scheme, entails two main challenges: i) the precoding matrix shall be separated into feed groups assigned to each gateway; ii) complete CSI is required at each gateway,

leading to a large communication overhead. In order to solve these problems, a design based on a regularized singular value block decomposition of the channel matrix is presented so that both inter-cluster (i.e. beams of different clusters) and intra-cluster (i.e. beams of the same cluster) interference is minimized.

In addition, different gateway cooperative schemes are analyzed in order to keep the inter-gateway communication low. Furthermore, the impact of the feeder link interference is analyzed and it is shown both numerically and analytically that the system performance is reduced severally whenever this interference occurs even though precoding reverts this additional interference. Note that this effect occurs whenever the payload feeder link receiver is not properly calibrated and certain pointing errors take place.

Finally, in contrast to the aforementioned beam pattern which employs a single user per codeword, we study the case where the satellite communications embed more than one user in each single codeword in order to increase the channel coding gain. This is referred to the so-called multigroup multicast model (see Figure 1.7).

In this context, the present work proposes a low complex on ground precoding scheme to deal with the multibeam interference in multicast transmissions. Our proposal offers higher spectral efficiencies than the conventional regularized ZF and the average MMSE schemes. In addition, considering that the CSI will be corrupted at the gateway, a robust scheme is presented based on the first perturbation theory of the eigenvectors and eigenvalues. The resulting precoding design remains low complex so that it can be implemented even if a very large number of feeds are considered.

Second, since the achievable rates decreases whenever the user channel vectors within one beam are not collinear, we propose a user grouping technique based on the spatial signature. With this, over all possible users to be serve for each beam we select the most adequate set of users to be served using a variation of the k-means algorithm.

Third, in case the data traffic is generated by multiple gateways, a precoding mechanism is presented for dealing with both CSI sharing challenge and the distributed precoding

matrix computation. Both a reduced inter-gateway communication for CSI sharing and a precoding matrix division among gateways are presented. Even though the achievable rates are decreased when the multiple gateway architecture is considered, the proposed scheme offers a good trade-off between communication overhead, payload complexity and overall throughput. The outline of the thesis is as follows

- **Chapter 2**

  First, In full frequency reuse pattern, a novel hybrid space-ground architecture is analyzed. In this context, an optimal on board beam generation process along with typical interference mitigation technique are presented for both forward and return links of a single gateway multibeam satellite communication system architecture. The contributions of this chapter were presented in the following publications:

  1. V. Joroughi, B. Devillers, M. Angel Vázquez and A. Ana Perez-Neira,*Design of an On Board Beam Generation Process for the Forward Link of a Multi-Beam Broadband Satellite System*, IEEE Global Telecommunications Conference (GLOBECOM). Atlanta (USA), December 2013.

  2. V. Joroughi, B. Devillers, M. Angel Vázquez and A. Ana Perez-Neira,*Design of an On Board Beam Generation Process for a Multi-Beam Broadband Satellite System*, a journal to appear in IEEE Transaction on wireless communication, Under review.

  Second, Deployment the aforementioned hybrid architecture in the forward link where both precoding and beam generation techniques are re-designed under per-feed power optimization. This is done in order to efficient and more realistic use of payload power resources. The results is published in the following conference:

  1. V. Joroughi, M. Angel Vázquez, B. Devillers and A. Ana Perez-Neira, *"Design of a hybrid ground/space architecture based on individual on board feed power*

optimization for the forward link of a multi-beam broadband satellite system," in Proc. 24th AIAA Int. Commun. Satell. Systems Conf. Florence (Italy), October 2013.

- **Chapter 3**

  Design and assessment of an individual on ground multiple gateway structure in order to drastically increase the performance in terms of efficient use of the available feeder link resources and reliability in the next satellite communication system. It addresses in the following publications:

  1. V. Joroughi, M. Angel Vázquez and A. Ana Perez-Neira, *" Multiple Gateway Precoding with Per Feed Power Constraints for Multibeam Satellite Systems"* , in Proceedings of European Wireless 2014, 14-16 May 2014, Barcelona (Spain).

  2. V. Joroughi, M. Angel Vázquez, B. Devillers and A. Ana Perez-Neira, *"Precoding in Multigateway Multibeam Satellite Systems,"* a journal to appear in IEEE Transaction on wireless communication, Submitted.

  3. V. Joroughi, M. Angel Vázquez and A. Ana Perez-Neira, *"Joint On-Board and Multiple Gateway Precoding Scheme for Multibeam Satellite Systems,"* a journal to appear in IEEE Transaction on wireless communication, in progress.

- **Chapter 4**

  We investigate forward link of an individual on-ground multicast multibeam satellite system where we develop several scenarios in order to design precoding schemes in single and multiple gateway architectures.

- **Chapter 5**

  The final chapter concludes the dissertation and points some possible future research directions.

Chapter 2

Hybrid space-ground processing

This chapter deals with the design of a hybrid space-ground architecture in multibeam satellite systems. In such architecture, the on board beam processing at the payload is used in order to reduce the traffic at the feeder link. In addition, we consider that the gateway employs a MMSE precoding scheme in the forward link and multiuser detecting in the return link aiming at suppressing multiuser interference.

2.1 System overview

The MISO broadcast channel is the inherent model behind practical problem where a multibeam hybrid space-ground architecture in full frequency reuse pattern is used. Therefore, from ground processing point of view, interference becomes the bottleneck of the network performance and it has to be alleviated in order to provide a reliable communication for the link pair. In this context, more advance interference mitigation techniques, as respectively precoding and multiuser detection mechanisms in forward and return links, have been considered [4],[9].

23

From the space point of view, since the amount of bandwidth resources in the feeder link are scarce, the generation of beams can be carried out by an on board beam generation process. However, the volume and calibration requirements of this on board processing is currently its main drawback.

A recent attempt is proposed to shift on board beam generation procedure on ground at the gateway [13]. For that case, the interference mitigation technique can be jointly designed with the beam generation process. Moreover, the generation of beams is realized on ground with all capabilities offered by on ground segment digital signal processing. The results were encouraging, as the system throughput was significantly improved. In addition, it provided a higher degree of flexibility and reduced payload complexity.

Nevertheless, the scenario overhead required a large amount of feeder link spectral resources since the feeder link signals have to be frequency multiplexed in both forward and return links. Furthermore, an excessive feeder link bandwidth leads to costly design a feeder link infrastructure and it maybe inefficient from satellite service provider outlook. Thus, aiming to some optimization of the trade-off between performance and complexity, implementing dis-joint on board beam generation and on ground interference mitigation technique is compulsory so that a sufficient degree of flexibility and efficiency on the feeder link obtains.

In this context, the satellite system designers are currently trying to profit from the significant research achievements in the area of a low complex on board beam processing along with on ground interference mitigation technique for developing future multibeam systems [14, 15].

The contribution of this chapter lies in finding an optimal on board beam generation process for link pair of a single gateway multibeam broadband satellite communication system. This work also predicts presence of an advance on ground interference mitigation technique at the gateway. Concretely, we will follow:

- Introducing a hybrid space-ground where an unitary channel adaptive on board

beam generation process along with LMMSE precoding technique in the forward link and LMMSE detection procedure in the return link are used as interference mitigation techniques.

Since the payload is used an unitary processing, we assume a total power constraint in the ground segment. It is important to remark that, unitary characteristic is considered in order to keep on board power loading complexity low so that the power loading procedure is only done in the ground unit and payload follows-up a constant.

- Examining the characteristic of employing unitary non-channel adaptive on board beam process in the proposed hybrid space-ground architecture even if the channel appears as a random variable. We formulate the robust MMSE optimization framework so that a fixed beam generation can be obtained despite user link channel variation. In fact, we deal optimizing the upper bound of the MSE in both links. Remarkably, the best issue is that the design for both forward and return links results the same, which makes it appropriate for the current multibeam satellite systems.

- Addressing more complicate scenario in the forward link and designing beam generation process under per-feed power optimization which leads to a non-unitary payload scheme. In practice, this constraint is more realistic where each on board transmit feed has its own power TWT amplifier. It is important to remark that, the state-of-the-art satellite communication systems will utilize multiple feeds per beam [1] where each feed is geographically served a specific areas, but cooperatively send data to the receiving units. In such systems, it is clear that each feed will have its own power restrictions. In addition, in order to maintaining low complexity, we employ a ZF precoding [24] instead of aforementioned LMME interference

---

[1]The multiple feeds will contribute to each beam. This implies that a feed is shared by multiple beams making TWTAs always operating in multicarrier mode.

technique, based on its relation to the theory of generalized inverse in the linear algebra.

2.2 Hybrid space-ground architecture with unitary on board processing

2.2.1 Signal model

Let us consider a multibeam satellite communication system, where a single geosynchronous satellite with multibeam coverage provides fixed broadband services to a large set of users. To this end, the satellite is equipped with an array fed reflector antenna whose number of feeds is denoted by N. The coverage area is divided into K beams, with

$$K < N, \tag{2.1}$$

and the users are assumed to be uniformly distributed within the beams. By employing a TDM scheme, at each time instant the gateway is serving a total of K single antenna users (i.e. exactly one user per beam), and it is transmitting (receiving) information to (from) the same number of the users through the satellite in the forward (return) link. Note that return link satellite systems generally operate in a MF-TDMA scheme so that in this work it is assumed that the channel is frequency flat the spectral response is the same for each return link sub-band.

In the rest of the study the return link is presented considering a single band transmission since due to the flatness of the channel frequency response the same procedure shall be mimicked for the remaining bands.

The satellite is assumed to linearly convert a set of N on board feed signals into the K feeder link signals which are transmitted to the gateway in a frequency multiplexed fashion. Reciprocally, in the forward link, the same linear processing strategy is used to
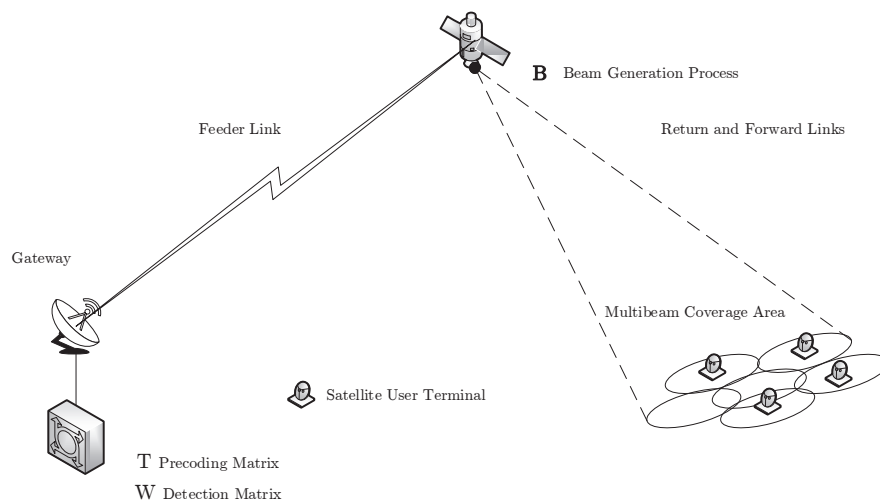
Figure 2.1: Block diagram of the forward and return links.

construct the N feed signals from the K feeder link signals. This on board procedure will be referred to as beam generation process in the forward link and pre-processing in the return link.

Moreover, as a high spectral efficiency of the system is targeted, full frequency reuse among beams is assumed so that all beams can share the same frequency resources. The feeder link is assumed perfectly calibrated and noiseless. Fig. 2.1 summarizes the transmission block diagram.

 The corresponding received signal model for both return and forward links are detailed in follows.

2.2.1.1   Return Link

As stated above, K denotes the number of users and N is the number of on board feeds. Then, the corresponding received signal at the gateway can be modelled as

$$\mathbf{y}_{\mathrm{RL}} = \sqrt{\beta}\mathbf{BHs} + \mathbf{Bn}, \tag{2.2}$$

where $\mathbf{y}_{RL} = [y_{RL,1}, ..., y_{RL,K}]^T$ is a $K \times 1$ vector containing the stack of received signals at the gateway. The $K \times 1$ vector $\mathbf{s}$ is the stack of the transmitted independent signals by all users such that $\mathrm{E}\{\mathbf{ss}^H\} = \mathbf{I}_K$. The constant β denotes equivalent isotropic radiated power which is referred to the user terminal transmit power and we assume to be the same for all the users.

In order to radiate the multibeam pattern, the satellite payload is equipped with a smart antenna system (generally an array fed reflector) coined as on board beam generation process. This system constructs the beam pattern for transmitting and receiving data from the coverage area. Mathematically, the effect of this beamforming appears as the rectangular $K \times N$ fat matrix $\mathbf{B}$.

Finally, the $N \times 1$ vector $\mathbf{n}$ accounts for the zero mean additive white Gaussian noise. We assume unit variance Gaussian noise samples such that

$$\mathrm{E}\{\mathbf{Bnn}^H\mathbf{B}^H\} = \mathbf{BB}^H. \tag{2.3}$$

For radio-frequency design convenience, we will assume that $\mathbf{B}$ is orthonormal so that the feed signals are decoupled at the payload.

Matrix $\mathbf{H}$ is the overall $N \times K$ user link channel matrix whose element h_{ij} presents the aggregate gain of the link between the i-th satellite feed and the j-th user (in the

j-th beam). The reader can refer to (1.6) for a more detailed description of the channel model.

2.2.1.2   Forward Link

Analogously to the return link, the signal model of the forward link becomes

$$\mathbf{y}_{\mathrm{FL}} = \gamma \mathbf{H}^T \mathbf{B}^T \mathbf{x} + \mathbf{w}, \tag{2.4}$$

where $K \times 1$ vector $\mathbf{y}_{\mathrm{FL}}$ is the stack of received signals at each user terminal, and $\mathbf{x}$ is a $K \times 1$ vector that contains the stack of transmitted symbols. Remarkably, in general wireless communication systems, the channel reciprocity does not hold as uplink and downlink operate in disjoint frequency bands. However, considering our channel modelling, the channel matrix in the forward link differs from the return link in the path loss, feed gain and atmospheric fading.

As a result, there exist a scaling factor γ that models the different frequency operations. It will be described in the study this rescaling factor does not influence the proposed optimization and; therefore, it can be omitted. Consequently, in the following it will be considered that $\gamma = 1$.

Similarly as in return link, $\mathbf{w}$ is a $K \times 1$ vector that represents the independent and identically distributed zero mean Gaussian random noise with unit variance such that

$$E\{\mathbf{w}\mathbf{w}^H\} = \mathbf{I}_K. \tag{2.5}$$

To generate a power flexibility which is essential for optimum resource allocation in multibeam system, we assume on board TWT amplifiers. In general, in TWT amplifiers symbols are perfectly oversampled and pulse-shaped with a square-root raised cosine filter and a small roll-off factor. Therefore, these high power amplifiers provide a large bandwidth and high signal power level with small level of interference among feeds'

signals. In fact, the total power obtained by a set of TWT amplifiers can be distributed among different feeds and the number of TWT amplifiers is related to the number of feeds used in the antenna. Under this context, multiple feeds will distribute the available power to each beam. As a result, the precoding design is based on total power constraint. Mathematically,

$$\text{trace}(\mathbf{T}\mathbf{T}^H) \leq P_T, \tag{2.6}$$

where P_T denotes the total transmit power in the forward link. Note that the transmit power constraint is set in without considering the beam generation process $\mathbf{B}$. This is because the power allocation mechanism is allocated before the array fed reflector system. In addition, it is assumed that the feeds can share the available transmit power. This can be implementable for instance with flexible power amplifiers as described in [25].

Now, we proceed to jointly optimize matrix $\mathbf{B}$ so that the overall system performance is improved. It is important to remark that $\mathbf{B}$ must be the same for both the optimization of the return and forward links. In addition, this matrix needs to be fixed in order to keep the payload complexity low and minimize the feeder link spectral resources.

2.2.2   Problem statement

Let us assume the gateway has perfect CSI and uses LMMSE as described in [19] for precoding in the forward link and LMMSE filtering for multiuser detection in the return link. These techniques have been pointed out as efficient methods due to both its interference rejection capabilities and fairness among beams while preserving a low computational complexity [24].

Concretely, let us briefly outline the overall mathematical derivation:

1. First, the MSE matrix of the return link is computed assuming LMMSE detection.

2. Secondly, the MSE matrix of the forward link is computed assuming LMMSE

precoding.

3. Thirdly, a channel adaptive design of on board beam processing is preliminary calculated.

4. Fourthly, an upper bound of the MSE minimization in the return link is presented.

5. Finally, considering the MSE upper bound in previous step, the design of the optimal $\mathbf{B}$ is imposed to be non channel dependent. Surprisingly, for the forward link we show that the optimal design yields to the same solution as it is obtained in the return link.

2.2.3 Return Link

As a first step, let us define $\mathbf{W}^H$ as the LMMSE filter that detects K received signals at the gateway. In this context, the MSE for i-th user is achieved as follows [20]

$$\text{MSE}_{RL,i} = \text{E}\{|\text{s}_i - \hat{\text{s}}_i|^2\} \tag{2.7}$$

where s_i represents the i-the element of transmit signal vector (for i-the user) of K users such that $\mathbf{s} = (s_1, ..., s_K)^T$. With $\hat{\mathbf{s}} = \mathbf{W}^H \mathbf{y}_{\text{RL}} = (\hat{s}_1, ..., \hat{s}_K)^T$, $\hat{\text{s}}_i$ denotes the i-th element of received signal (for i-the user) in the gateway.

Typically, the mathematical expression of LMMSE filter calculated from (2.2) becomes [20]

$$\mathbf{W}^H = \mathbf{R}_{\hat{s}}^{-1} \mathbf{R}_{\hat{s}s} = \mathbf{H}^H \mathbf{B}^H (\mathbf{I}_K + \mathbf{B}\mathbf{H}\mathbf{H}^H \mathbf{B}^H)^{-1} \tag{2.8}$$

where $\mathbf{R}_{(.)}$ denotes the covariance matrix of respective elements. The received MSE in matrix notation is calculated by the following error covariance matrices [20]

$$\mathbf{MSE}_{RL} = \text{E}\{(\mathbf{W}^H \mathbf{y}_{\text{RL}} - \mathbf{s})(\mathbf{W}^H \mathbf{y}_{\text{RL}} - \mathbf{s})^H\} = \mathbf{R}_{s\hat{s}} - \mathbf{R}_s \mathbf{R}_{\hat{s}}^{-1} \mathbf{R}_{\hat{s}s} = \left(\mathbf{I}_K + \mathbf{H}^H \mathbf{B}^H (\mathbf{B}\mathbf{B}^H)^{-1} \mathbf{B}\mathbf{H} \right)^{-1}$$
$$\tag{2.9}$$

It makes sense that the total MSE (i.e. SMSE) is given by

$$\text{trace}(\mathbf{MSE}_{\text{RL}}) = \sum_{i=1}^{K} \text{MSE}_{\text{RL},i} \tag{2.10}$$

Thus, the resulting (2.10) can be used as a performance metric and the related SMSE calculated as

$$\text{SMSE}_{\text{RL}} = \sum_{i=1}^{K} \text{MSE}_{\text{RL},i} = \text{trace}\left[\left(\mathbf{I}_K + \mathbf{H}^H \mathbf{B}^H \mathbf{B} \mathbf{B}^H \mathbf{B} \mathbf{H}\right)^{-1}\right]. \tag{2.11}$$

As mentioned before, we restrict $\mathbf{B}$ to be orthonormal such that $\mathbf{B}\mathbf{B}^H = \mathbf{I}_K$. Thus, the SMSE_{RL} in (2.11) is rewritten as

$$\text{SMSE}_{\text{RL}} = \text{trace}[(\mathbf{I}_K + \mathbf{H}^H \mathbf{B}^H \mathbf{B} \mathbf{H})^{-1}]. \tag{2.12}$$

Let's continue with the forward link.

2.2.4   Forward Link

In the forward link, the LMMSE with a regularized inversion is assumed. In this case, the linear precoding is expressed as

$$\mathbf{x} = \mathbf{T}\mathbf{c} \tag{2.13}$$

where $\mathbf{T}$ is the $N \times K$ precoding matrix and $\mathbf{c}$ is the $K \times 1$ transmit symbol vector at all feeds such that $\text{E}\{\mathbf{c}\mathbf{c}^H\} = \mathbf{I}_K$. In this context, by the regularized inverse approach in [19], the respective precoder can be expressed as

$$\mathbf{T} = \sqrt{\rho}\mathbf{B}^* \mathbf{H}^* \left(\frac{K}{P_{\text{FL}}}\mathbf{I}_K + \mathbf{H}^T \mathbf{B}^T \mathbf{B}^* \mathbf{H}^*\right)^{-1} \tag{2.14}$$

where the value of the constants ρ has to be such to comply with the forward link power constraint as follows

$$\text{trace}\left(\mathbf{B}^T\mathbf{T}\mathbf{T}^H\mathbf{B}^*\right) \leq P_{\text{FL}}. \tag{2.15}$$

This particular kind of precoder is used to find an optimal balance between achieving signal gain and limiting the multiuser interference. Similar to the return link, $\text{MSE}_{FL,i}$ is defined as

$$\text{MSE}_{FL,i} = \text{E}\{|c_i - \hat{c}_i|^2\} \tag{2.16}$$

where $\text{MSE}_{\text{FL},i}$ refers to the MSE received by i-th user. $\mathbf{c} = (c_1, ..., c_K)^T$ and $\hat{\mathbf{c}} = (\sqrt{\rho})^{-1}\mathbf{y}_{FL} = (\hat{c}_1, ..., \hat{c}_K)^T$ are transmitted signal and the received signal for K users, respectively. In this context, c_i represents the transmitted signal for i-the user and $\hat{c}_i$ denotes the signal received by user i-th.

To this end, the MSE in the forward link can be calculated as follows

$$\mathbf{MSE}_{FL} = \text{E}\{\left((\sqrt{\rho})^{-1}\mathbf{y}_{FL} - \mathbf{c}\right)\left((\sqrt{\rho})^{-1}\mathbf{y}_{FL} - \mathbf{c}\right)^H\}$$

$$= \frac{K}{P_{\text{FL}}}\left[(\mathbf{H}^T\mathbf{B}^T\mathbf{B}^*\mathbf{B}^T\mathbf{B}^*\mathbf{H}^* + \frac{K}{P_{\text{FL}}}\mathbf{I}_K)(\mathbf{H}^T\mathbf{B}^T\mathbf{B}^*\mathbf{H}^* + \frac{K}{P_{\text{FL}}}\mathbf{I}_K)^{-2}\right]. \tag{2.17}$$

Thus, the overall SMSE_{FL} associated with the precoder (2.14) is expressed as follows

$$\text{trace}(\mathbf{MSE}_{\text{FL}}) = \sum_{i=1}^{K} \text{MSE}_{\text{FL},i} \tag{2.18}$$

Thus,

$$\text{SMSE}_{FL} = \sum_{i=1}^{K} \text{MSE}_{\text{FL},i} = \frac{K}{P_{\text{FL}}}\text{trace}\left[(\mathbf{H}^T\mathbf{B}^T\mathbf{B}^*\mathbf{B}^T\mathbf{B}^*\mathbf{H}^* + \frac{K}{P_{\text{FL}}}\mathbf{I}_K)(\mathbf{H}^T\mathbf{B}^T\mathbf{B}^*\mathbf{H}^* + \frac{K}{P_{\text{FL}}}\mathbf{I}_K)^{-2}\right]. \tag{2.19}$$

Analogously to the return link, we assume that $\mathbf{B}\mathbf{B}^H = \mathbf{I}_K$. With the following property,

$\text{trace}(\mathbf{A}) = \text{trace}(\mathbf{A}^T)$ where $\mathbf{A}$ is any arbitrary matrix, then we have that

$$\text{SMSE}_{FL} = \frac{K}{P_{\text{FL}}} \text{trace}(\mathbf{H}^H \mathbf{B}^H \mathbf{B} \mathbf{H} + \frac{K}{P_{\text{FL}}} \mathbf{I}_K)^{-1}. \tag{2.20}$$

In the following section we will propose an appropriate solution to the problems (2.12) and (2.20).

2.2.5   On board processing optimization

2.2.5.1   Channel adaptive beam generation process

For a moment let us assume that $\mathbf{B}$ can be channel adaptive. Then, the corresponding problem in the return link would be formulated as

$$\min_{\mathbf{B}} \quad \text{trace}[(\mathbf{I}_K + \mathbf{H}^H \mathbf{B}^H \mathbf{B} \mathbf{H})^{-1}] \tag{2.21}$$

$$s.t. \qquad \mathbf{B}\mathbf{B}^H = \mathbf{I}_K$$

where $\mathbf{B}\mathbf{B}^H = \mathbf{I}_K$ is the constraint on $\mathbf{B}$ which was explained above. It is important to remark that [14] showed the effect of $\mathbf{B}$ increases the SMSE_{RL} in the gateway, that is,

$$\text{trace}[(\mathbf{I}_K + \mathbf{H}^H \mathbf{B}^H \mathbf{B} \mathbf{H})^{-1}] \geq \text{trace}[(\mathbf{I}_K + \mathbf{H}^H \mathbf{H})^{-1}]. \tag{2.22}$$

With the following SVD of the channel $\mathbf{H} = \mathbf{U}\mathbf{\Phi}\mathbf{V}^H$, an optimal design of $\mathbf{B}$ can be worked out as

$$\mathbf{B} = \mathbf{U}_{1:K}^H \tag{2.23}$$

where $\mathbf{U}_{1:K}^H$ denotes the K first rows of the matrix $\mathbf{U}^H$. In fact, it can easily be seen that this particular solution reaches equality in (2.22) and; therefore it minimizes the SMSE_{RL}.

However, the considered problem in this work is more challenging. This is due to the beam processing mechanism must update respect to the variation of the channel within time instants. This is done in order to more realistic use of payload resources and keep the complexity low. This will be justified in the following section.

Note that, the sketch of the design for the forward link is similar to the one presented in (2.23) and; thus, we only comment it. The idea is to check whether the term $\frac{K}{P_{\text{FL}}}$ does not influence the optimal value of (2.20). Let us continue with non-channel adaptive design of $\mathbf{B}$ in the following section.

2.2.5.2   Non-channel adaptive beam generation process

Now, $\mathbf{B}$ is assumed to be non-channel adaptive such that the design of $\mathbf{B}$ in (2.23) can not be considered. Even though the channel appears as a random variable, we aim at finding the best possible non-channel adaptive design of $\mathbf{B}$. In this context, let us decompose the channel as follows

$$\mathbf{H} \triangleq \bar{\mathbf{H}} + \boldsymbol{\Delta} \tag{2.24}$$

where:

- $\bar{\mathbf{H}}$ represents the mean value of the channel.

- $\boldsymbol{\Delta}$ models the difference between the actual value of the channel and its mean. It indicates the variability of the channel in consecutive time instants as already explained in section I. In this context, we define α as the maximum value that the Frobenius norm of $\boldsymbol{\Delta}$ can be, i.e. $||\boldsymbol{\Delta}|| \leq \alpha$. The bigger the value of α, the greater the variability of the channel will be.

Interestingly, the channel model in (2.24) resembles to the modeling of a MIMO system when imperfect CSI at the transmitter is assumed. With this perspective, the worst case

robust design, which leads to a maximin or minimax formulation, can be proposed to
optimize the system performance [21]. By employing the worst case approach to (2.21),
we get the following optimization problem

$$\min_{\mathbf{B}} \quad \max_{\Delta} \quad \text{trace}[(\mathbf{I}_K + \mathbf{H}^H \mathbf{B}^H \mathbf{B} \mathbf{H})^{-1}] \tag{2.25}$$

$$s.t. \quad \mathbf{B} \mathbf{B}^H = \mathbf{I}_K,$$

where $\mathbf{H}$ is decomposed in (2.24). It is important to remark that by substituting
$\text{trace}[(\mathbf{H}^H \mathbf{B}^H \mathbf{B} \mathbf{H} + \frac{K}{P_{\text{FL}}} \mathbf{I}_K)^{-1}]$ in (2.25) the sketch of the optimization problem for the
forward link is the same return link.
In the following section we will propose an appropriate approximate solution to the
problems (2.25).

2.2.5.3 Return link

First, by considering $\mathbf{A} \triangleq \mathbf{B} \mathbf{H}$, let us present a matrix inversion lemma as follows

$$\text{trace}(\mathbf{I}_K + \mathbf{A} \mathbf{A}^H)^{-1} = \text{trace}(\mathbf{I}_K + \mathbf{A}^H \mathbf{A})^{-1} \tag{2.26}$$

where $\mathbf{A}$ is a random square matrix of size $K \times K$.

Proof. See Appendix 2.5.1. □

Then, the SMSE_{RL} in problem (2.25) can be rewritten as

$$\text{trace}[(\mathbf{I}_K + \mathbf{B} \mathbf{H} \mathbf{H}^H \mathbf{B}^H)^{-1}] = \text{trace}[(\mathbf{I}_K + \mathbf{B} \mathbf{Z} \mathbf{B}^H)^{-1}] \tag{2.27}$$

where $\mathbf{Z}$ is a $N \times N$ matrix so that

$$\mathbf{Z} = \mathbf{H}\mathbf{H}^H = \bar{\mathbf{H}}\bar{\mathbf{H}}^H + \bar{\mathbf{H}}\boldsymbol{\Delta}^H + \boldsymbol{\Delta}\bar{\mathbf{H}}^H + \boldsymbol{\Delta}\boldsymbol{\Delta}^H \qquad (2.28)$$

We propose an upper bound of SMSE_{RL} as follows

Theorem 2.1. *The worst case (upper-bound) of $SMSE_{RL}$ as follows*

$$trace[(\mathbf{I}_K + \mathbf{B}\mathbf{Z}\mathbf{B}^H)^{-1}] \leq trace[(\mathbf{I}_K + \mathbf{B}\check{\mathbf{Z}}\mathbf{B}^H)^{-1}] \qquad (2.29)$$

with the following eigenvalue decomposition $\bar{\mathbf{H}}\bar{\mathbf{H}}^H = \bar{\mathbf{L}}\bar{\boldsymbol{\Sigma}}\bar{\mathbf{L}}^H$, $\check{\mathbf{Z}}$ is defined as

$$\check{\mathbf{Z}} \triangleq \bar{\mathbf{L}}(\bar{\boldsymbol{\Sigma}} - \epsilon_H \mathbf{I}_N)^+ \bar{\mathbf{L}}^H \qquad (2.30)$$

where $\epsilon_H \triangleq 2\alpha\delta_{max}(\bar{\mathbf{H}})$, and $\delta_{max}(.)$ denotes the maximum singular value.

Proof. See Appendix 2.5.2. □

In order to see more details of the upper-bound, the reader can refer to [22, Sec.7.3]. In fact, a worst-case of SMSE_{RL} can be obtained in practice by using the lower bound $\check{\mathbf{Z}}$ in lieu of $\mathbf{Z}$. The reader refers to [22] for more details about the worst case design. It is important to mention that some values of α lead to unfeasible MSE_{RL} solutions, that is, for a large value of α the matrix (2.30) might become semi definite negative. In order to avoid this circumstance, the value of α has to be checked and, if necessary, decreased so that the feasibility condition of the problem (2.25) is hold. Note that feasibility of the problem implies to the likelihood of success and the expected cost of solving the problem. Besides, it also has to be satisfied all their constraints.

Now, the target is to minimize the proposed upper-bound of SMSE_{RL} in (2.29). In

this case, the corresponding problem would be formulated as

$$\min_{\mathbf{B}} \quad \text{trace}[(\mathbf{I}_K + \mathbf{B}\check{\mathbf{Z}}\mathbf{B}^H)^{-1}] \tag{2.31}$$

$$s.t. \qquad \mathbf{B}\mathbf{B}^H = \mathbf{I}_K \qquad .$$

Similar to the problem (2.21), the particular solution in order to minimize the upper bound of the SMSE in (2.31), is a direct consequence of the following theorem.

Theorem 2.2. *Let* $\mathbf{B}$ *and* $\bar{\mathbf{L}}^H$ *be two matrices of size* $K \times N$ *and* $N \times N$, *respectively. Then, the upper bound of SMSE is minimized if* $\mathbf{B}$ *is selected by first* K *rows of the matrix* $\bar{\mathbf{L}}^H$, *that is*

$$\mathbf{B}^{\star} = \bar{\mathbf{L}}^H_{1:K} \tag{2.32}$$

where $\mathbf{B}^{\star}$ *denotes the optimal design of* $\mathbf{B}$.

Proof. See Appendix 2.5.3. □

Let's now proceed with the forward link optimization.

2.2.5.4 Forward Link

Interestingly, the forward link can be conceptually modeled very similar to that of the return link. The corresponding SMSE_{FL} in (2.20) can be rewritten similar to the Appendix 2.5.1 as

$$\text{trace}[(\mathbf{B}\mathbf{Z}\mathbf{B}^H + \frac{K}{P_{\text{FL}}}\mathbf{I}_K)^{-1}] \tag{2.33}$$

Then, the SMSE_{FL} is upper bounded as

$$\text{trace}[(\mathbf{B}\mathbf{Z}\mathbf{B}^H + \frac{K}{P_{\text{FL}}}\mathbf{I}_K)^{-1}] \leq \text{trace}[(\mathbf{B}\check{\mathbf{Z}}\mathbf{B}^H + \frac{K}{P_{\text{FL}}}\mathbf{I}_K)^{-1}] \tag{2.34}$$

Then, the optimizing problem can be formulated as follows

$$\min_{\mathbf{B}} \quad \text{trace}[(\mathbf{B}\check{\mathbf{Z}}\mathbf{B}^H + \frac{K}{P_{\text{FL}}}\mathbf{I}_K)^{-1}] \tag{2.35}$$

$$s.t. \quad \mathbf{B}\mathbf{B}^H = \mathbf{I}_K$$

The sketch of the proof is similar to the one presented previously for the return link and; thus, we only comment it. The idea is to check whether the term $\frac{K}{P_{\text{FL}}}$ does not influence the optimal value of (2.35) which can be easily observe in appendix 2.5.2. Consequently, the scaling factor due to the channel variations γ does not influence the optimization, either. Note that the robust beamforming design has the same eigenvectors as the nominal channel matrix $\bar{\mathbf{H}}\bar{\mathbf{H}}^H$. In other words, the presented robust design only considers eigenvalue variations due to the different user positions. In the next section, the impact on the eigenvectors is analyzed.

2.2.6   First order perturbation analysis

As discussed in the previous sections, the underlying optimization problem (2.31) shall be lower bounded in order to obtain a closed-form solution. This is done by means of considering upper bounds of $\mathbf{Z}$. Indeed, the proposed perturbation model can be described as

$$\mathbf{Z} = \left(\bar{\mathbf{U}}_s + \Delta\mathbf{U}_s\right)\left(\bar{\mathbf{\Sigma}}_s + \Delta\mathbf{\Sigma}_s\right)\left(\bar{\mathbf{U}}_s + \Delta\mathbf{U}_s\right)^H + \left(\bar{\mathbf{U}}_n + \Delta\mathbf{U}_n\right)\left(\bar{\mathbf{\Sigma}}_n + \Delta\mathbf{\Sigma}_n\right)\left(\bar{\mathbf{U}}_n + \Delta\mathbf{U}_n\right)^H, \tag{2.36}$$

where the $\mathbf{U}$ denotes the matrix containing the eigenvectors and $\mathbf{\Sigma}$ is a diagonal matrix, which contains the eigenvalues. In addition, subindex s denotes the non-zero signal space whereas n the signal space that is spanned by the zero valued eigenvalues (i.e. the null

space of $\mathbf{Z}$. All $\Delta \mathbf{U}_s, \Delta \Sigma_s, \Delta \mathbf{U}_n, \Delta \Sigma_n$ are generated by a perturbed version of $\bar{\mathbf{Z}}$:

$$\mathbf{Z} = \bar{\mathbf{Z}} + \Delta \mathbf{Z}, \tag{2.37}$$

where

$$\bar{\mathbf{Z}} = \bar{\mathbf{H}}\bar{\mathbf{H}}^H, \tag{2.38}$$

and

$$\Delta \mathbf{Z} = \bar{\mathbf{H}}\Delta^H + \Delta\bar{\mathbf{H}}^H + \Delta\Delta^H. \tag{2.39}$$

Under this context, $\bar{\mathbf{U}}$ denotes the eigenvector of the nominal matrix $\bar{\mathbf{Z}}$ whereas $\bar{\Sigma}$ a matrix containing its eigenvalues. The other matrices with the $\Delta\cdot$ prefix denote the corresponding perturbation matrices.

The previous section has implicitly considered two assumptions. First, it has been assumed that the channel variations do not modify the dimension of the null space so that $\Delta\Sigma_n$ remains as a zero matrix. Second, it has been assumed that $\Delta\mathbf{U}_s = 0$,which might not be true in certain cases. The aim of this section is to consider the effect of this later perturbation in order to obtain a tighter upper bound of $\mathbf{Z}$ than the presented in the previous section. Remarkably, the first assumption does not influence the overall matrix.

Remarkably, the following inequality holds

$$\mathbf{Z} \geq \widehat{\mathbf{Z}} \geq \widecheck{\mathbf{Z}}, \tag{2.40}$$

where $\widecheck{\mathbf{Z}}$ only considers perturbations at the eigenvalues whereas $\widehat{\mathbf{Z}}$ considers both perturbations at both eigenvalues and eigenvectors($\Delta\mathbf{U}_s$) . Next theorem provides an approximate solution whenever these both perturbations are considered.

Theorem 2.3. The beamforming matrix that optimizes a MSE upper bound when

considering both eigenvector and eigenvalue perturbations is

$$\widehat{\mathbf{B}^*} = \widehat{\mathbf{L}} \left(\bar{\mathbf{\Sigma}} - \epsilon_H \mathbf{I}_N \right)^+ \widehat{\mathbf{L}}^H, \tag{2.41}$$

where

$$\widehat{\mathbf{L}} = \bar{\mathbf{U}}_s + \epsilon_H \bar{\mathbf{U}}_s \widehat{\mathbf{R}} + \epsilon_H \bar{\mathbf{U}}_n \bar{\mathbf{U}}_n^H \bar{\mathbf{U}}_s \bar{\mathbf{\Sigma}}_s^{-1}, \tag{2.42}$$

and

$$\widehat{\mathbf{R}} = \mathbf{D} \cdot \left(\epsilon_H \mathbf{U}_s^H \mathbf{U}_s \bar{\mathbf{\Sigma}} + \epsilon_H \bar{\mathbf{\Sigma}} \mathbf{U}_s^H \mathbf{U}_s \right), \tag{2.43}$$

and the g, f-th entry of $\mathbf{D}$ is

$$\frac{1}{\lambda_f - \lambda_g}, \tag{2.44}$$

for $f \neq g$ and λ_f for $f = 1, \ldots, N$ denote the eigenvalues of $\bar{\mathbf{H}} \bar{\mathbf{H}}^H$.

Proof. See Appendix 2.5.4. □

Note that for this case, the eigenvectors of the beamforming matrix take a different value from the nominal matrix. In addition, the larger α the more different are the eigenvectors from the nominal channel matrix.

Now, it is time to develop the beam generation process under per-feed power optimization in the forward link so that the on board process leads to be non-unitary.

2.3 Hybrid space-ground architecture with non-unitary payload

As stated above, the hybrid space-ground architecture is traditionally designed under the assumption of an average power constraint among feeds which leads to using an unitary payload processing. In practice, there is increasing interest in addressing more complicated scenarios, such as individual per feed power constraints. In fact, these con-

straints are more realistic since each on board transmit feed has its own power amplifier so that a non-unitary payload processing results.

In this way, this section progress the aforementioned hybrid space-ground architecture in the forward link.

From ground point of view, in order to achieve a promising trade-off between complexity and performance, here, we develop a linear ZF precoding [24] (instead of aforementioned LMMSE in (2.13)) based on its relation to the theory of generalized inverse in the linear algebra. To this end, we formulate the precoding problem with individual on board feed power constraint in order to efficient and more realistic use of payload power resources. From space point of view, in contrast to the previous case, we will consider an adaptive payload so that at each frame the satellite is able to optimize its individual per feed power.

Consider the same forward link system architecture described in section 2.2.1.2. In such system, in order to simplify mathematical notation the signal model in(2.4) is rewritten as

$$\mathbf{y}_{\mathrm{FL}} = \mathbf{HBTc} \tag{2.45}$$

where we assume user link channel and beam generation matrices $\mathbf{H}$ and $\mathbf{B}$ are the same size and properties of $\mathbf{H}^T$ (of size $K \times N$) and $\mathbf{B}^T$ (of size $N \times K$) , respectively. Here, $\mathbf{T}$ denotes ZF precoding matrix of size $K \times K$. $\mathbf{y}_{\mathrm{FL}}$ and $\mathbf{c}$ are the stack of received and transmit signals of size $K \times 1$, respectively.

The received SINR for k-th user is expressed as

$$\mathrm{SINR}_k = \frac{|(\mathbf{HBT})_{kk}|^2}{\sum_{j \neq k}^{K} |(\mathbf{HBT})_{kj}|^2 + 1} \quad k = 1, ..., K. \tag{2.46}$$

Conventionally, the design of precoders based on total power constraint can be formed as

$$\mathrm{E}\{||\mathbf{Bx}||^2\} = \mathrm{trace}(\mathbf{BTT}^H\mathbf{B}^H) \leq P \tag{2.47}$$

Remind that P denotes the total transmit power at the satellite. In fact, many satellite systems have to be designed based on per on board feed power constraint so that

$$\mathrm{E}\{|(\mathbf{B}\mathbf{x})_n|^2\} = (\mathbf{B}\mathbf{T}\mathbf{T}^H\mathbf{B}^H)_{nn} \leq \frac{P}{N} \quad n = 1, ..., N. \tag{2.48}$$

2.3.1 Generalized inverse

The concept of generalized inverse in linear algebra has a close meaning of designing a ZF precoder in multiuser system framework [26]. Typically, $K \times K$ rectangular matrix $(\mathbf{HB})^-$ denotes the generalized inverse of matrix $(\mathbf{HB})$ of size $K \times K$ such that $(\mathbf{HB})^- = (\mathbf{HB})^{-1}$. In this context, $(\mathbf{HB})^-$ is defined as follows

$$\mathbf{HB}^- \triangleq (\mathbf{HB})^{\dagger} + \mathbf{R}_{\perp}\mathbf{Q} \tag{2.49}$$

where $(\mathbf{HB})^{\dagger}$ is defined as $(\mathbf{HB})^{\dagger} \triangleq \mathbf{H}^H\mathbf{B}^H(\mathbf{HBB}^H\mathbf{H}^H)^{-1}$. Moreover, $\mathbf{R}_{\perp} \triangleq (\mathbf{HB})^{\dagger}(\mathbf{HB})$ is the orthogonal projection onto the null space of $\mathbf{HB}$ and matrix $\mathbf{Q}$ represents an arbitrary matrix. This changes the precoder design problem to an optimization via the elements of $\mathbf{R}_{\perp}$ and generalized inverse via $\mathbf{Q}$.

Let's now proceed with the design of hybrid space/ground architecture in the forward link.

2.3.2 Ground unit

2.3.2.1 A brief overview on designing ZF precoding under total power optimization

This subsection provides an appropriate design of precoding (2.45) under a total power constraint. We employ a ZF precoding technique in order to transmit symbols at the gateway. We focus on ZF precoding due to its achieving zero interference among users. The reason is that the ZF lies on complete cancellation of the inter-user interference by

employing pseudo inverse of $(\mathbf{HB})$. Moreover, it provides a promising trade-off between complexity and performance which is proven in [20]. Hence, $\mathbf{T}$ is destined to achieve zero interference among users, i.e. $[\mathbf{HBT}]_{kj} = 0$.

Now, let us rewrite again the ZF precoding in (2.45) based on the concept of SNR in (2.46) as follows

$$\mathbf{HBT} = \mathrm{diag}\sqrt{\mathbf{SNR}} \tag{2.50}$$

where $\sqrt{\mathbf{SNR}} = [\sqrt{\mathrm{SNR}}_1, ..., \sqrt{\mathrm{SNR}}_K]^T$ is a vector of SNRs with non-negative elements. Then, by using the the generalized inverse criterion in (2.49), the precoder in (2.50) can be expressed as

$$\mathbf{T} = \sqrt{\rho}((\mathbf{HB})^{\dagger} + \mathbf{R}_{\perp}\mathbf{Q})\mathrm{diag}\sqrt{\mathbf{SNR}} \tag{2.51}$$

where the value of the constants ρ has to be such to comply with (2.47) and (2.48). The objective of optimizing ground processing problem based on per-feed power constraints is to maximize an arbitrary function of SNR (i.e. $f(\mathbf{SNR})$). If we assume $f(.)$ is a arbitrary function of any matrix, the optimization problem then can be formulated as

$$\max_{\mathbf{SNR} \geq 0, \mathbf{T}} \quad f(\mathbf{SNR}) \tag{2.52}$$

$$s.t. \quad \mathbf{HBT} = \mathrm{diag}\sqrt{\mathbf{SNR}}$$

$$. \qquad \mathrm{trace}(\mathbf{BTT}^H\mathbf{B}^H) \leq P.$$

By employing the (2.50), the problem (2.52) can be rewritten as

$$\max_{\mathbf{SNR} \geq 0, \mathbf{T}} \quad f(\mathbf{SNR}) \tag{2.53}$$

$$s.t. \quad \mathrm{trace}[(\mathbf{HB}^{\dagger} + \mathbf{R}_{\perp}\mathbf{Q})\mathrm{diag}(\mathbf{SNR})(\mathbf{HB}^{\dagger} + \mathbf{R}_{\perp}\mathbf{Q})^H] \leq P.$$

Since $\mathbf{Q} = 0$, the problem reduces to

$$\max_{\mathbf{SNR} \geq 0, \mathbf{T}} \quad f(\mathbf{SNR}) \tag{2.54}$$

$$s.t. \quad \text{trace}[(\mathbf{HB})^{\dagger}\text{diag}(\mathbf{SNR})\left((\mathbf{HB})^{\dagger}\right)^{H}] \leq P.$$

Then, the above problem also can be expressed as

$$\max_{\mathbf{SNR} \geq 0, \mathbf{T}} \quad f(\mathbf{SNR}) \tag{2.55}$$

$$s.t. \quad \sum_{k} \text{SNR}_{k}[\left((\mathbf{HB})^{\dagger}\right)^{H}(\mathbf{HB})^{\dagger}] \leq P.$$

where SNR_k denotes the SNR of k-th user in the coverage area. As a consequence the problem (2.55) is a simple power allocation problem such that is concave maximization with a linear constraint. In this way, $f(\mathbf{SNR})$ is a concave function in $\mathbf{SNR} \geq 0$. In [27, 28], the authors boil down this problem to

$$\max_{\mathbf{SNR} \geq 0, \mathbf{T}} \quad \sum_{k} \log(1 + \text{SNR}_{k}) \tag{2.56}$$

$$s.t. \quad \sum_{k} \text{SNR}_{K}[\left((\mathbf{HB})(\mathbf{HB})^{H}\right)^{-1}]_{kk} \leq P$$

which is solved by water filling solution. We refer the reader to study provided references [27, 28] and this problem is beyond the scope of this thesis.

Next subsection provides the provides precoding design (2.45) under per-feed power optimization.

2.3.2.2   Precoding design with per-feed power optimization

Here, we propose an optimal design of ZF precoding technique based on on board individual per-feed power constraints.

Similar to the total power constraint, the objective problem respect to the arbitrary function of SNR (i.e. $f(\mathbf{SNR})$) can be formulated as

$$\max_{\mathbf{SNR} \geq 0, \mathbf{T}} \quad f(\mathbf{SNR}) \tag{2.57}$$

$$s.t. \quad \mathbf{HBT} = \mathrm{diag}\sqrt{\mathbf{SNR}}$$

$$. \quad\quad [\mathbf{BTT}^H\mathbf{B}^H]_{nn} \leq \tfrac{P}{N} \quad\quad \forall n.$$

In general, (2.57) is a difficult non-convex problem. To tackle with this, let us reformulate (2.57) as a fairness typical performance measure such that $f(\mathbf{SNR}) = \min_k \mathrm{SNR}_k$. Thus, we can have that

$$\max_{\mathbf{SNR} \geq 0, \mathbf{T}} \quad \min_k \; \mathrm{SNR}_k \tag{2.58}$$

$$s.t. \quad \mathbf{HBT} = \mathrm{diag}\sqrt{\mathbf{SNR}}$$

$$. \quad\quad [\mathbf{BTT}^H\mathbf{B}^H]_{nn} \leq \tfrac{P}{N} \quad\quad \forall n.$$

Then, the fairness criterion implies that

$$\mathbf{SNR} = \mathrm{s}_f \mathbf{1} \tag{2.59}$$

where s_f is optimal and feasible value of SINR in all K users. Thus, respect to the

feasible point obtained in (2.59), the precoding matrix $\mathbf{T}$ can be worked out as

$$\mathbf{T} = \sqrt{\rho}\sqrt{s_f}\left((\mathbf{HB})^-\right) = \sqrt{\rho}\sqrt{s_f}\left((\mathbf{HB})^\dagger + \mathbf{R}_\perp \mathbf{Q}\right) \quad (2.60)$$

Note that a similar idea has studied in terrestrial networks in [29]. This new statement for $\mathbf{T}$ is reduced the problem (2.57) for some $\mathbf{Q}$ as

$$\max_{s_f \geq 0, \mathbf{T}} \quad s_f \quad (2.61)$$

$$s.t. \quad s_f ||[\mathbf{B}\left((\mathbf{HB})^\dagger + \mathbf{R}_\perp \mathbf{Q}\right)]^H \mathbf{a}_n||^2 \leq \frac{P}{N} \quad \forall n$$

Obviously, we can have that

$$s_f = \frac{P}{N \max_n ||[\mathbf{B}\left((\mathbf{HB})^\dagger + \mathbf{R}_\perp \mathbf{Q}\right)]^H \mathbf{a}_n||^2} \quad (2.62)$$

where $\mathbf{Q}$ is the solution to

$$\min_{\mathbf{Q}, r} \quad r \quad (2.63)$$

$$s.t. \quad ||[\mathbf{B}\left((\mathbf{HB})^\dagger + \mathbf{R}_\perp \mathbf{Q}\right)]^H \mathbf{a}_n|| \leq r \quad \forall n$$

The problem (2.63) is a convex second order cone program and it can be solved easily by standard optimization package [30].

2.3.3   Space unit

2.3.3.1   Channel adaptive payload processing

Now, the target is to provide an appropriate design of on board $\mathbf{B}$ respect to novel precoding ZF technique in (2.60).

For a moment, in order to simplify mathematical expression, let us assume $\mathbf{Q} = \mathbf{0}$. Then,

the resulting total SNR from (2.47) and (2.60) can be rewritten as

$$\text{SNR} = \frac{P}{\text{trace}\left(\mathbf{B}\left(\mathbf{B}^H \mathbf{H}^H \mathbf{H} \mathbf{B}\right)^{-1} \mathbf{B}^H\right) \mathbf{s}_f} \tag{2.64}$$

Then, the particular design of $\mathbf{B}$ in order to improve the SNR in (2.64), is a direct consequence of the following theorem.

Theorem 2.4. *Let $\boldsymbol{B}$ and $\boldsymbol{L}$ be two matrices of size $N \times K$ and $N \times N$, respectively, so that $\mathbf{H} = \mathbf{U}\boldsymbol{\Sigma}\mathbf{L}^H$. Then, the SNR is maximized if $\boldsymbol{B}$ is selected by K columns of matrix $\boldsymbol{L}$, that is*

$$\boldsymbol{B}^\star = \boldsymbol{L}_{1:K} \tag{2.65}$$

where $\boldsymbol{B}^\star$ denotes the optimal design of $\boldsymbol{B}$. Then, the following inequality holds

$$\text{trace}[\mathbf{B}^\star(\mathbf{B}^{\star,H}\mathbf{H}^H\mathbf{H}\mathbf{B}^\star)^{-1}\mathbf{B}^{\star,H}] \leq \text{trace}[\mathbf{B}(\mathbf{B}^H\mathbf{H}^H\mathbf{H}\mathbf{B})^{-1}\mathbf{B}^H] \tag{2.66}$$

Proof. See Appendix 2.5.5. $\qquad\qquad\qquad\qquad\qquad\qquad\qquad\qquad\qquad\qquad\square$

Let us continue with non-channel adaptive design of $\mathbf{B}$ in the following section.

2.3.3.2   Non-channel adaptive payload processing

As stated before, in order to reduce payload complexity, we aim at finding the best possible non-channel adaptive design of $\mathbf{B}$ while the channel matrix $\mathbf{H}$ is a random variable. In this context, the channel in (2.24) has to be considered.

By employing the robust approach for (2.64), we get the following optimization problem

$$\min_{\mathbf{B}} \quad \max_{\boldsymbol{\Delta}} \quad \text{trace}\left(\mathbf{B}\left(\mathbf{B}^H\mathbf{H}^H\mathbf{H}\mathbf{B}\right)^{-1}\mathbf{B}^H\right)\mathbf{s}_f \tag{2.67}$$

$$s.t. \qquad \mathbf{B} \quad is \quad fixed$$

In order to simplify mathematical expression, let us consider eigen values upper-bound of the problem (2.67). Similar to (2.29), with the following definition $\mathbf{R} \triangleq \mathbf{H}^H \mathbf{H} = \bar{\mathbf{H}}^H \bar{\mathbf{H}} + \bar{\mathbf{H}}^H \boldsymbol{\Delta} + \boldsymbol{\Delta}^H \bar{\mathbf{H}} + \boldsymbol{\Delta}^H \boldsymbol{\Delta}$ of size $N \times N$, the upper-bound of (2.67) can be expressed as

$$\text{trace} \left(\mathbf{B} \left(\mathbf{B}^H \mathbf{R} \mathbf{B} \right)^{-1} \mathbf{B}^H \right) \mathbf{s}_f \leq \text{trace} \left(\mathbf{B} \left(\mathbf{B}^H \breve{\mathbf{R}} \mathbf{B} \right)^{-1} \mathbf{B}^H \right) \mathbf{s}_f \qquad (2.68)$$

where $\bar{\mathbf{H}}^H \bar{\mathbf{H}} = \bar{\mathbf{L}} \bar{\boldsymbol{\Sigma}} \bar{\mathbf{L}}^H$ denotes eigenvalue decomposition of matrix $\bar{\mathbf{H}}^H \bar{\mathbf{H}}$. In this context $\breve{\mathbf{R}}$ is obtained as $\breve{\mathbf{Z}}$ in (2.30).

Proof. See Appendix 2.5.6. □

Then, the particular design of $\mathbf{B}$ in order to improve the SNR in (2.64) is obtained by selecting K columns of matrix $\bar{\mathbf{L}}$ such that

$$\mathbf{B}^\star = \bar{\mathbf{L}}_{1:K} \qquad (2.69)$$

The sketch of the proof is similar to (2.65) and skip in order to the sake of brevity. Let us continue by comparing joint and individual design of space-ground architectures in the throughput of a multibeam satellite system.

2.4 Numerical results and interpretation

2.4.1 The space/ground architecture under total power constraint

In order to show the performance of our proposal in section 2.2, here we present a numerical evaluation of the considered techniques. Our baseline scenario is an array fed reflector antenna and matrix $\mathbf{B}$ that have been provided by ESA in the framework of a

study on next generation multibeam satellite systems. The number of feeds is assumed to be $N = 155$ and $K = 100$ beams that are covering the whole Europe area. Fig. 2.2 depicts 3dB contour plot of on ground feed radiation pattern whereas each of them is indicated by a number. Besides, we assume K users are served at a given time instant and they are spread over the coverage area.

Results have been averaged for a total of 1000 user link channel realizations and it is
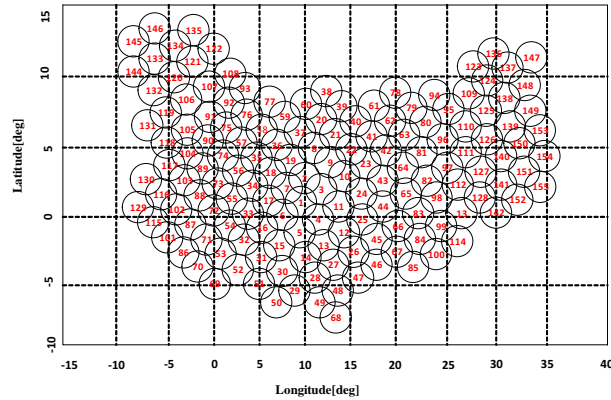
Figure 2.2: Beam pattern on Earth of the base line scenario. Concretely, the contour plot at 3 dBs is presented. It is important to observe the beam overlapping which lead to high interference scenario in case full frequency reuse is carried out without interference mitigation techniques.

also assumed that the user link has a total of 500 MHz available bandwidth. Note that, only atmospheric fading due to rain effect is considered in the user link channel and further refinements of the channel are neglected. Note that this simple characterization is useful for the intended comparisons and it is a general practice in the evaluation of multibeam satellite systems.

The randomness of the channel is due to the user positions which are assumed to be uniformly distributed within the beams. For the sake of completeness, the rest of parameters are collected in Table 2.1.

Recall that, full frequency reuse among beams and noiseless feeder link have been considered in this evaluation. In the sequel, we compute two performance metrics. First, the

SINR for each user, after employing interference mitigation among beams. With that SINR value, the throughput is inferred according to DVB-RCS and DVB-S2 standards for the return and forward links, respectively. Furthermore, the simulation results also provide the associated CDF of SINR, which shows the availability of the user link. In this case, the instantaneous availability indicator for the k-th user is given by

$$A_k = g(\text{SINR}_k) \tag{2.70}$$

which is equal to 0 if the user link is unavailable (i.e, if the instantaneous SINR is lower than that required by the lowest ModCod of Table 2.2 for the return link, i.e. $\text{SINR}_k < 1.7\text{dB}$, and Table 2.3 for the forward link, i.e. $\text{SINR}_k < -2.72\text{dB}$) and is equal to 1 otherwise. We also present the Shannon capacity obtained from the user SINR and assuming that interference is treated as Gaussian noise. This measurement serves us to see the potential of our work independently of the satellite standard modulations and codes both for the forward and return links.

Then, we consider the fairness among beams as an another performance metric. Note that this is of great interest for satellite operators where near to equal achievable data rates per beam are the target. For this purpose, we present the throughput index of dispersion which defines as

$$\text{Index of Dispersion} = \frac{\sigma_{\text{Th}}}{\mu_{\text{Th}}}, \tag{2.71}$$

where σ_{Th} and μ_{Th} correspond to the variance and the mean of the user throughput, respectively. This metric provides an indicator of how the data rates are dispersed with respect to the mean. The larger the index of dispersion is, the less the fairness the system achieves.

For a best practice, as upper bound for the achievable rates we consider only on ground processing at the gateway (i.e. no on board processing) as it is described in [13]. From

the return link point of view, the received signal (2.2), which is based on this on ground scenario, is rewritten as

$$\mathbf{y}_{\text{RL}} = \mathbf{T}^{H}_{\text{on-ground}} \left(\mathbf{H}\mathbf{s} + \mathbf{n} \right), \tag{2.72}$$

where

$$\mathbf{W}_{\text{on-ground}} = \mathbf{H} \left(\mathbf{H}\mathbf{H}^{H} + \mathbf{I}_{K} \right)^{-1} \tag{2.73}$$

denotes the LMMSE detector filter at the gateway. Note that the linear processing is similar to (2.8) but in this case it has been assumed that no beam processing is done. Considering the forward link, the received signal by the user terminals with this on ground technique can be represented as

$$\mathbf{y}_{\text{FL}} = \mathbf{H}^{T} \mathbf{T}_{\text{on-ground}} \mathbf{x} + \mathbf{w}. \tag{2.74}$$

It is important to remind that although larger data rates can be obtained if all the processing is carried out on ground, the required feeder link spectral resources exponentially increase, leading to an inefficient system.

To sum up, in order to test the validity of the derived theoretical results in section IV, we compute the spectral efficiency of the following multibeam satellite system using precoding and detection algorithms for forward and return links respectively:

- $\mathbf{B}$ provided by ESA (reference).

- $\mathbf{B}^{*}$ proposed by this study in Theorem 2.2.

- $\mathbf{B}$ designed in (2.23).

- On ground processing (system upper bound).

- $\widehat{\mathbf{B}}^{*}$ provided by this study in (2.2.6)
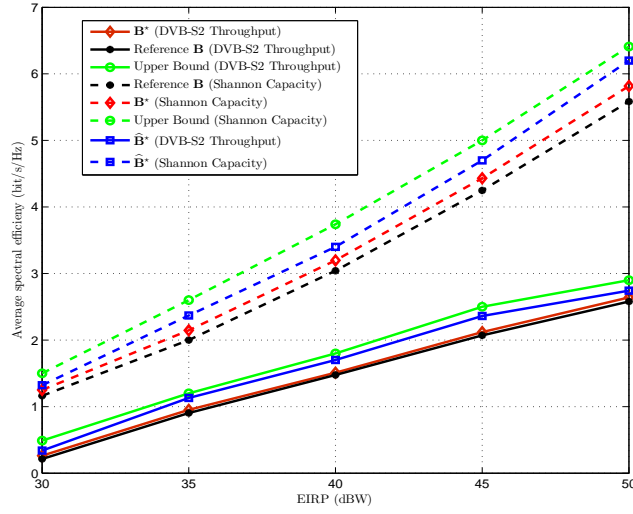
Figure 2.3: Return link throughput values over different user EIRP.
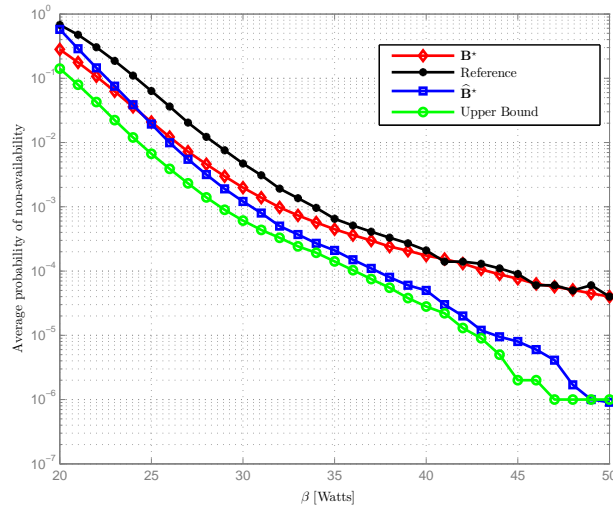
Figure 2.4: Return link non-availability comparison with proposed $\mathbf{B}$ over EIRP .

In the sequel, the results are separated into two different subsections, return and forward link. In this context, the same fixed optimal design of on board beamforming matrix is computed since this optimal design depends on the right eigen vector of channel average matrix, $\bar{\mathbf{H}}$. This is computed empirically considering the aforementioned 1000 channel
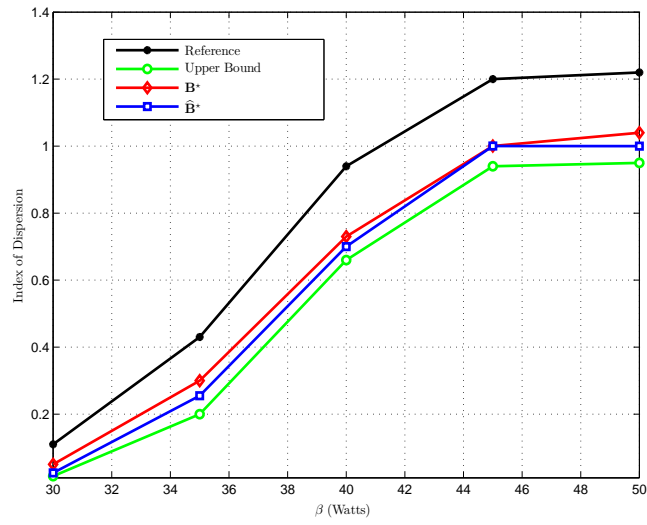
Figure 2.5: Return link throughput index of dispersion.
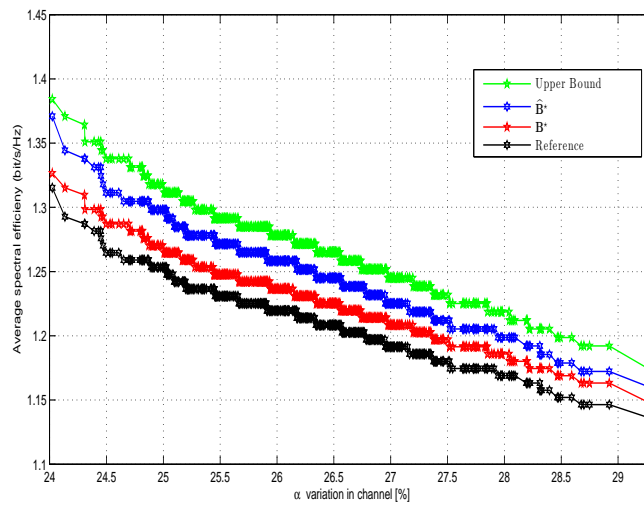
Figure 2.6: Return link throughput with respect to channel variations.

user realizations.
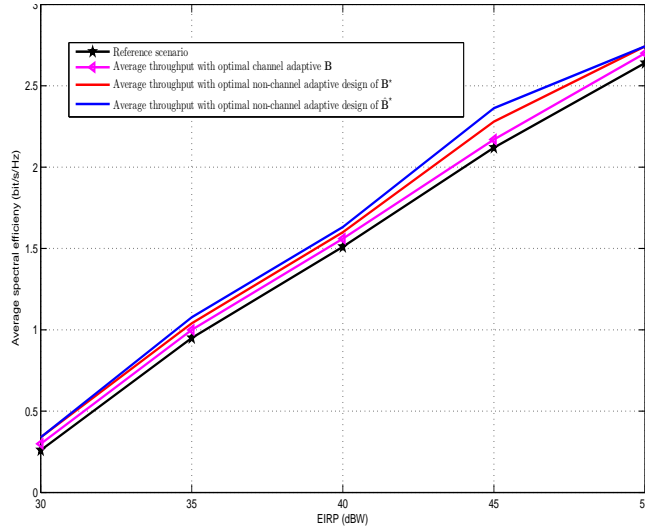
Figure 2.7: Return link throughput comparison based on DVB-RCS with employing **B** channel adaptive and fixed.

2.4.2   Return Link

The return link operates at 30GHz, and is based on DVB-RCS standard [36]. We target a PER of 10^{-7}. Table 2.2 provides a one-to-one relationship between the required received SINR and the spectral efficiency (bits/symbol) achieved by DVB-RCS standard.

Figure 2.3 depicts the evolution of the total average throughput (bits/symbol) as a function of the user EIRP (β) for different scenarios. Although by means of using the DVB-RCS standard the obtained throughput gain is limited when the Shannon capacity is considered, higher gains are obtained with respect to the reference scenario . In other words, other modcods design would improve the benefits of the proposed technique with respect to the reference scenario. Note that the proposed robust design that consider the eigenvector perturbation improves the system throughput with respect to the design that only considers eigenvalue variations. Indeed, our proposal is approaching the upper bound of the on ground design.

The corresponding availability probability is also provided in Figure 2.4. In this case,
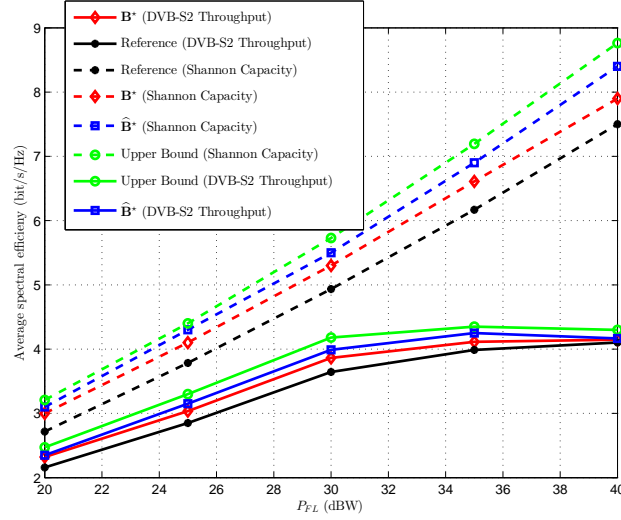
Figure 2.8: Forward link throughput values over P_{FL}= 30 dBW.

our proposal also improves the reference scenario, leading to an increase of the system availability. Remarkably, the fairness among beams is also improved as it is depicted in Figure 2.5. Lower values of dispersion index are obtained with our technique with respect to the reference design.

Finally, we study the impact of the channel variations on the beam processing design. Bearing in mind that α in (2.30) determines this variation, we compute this value and we present its corresponding average throughput values in Figure 2.6. The values of α are selected so that the feasibility of $\mathrm{MSE}_{\mathrm{RL}}$ in (2.9) holds. It implies that

$$(\bar{\boldsymbol{\Sigma}} - \epsilon_H \mathbf{I}_N)_{ii} \geq 0 \qquad \forall i = 1, ..., N. \tag{2.75}$$

For a large value of α the matrix (2.75) might become semidefinite negative and; thus, changes the nature of the problem. In order to avoid this, α has to be checked so that the matrix (2.75) always remains semidefinite positive. It is observed that the larger α values, the less the throughput is obtained due to the channel mismatch.
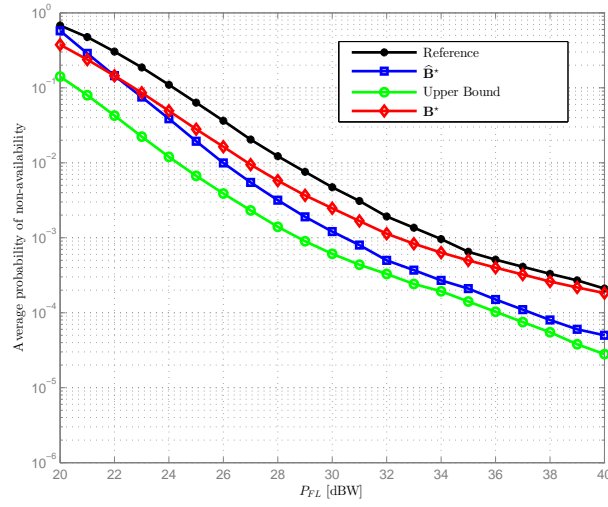
Figure 2.9: Forward link non-availability comparison with proposed $\mathbf{B}$ over P_{FL}.
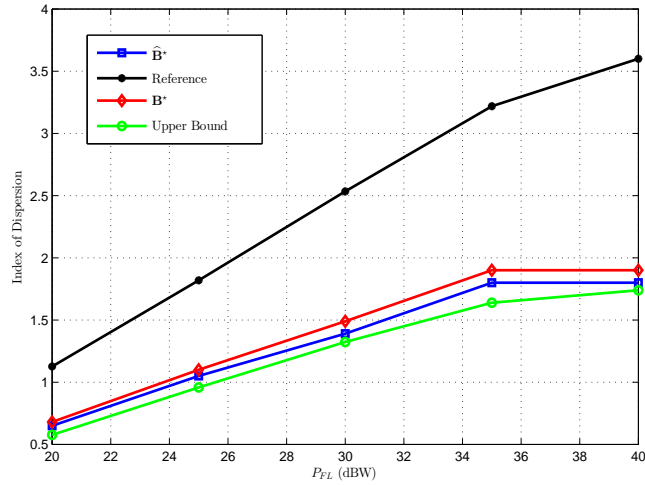
Figure 2.10: Forward link throughput index of dispersion.

For the sake of completeness, Figures 2.7 compares the impact of the channel adaptive and fixed on the beam processing design in the overall system performance.

It is shown that the fixed $\mathbf{B}$ has the lowest achievable rate due to lack of variation at the time instants. Still, the corresponding relative gain of system with the proposed beam
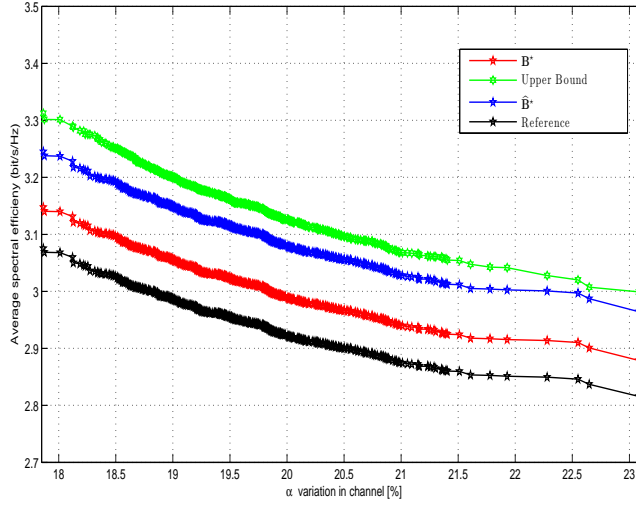
Figure 2.11: Forward link throughput with respect to channel variations.

processings go up to $\mathbf{B}^*$: 9% and $\widehat{\mathbf{B}}^*$: 11.4 % of that of beam generation process provided by ESA. Therefore, our proposals could generate a better tradeoff between complexity and throughput and would be converseable in the next generation hybrid networks.

Eventually, Fig.2.13 shows the corresponding average SINR distribution among users in one channel realization (for a definite available total power). It can be seen that the system with the proposed designs of pre-processing achieves better average SINR distribution ($\mathbf{B}^*$: 2.5 Mb/s and $\widehat{\mathbf{B}}^*$: 3.067 Mb/s) with respect to the reference scenario (2.1 Mb/s). In any case, our proposals perform better than the reference scenario.

2.4.3   Forward Link

The forward link is assumed to operate at 20GHz and is based on DVB-S2 standard with a PER of 10^{-6}. Note that the working points were extrapolated from the PER curves reported in the DVB-S2 guidelines document [36]. Table 2.3 provides a relationship between the required received SINR and the spectral efficiency achieved by DVB-S2 standard.
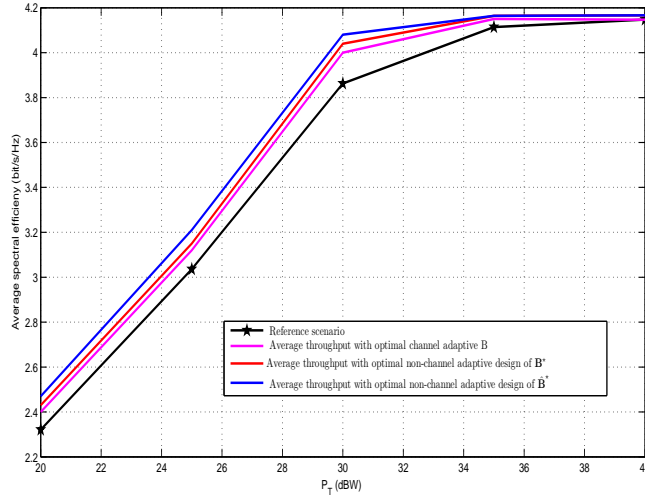
Figure 2.12: Forward link throughput comparison based on DVB-S2 with employing **B** channel adaptive and fixed.

The results are presented for the total bandwidth and as a function of the total available power denoted by P_{FL}. Figure 2.8 depicts the achieved results of spectral efficiency and Figure 2.9 shows the availability of the users in the forward link. Clearly, the proposed techniques perform better than the benchmark system and again the robust design based on the eigenvector perturbations behaves better than the one that only considers the eigenvalues.

The expected result of throughputs in 2.8 is justified by the availability 2.9. In other words, the system with new proposed design of $\widehat{\mathbf{B}}^*$ is closer to upper bound scenario than the reference. Moreover, the impact of channel variations can be observed in Figure 2.11. It is clear that our proposal results in higher throughputs even when the channel variations are high. Remarkably, for the forward link the performance difference is higher than the one obtained in the return link. Note that, similar to the return link, the values of α are selected so that the feasibility of MSE_{FL} in (2.20) is hold.

Finally, the dispersion index among users is analysed and represented in Figure 2.10. For this case, the dispersion values are even higher for the reference scenario and our
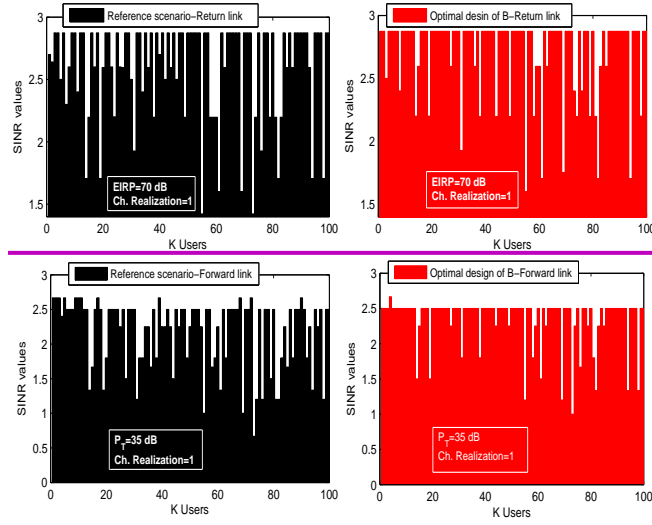
Figure 2.13: Average SINR distribution for one channel realization.

approach leads to higher fairness between beams.

Fig. 2.12 depicts the evolution of the total average throughput as a function of the user total power for both fixed and channel adaptive $\mathbf{B}$ system. It is seen that fixed $\mathbf{B}$ establishes a significant degradation in the average throughput respect to channel adaptive one. Given Figure 2.12, for instance our proposal $\mathbf{B}^*$ (res. can be easily confirmed for $\widehat{\mathbf{B}}^*$) presents an adequate trade off between complexity and throughput where the channel adaptive $\mathbf{B}$ with high complexity (due to channel variation) and fixed $\mathbf{B}$ provided by ESA result a bottleneck in order to design next generation multibeam satellite systems. Finally, similar to the return link, the dispersion index among users is analyzed and represented in Figure 2.10. For this case, the dispersion values are even higher for the reference scenario and our approaches lead to higher fairness between beams.

Moreover, Fig.2.13 depicts the average SINR distribution among users for one channel realization. We are seen that our proposals for $\mathbf{B}$ obtain better average SINR distribution ($\mathbf{B}^*$: 2.31 Mb/s and $\widehat{\mathbf{B}}^*$: 3.92 %) respect to the reference scenario (1.80 Mb/s). In any

case, our proposals perform better than the reference scenario.
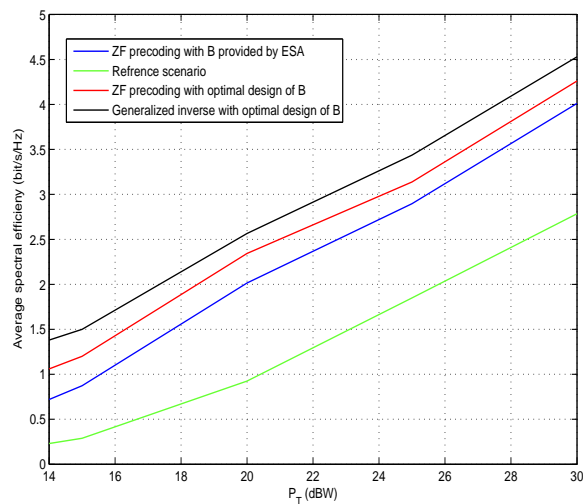
Figure 2.14: Generalized inverse precoding based on per feed power optimization: Throughput.
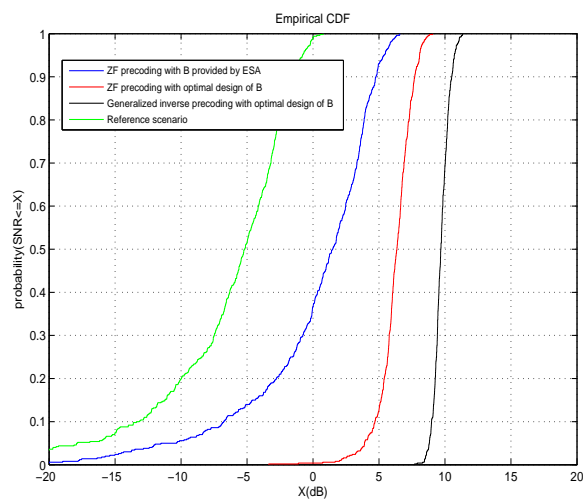
Figure 2.15: Generalized inverse precoding based on per feed power optimization: Availability.
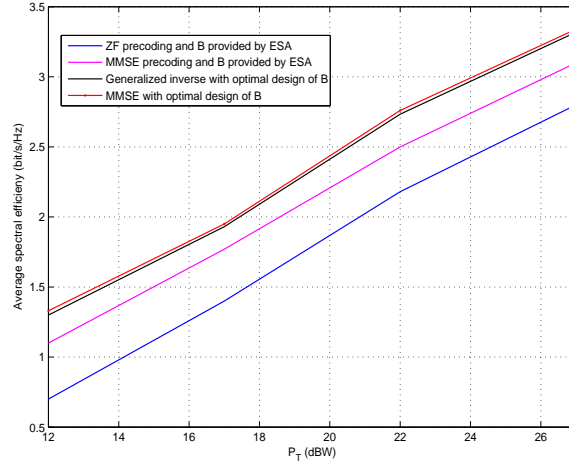
Figure 2.16: Generalized inverse precoding and MMSE comparison: Throughput.

2.4.4   The space/ground architecture under per-feed power constraint

This section presents further compare the performance of the proposed interference mitigation technique and beam generation process scheme in section 2.3. The features of the chosen reference scenario are:

1. Fixed on board beamforming $\mathbf{B}$ provided by ESA with a LMMSE precoder

2. Fixed on board beamforming $\mathbf{B}$ provided by ESA with a linear ZF precoder

3. Fixed on board beamforming $\mathbf{B}$ provided by this study in (2.69) with generalized inverse precoder

4. Fixed on board beamforming $\mathbf{B}$ provided by this study in (2.69) with a LMMSE precoder

Fig. 2.14 depicts performance in terms of average throughput as a function of P_T/P_{FL}. For instance, at $P_{FL}/P_T = 30$ dBW the corresponding relative gain for new design in (2.69) goes up to 11% of that of ESA provided $\mathbf{B}$. Moreover, the corresponding CDF of

the SINR is provided in Figure 2.15. It shows the availability condition of users is also improved by novel proposed hybrid architecture.

As it is seen in Fig.2.16 the MMSE and generalized inverse precoding technique are almost same results. But, the important benefit of proposed generalized inverse precoding technique is to better interference rejection (same as ZF precoder) rather than MMSE precoder that is not able to do this. Moreover, this method save the power of the signals as a MMSE precoder.

2.5   Appendix

2.5.1   Proof of equality (2.26)

This Appendix presents the following property

$$\text{trace}(\mathbf{I}_K + \mathbf{A}^H\mathbf{A})^{-1} = \text{trace}(\mathbf{I}_K + \mathbf{A}\mathbf{A}^H)^{-1} \tag{2.76}$$

By employing the conversion lemma in [34, sec.3.2.3], the left hand side of the equality (2.76) can be rewritten as follows

$$\text{trace}(\mathbf{I}_K + \mathbf{A}^H\mathbf{A})^{-1} = \text{trace}(\mathbf{I}_K) - \text{trace}[\mathbf{A}^H(\mathbf{I}_K + \mathbf{A}\mathbf{A}^H)^{-1}\mathbf{A}]$$

$$= \text{trace}(\mathbf{I}_K) - \text{trace}[\mathbf{A}\mathbf{A}^H(\mathbf{I}_K + \mathbf{A}\mathbf{A}^H)^{-1}]$$

$$= \text{trace}[\mathbf{I}_K - \mathbf{A}\mathbf{A}^H(\mathbf{I}_K + \mathbf{A}\mathbf{A}^H)^{-1}] \tag{2.77}$$

With the following property $\mathbf{I}_K = (\mathbf{I}_K + \mathbf{A}\mathbf{A}^H)(\mathbf{I}_K + \mathbf{A}\mathbf{A}^H)^{-1}$, (2.77) can be rewritten as follows

$$\text{trace}[(\mathbf{I}_K + \mathbf{A}\mathbf{A}^H)(\mathbf{I}_K + \mathbf{A}\mathbf{A}^H)^{-1} - \mathbf{A}\mathbf{A}^H(\mathbf{I}_K + \mathbf{A}^H\mathbf{A})^{-1}]$$

$$. \qquad\qquad = \text{trace}[\left(\mathbf{I}_K + \mathbf{A}\mathbf{A}^H - \mathbf{A}\mathbf{A}^H\right)(\mathbf{I}_K + \mathbf{A}\mathbf{A}^H)^{-1}]$$

$$= \text{trace}(\mathbf{I}_K + \mathbf{A}\mathbf{A}^H)^{-1} \tag{2.78}$$

Thus the equality is obtained.

2.5.2   The proof of inequality (2.29)

This Appendix deals finding the upper bound of SMSE_{RL} in (2.29) which is expressed as

$$(\mathbf{I}_K + \mathbf{B}\mathbf{Z}\mathbf{B}^H)^{-1} \leq (\mathbf{I}_K + \mathbf{B}\check{\mathbf{Z}}\mathbf{B}^H)^{-1} \tag{2.79}$$

where $\check{\mathbf{Z}}$ is defined in (2.30).

First, for any rectangular matrices $\mathbf{X}$ of size $N \times M$ and $\mathbf{Y}$ of size $N \times M$, the authors in [22, Lemma 7.1] have proved that

$$\mathbf{X}\mathbf{Y}^H + \mathbf{Y}\mathbf{X}^H \leq 2\sigma_{\max}(\mathbf{X})\sigma_{\max}(\mathbf{Y})\mathbf{I}_N \tag{2.80}$$

And,

$$\mathbf{X}\mathbf{X}^H \leq \lambda_{\max}(\mathbf{X}\mathbf{X}^H)\mathbf{I}_N \tag{2.81}$$

where $\sigma_{\max}(.)$ and $\lambda_{\max}(.)$ denote the maximum singular value and eigen value of respective matrix, respectively.

With the presented channel decomposition in (2.24), $\mathbf{Z}$ can be defined again as follows

$$\mathbf{Z} = \mathbf{H}\mathbf{H}^H \triangleq \mathbf{Z}_H + \mathbf{Z}_\Delta \tag{2.82}$$

where

$$\mathbf{Z}_H \triangleq \bar{\mathbf{H}}\bar{\mathbf{H}}^H$$

$$\mathbf{Z}_\Delta \triangleq \bar{\mathbf{H}}\boldsymbol{\Delta}^H + \boldsymbol{\Delta}\bar{\mathbf{H}}^H + \boldsymbol{\Delta}\boldsymbol{\Delta}^H \tag{2.83}$$

By employing (2.80) and (2.81), $\mathbf{R}_\Delta$ is bounded as

$$|\lambda_i(\mathbf{Z}_\Delta)| \leq 2\alpha\sigma_{\max}(\bar{\mathbf{H}}) + \alpha^2 \tag{2.84}$$

where $\lambda_i(.)$ represents the i-th eigen value of respective matrix. Remind that we assumed $||\mathbf{\Delta}|| = \sigma_{\max}(\mathbf{\Delta}) = \sqrt{\lambda_{\max}(\mathbf{\Delta}\mathbf{\Delta}^H)} \leq \alpha$.

Since $\alpha << \sigma_{\max}(\bar{\mathbf{H}})$, the expression (2.84) can be reduce to

$$|\lambda_i(\mathbf{Z}_\Delta)| \leq \epsilon_H \tag{2.85}$$

where $\epsilon_H \triangleq 2\alpha\sigma_{\max}(\bar{\mathbf{H}})$. By employing the following eigen value decomposition $\mathbf{Z}_H = \bar{\mathbf{L}}\bar{\mathbf{\Sigma}}\bar{\mathbf{L}}^H$, the eigen values of $\mathbf{Z}$ in (2.82) can be shown to be lower bounded as

$$\lambda_{min}(\mathbf{Z}_H + \mathbf{Z}_\Delta) \leq \lambda_{min}(\mathbf{Z}_H - \epsilon_H)^+ \tag{2.86}$$

$$\vdots$$

$$\lambda_i(\mathbf{Z}_H + \mathbf{Z}_\Delta) \leq \lambda_i(\mathbf{Z}_H - \epsilon_H)^+ \tag{2.87}$$

$$\vdots$$

$$\lambda_1(\mathbf{Z}_H + \mathbf{Z}_\Delta) \leq \lambda_1(\mathbf{Z}_H - \epsilon_H)^+ \tag{2.88}$$

where $\lambda_i(.)$ represents the i-th eigen value of matrix $\bar{\mathbf{\Sigma}}$ in decreasing order. Thus, (2.86)-(2.88) implies that

$$\mathbf{Z} \geq \breve{\mathbf{Z}} \triangleq \bar{\mathbf{L}}(\bar{\mathbf{\Sigma}} - \epsilon_H\mathbf{I}_N)^+\bar{\mathbf{L}}^H \tag{2.89}$$

Finally, the lower of $\mathbf{Z}$ in (2.89) implies the following upper bound (i.e. worst case) on the $\mathbf{MSE}_{\mathrm{RL}}$:

$$\mathbf{E} \leq (\mathbf{I}_K + \mathbf{B}\breve{\mathbf{Z}}\mathbf{B}^H)^{-1} \tag{2.90}$$

where $\mathbf{E} \triangleq (\mathbf{I}_K + \mathbf{B}\mathbf{Z}\mathbf{B}^H)^{-1}$. Therefore, worst case (upper bound) can be obtained in practice by using the lower bound $\breve{\mathbf{Z}}$ in lieu $\mathbf{Z}$. It implies that this upper bound is obtained by slightly decreasing the eigenvalues of the squared whitened channel matrix.

2.5.3 Proof of the Theorem 2.2

The goal is to prove, the proposed optimal design of $\mathbf{B}$ in (2.32) can be minimize the upper-bound of SMSE_{RL} in (2.31). First, by employing the eigenvalue decomposition of $\check{\mathbf{Z}}$ in (2.30), problem (2.31) can be rewritten as

$$\min_{\mathbf{M}_{RL}} \quad \text{trace}(\mathbf{I}_K + \mathbf{M}_{RL}\mathbf{D}_{RL}\mathbf{M}_{RL}^H)^{-1} \tag{2.91}$$

$$s.t. \qquad \mathbf{M}_{RL}\mathbf{M}_{RL}^H = \mathbf{I}_K$$

with the following definitions

$$\mathbf{M}_{RL} \triangleq \mathbf{B}\bar{\mathbf{L}} \tag{2.92}$$

and,

$$\mathbf{D}_{RL} \triangleq (\bar{\boldsymbol{\Sigma}} - \epsilon_H \mathbf{I}_N)^+ = \begin{pmatrix} (\bar{\boldsymbol{\Sigma}}_{1:K} - \epsilon_H \mathbf{I}_K)^+ & \mathbf{0}_{K \times (N-K)} \\ \mathbf{0}_{(N-K) \times K} & \mathbf{0}_{(N-K) \times (N-K)} \end{pmatrix}$$

$$\tag{2.93}$$

where $\bar{\boldsymbol{\Sigma}}$ has only K non-zero eigenvalues, as $\bar{\mathbf{H}}\bar{\mathbf{H}}^H$ has rank equal to K. Actually, the problem (2.91) can be written as

$$\min_{\mathbf{M}_{RL}} \quad \sum_{i=1}^{K} \frac{1}{1 + \lambda_i\left(\mathbf{M}_{RL}\mathbf{D}_{RL}\mathbf{M}_{RL}^H\right)} \tag{2.94}$$

$$s.t. \qquad \mathbf{M}_{RL}\mathbf{M}_{RL}^H = \mathbf{I}_K$$

where $\lambda_i(.)$ denotes the i-th largest eigenvalue of the respective matrix. Obviously, $\mathbf{MDM}^H$ is a hermitian matrix whose eigenvalues are always positive. Then, it follows that

$$g(\lambda_i) = \frac{1}{1 + \lambda_i\left(\mathbf{M}_{RL}\mathbf{D}_{RL}\mathbf{M}_{RL}^H\right)} \qquad i = 1, ..., K \tag{2.95}$$

is convex function on $\lambda_i(\mathbf{M}_{RL}\mathbf{D}_{RL}\mathbf{M}_{RL}^H)$. By using the theorem 3.C.1 in [37], we have that

$$\phi(\boldsymbol{\lambda}) = \sum_{i=1}^{K} \frac{1}{1 + \lambda_i\left(\mathbf{M}_{RL}\mathbf{D}_{RL}\mathbf{M}_{RL}^H\right)} = \sum_{i=1}^{K} g\left(\lambda_i(\mathbf{M}_{RL}\mathbf{D}_{RL}\mathbf{M}_{RL}^H)\right) \qquad (2.96)$$

where $\boldsymbol{\lambda} = \left(\lambda_1(\mathbf{M}_{RL}\mathbf{D}_{RL}\mathbf{M}_{RL}^H), ..., \lambda_K(\mathbf{M}_{RL}\mathbf{D}_{RL}\mathbf{M}_{RL}^H)\right)^T$, and $\phi(.)$ is a schur-convex function operator. On other hand, the theorem B.1 in [37] proved that

$$\mathbf{d} \prec \boldsymbol{\lambda} \qquad (2.97)$$

where $\mathbf{d}$ denotes $K{\times}1$ vector formed by the diagonal elements of the matrix $\mathbf{M}_{RL}\mathbf{D}_{RL}\mathbf{M}_{RL}^H$, i.e. $\mathbf{d} = \left(d_1(\mathbf{M}_{RL}\mathbf{D}_{RL}\mathbf{M}_{RL}^H), ..., d_K(\mathbf{M}_{RL}\mathbf{D}_{RL}\mathbf{M}_{RL}^H)\right)^T$. Finally, combining of (2.97) with the schur convexity of $\phi(.)$, we have that $\phi(\mathbf{d}) \leq \phi(\boldsymbol{\lambda})$, i.e.

$$\sum_{i=1}^{K} \frac{1}{1 + d_i\left(\mathbf{M}_{RL}\mathbf{D}_{RL}\mathbf{M}_{RL}^H\right)} \leq \sum_{i=1}^{K} \frac{1}{1 + \lambda_i\left(\mathbf{M}_{RL}\mathbf{D}_{RL}\mathbf{M}_{RL}^H\right)}. \qquad (2.98)$$

Moreover, the equality in (2.98) is reached whenever $\mathbf{M}_{RL}\mathbf{D}_{RL}\mathbf{M}_{RL}^H$ is diagonal. To this end, it is clear that $\mathbf{M}$ has to be diagonal such that

$$\mathbf{M}_{RL} = [\mathbf{I}_K \qquad \mathbf{0}_{K\times(N-K)}] \qquad (2.99)$$

Given (2.92), it implies that $\mathbf{B}$ has to be made of the K first rows of the matrix $\bar{\mathbf{L}}^H$, that is

$$\mathbf{B} = \bar{\mathbf{L}}_{1:K}^H \qquad (2.100)$$

and concludes the proof.

2.5.4 Proof of the Theorem 2.2.6

This Appendix deals finding the upper bound of SMSE_{RL} in (2.29) which is expressed as

$$(\mathbf{I}_K + \mathbf{B}\mathbf{Z}\mathbf{B}^H)^{-1} \le (\mathbf{I}_K + \mathbf{B}\breve{\mathbf{Z}}\mathbf{B}^H)^{-1}, \tag{2.101}$$

where $\breve{\mathbf{Z}}$ is defined in (2.30).

First, for any rectangular matrices $\mathbf{X}$ of size $N \times M$ and $\mathbf{Y}$ of size $N \times M$, the authors in [22, Lemma 7.1] have proved that

$$\mathbf{X}\mathbf{Y}^H + \mathbf{Y}\mathbf{X}^H \le 2\delta_{\max}(\mathbf{X})\delta_{\max}(\mathbf{Y})\mathbf{I}_N. \tag{2.102}$$

And,

$$\mathbf{X}\mathbf{X}^H \le \lambda_{\max}(\mathbf{X}\mathbf{X}^H)\mathbf{I}_N, \tag{2.103}$$

where $\lambda_{\max}(.)$ denotes the maximum eigen value of the respective matrix. With the presented channel decomposition in (2.24), $\mathbf{Z}$ can be defined again as follows

$$\mathbf{Z} = \bar{\mathbf{Z}} + \Delta\mathbf{Z}, \tag{2.104}$$

where $\bar{\mathbf{Z}} = \bar{\mathbf{H}}\bar{\mathbf{H}}^H$ and

$$\Delta\mathbf{Z} = \bar{\mathbf{H}}\Delta^H + \Delta\bar{\mathbf{H}}^H + \Delta\Delta^H, \tag{2.105}$$

By employing (2.102) and (2.103), $\mathbf{R}_\Delta$ is bounded as

$$|\lambda_i(\Delta\mathbf{Z})| \le 2\alpha\sigma_{\max}(\bar{\mathbf{H}}) + \alpha^2, \tag{2.106}$$

where $\lambda_i(.)$ represents the i-th eigen value of respective matrix. Remind that we assumed $||\Delta|| = \sigma_{\max}(\Delta) = \sqrt{\lambda_{\max}(\Delta\Delta^H)} \le \alpha$. Since $\alpha << \sigma_{\max}(\bar{\mathbf{H}})$, the expression (2.106)

can be reduce to

$$|\lambda_i(\Delta \mathbf{Z})| \le \epsilon_H, \tag{2.107}$$

where $\epsilon_H \triangleq 2\alpha \sigma_{\max}(\bar{\mathbf{H}})$. By employing the following eigen value decomposition $\mathbf{Z}_H = \bar{\mathbf{L}}\bar{\mathbf{\Sigma}}\bar{\mathbf{L}}^H$, the eigen values of $\mathbf{Z}$ in (2.104) can be shown to be lower bounded as

$$\lambda_{min}(\bar{\mathbf{Z}} + \Delta \mathbf{Z}) \le \lambda_{min}(\bar{\mathbf{Z}} - \epsilon_H)^+, \tag{2.108}$$

$$\vdots$$

$$\lambda_i(\bar{\mathbf{Z}} + \Delta \mathbf{Z}) \le \lambda_i(\bar{\mathbf{Z}} - \epsilon_H)^+,$$

$$\vdots$$

$$\lambda_1(\bar{\mathbf{Z}} + \Delta \mathbf{Z}) \le \lambda_1(\bar{\mathbf{Z}} - \epsilon_H)^+,$$

where $\lambda_i(.)$ represents the i-th eigen value of matrix $\bar{\mathbf{\Sigma}}$ in decreasing order. Thus, (2.108) implies that

$$\mathbf{Z} \le \breve{\mathbf{Z}} \triangleq \bar{\mathbf{L}}(\bar{\mathbf{\Sigma}} - \epsilon_H \mathbf{I}_N)^+ \bar{\mathbf{L}}^H. \tag{2.109}$$

Note that, the operator $()^+$ is included for mathematical rigorousness but; however, it is expected that the system designer uses a value of α so that the diagonal entries of

$$\bar{\mathbf{\Sigma}} - \epsilon_H \mathbf{I}_N, \tag{2.110}$$

are positive. Otherwise, the upper bound will lead to a low rank solution which is an inappropriate relaxation.Finally, the lower of $\mathbf{Z}$ in (2.109) implies the following upper

bound (i.e. worst case) on the $\mathbf{MSE}_{\mathrm{RL}}$:

$$\mathbf{E} \le (\mathbf{I}_K + \mathbf{B}\breve{\mathbf{Z}}\mathbf{B}^H)^{-1}, \tag{2.111}$$

where $\mathbf{E} \triangleq (\mathbf{I}_K + \mathbf{B}\mathbf{Z}\mathbf{B}^H)^{-1}$. Therefore, worst case (upper bound) can be obtained in practice by using the lower bound $\breve{\mathbf{Z}}$ in lieu $\mathbf{Z}$. It implies that this upper bound is obtained by slightly decreasing the eigenvalues of the squared whitened channel matrix.

2.5.5   Proof of the Theorem 2.4

The goal is to prove

$$\mathrm{trace}[\mathbf{B}^\star(\mathbf{B}^{\star,H}\mathbf{H}^H\mathbf{H}\mathbf{B}^\star)^{-1}\mathbf{B}^{\star,H}] \le \mathrm{trace}[\mathbf{B}(\mathbf{B}^H\mathbf{H}^H\mathbf{H}\mathbf{B})^{-1}\mathbf{B}^H] \tag{2.112}$$

First, with the following SVD of the channel matrix $\mathbf{H} = \mathbf{U}\boldsymbol{\Phi}\mathbf{V}^H$, let us simplify the left-hand side of (2.112) thanks to the definition of $\mathbf{B}^\star$ in (2.65) as follows

$$\mathrm{trace}(\mathbf{F}^H\mathbf{F})^{-1} = \sum_{k=1}^{K} \frac{1}{\lambda_k(\mathbf{F}^H\mathbf{F})} \tag{2.113}$$

where $\mathbf{F} \triangleq \boldsymbol{\Phi}_{1:K}$ such that $\boldsymbol{\Phi}_{1:K}$ denotes the K columns of matrix $\boldsymbol{\Phi}$. Moreover, $\lambda_k(.)$ denotes the k-th largest eigenvalue of respective matrix.

Similarly, with $\mathbf{B} = \mathbf{M}\boldsymbol{\Sigma}\mathbf{L}^H$, the right-hand side in (2.112) can be worked out as

$$\mathrm{trace}[\mathbf{B}(\mathbf{B}^H\mathbf{H}^H\mathbf{H}\mathbf{B})^{-1}\mathbf{B}^H] = \mathrm{trace}[(\mathbf{A}_1^H\mathbf{A}_1)^{-1}(\mathbf{F}^H\mathbf{F})^{-1}] = \sum_{k=1}^{K} \frac{1}{\lambda_k\big((\mathbf{A}_1^H\mathbf{A}_1)(\mathbf{F}^H\mathbf{F})\big)} \tag{2.114}$$

where $\mathbf{A}_1$ is defined as follows

$$\mathbf{A} \triangleq \mathbf{M}^H\mathbf{V} = \begin{pmatrix} \mathbf{A}_1 & \mathbf{A}_2 \\ \mathbf{A}_3 & \mathbf{A}_4 \end{pmatrix} \tag{2.115}$$

with the submatrix $\mathbf{A}_1$ is of size $K \times K$. Moreover, $\mathbf{A}_2$ and $\mathbf{A}_3^H$ both are submatrices

of size $K \times (N - K)$, and submatrix $\mathbf{A}_4$ is of size $(N - K) \times (N - k)$.

By using the theorem H.1.g in [37], we have that

$$\lambda_k\left((\mathbf{A}_1^H \mathbf{A}_1)(\mathbf{F}^H \mathbf{F})\right) \leq \lambda_k(\mathbf{A}_1^H \mathbf{A}_1)\lambda_k(\mathbf{F}^H \mathbf{F}) \leq \lambda_k(\mathbf{F}^H \mathbf{F}) \qquad (2.116)$$

Now, we have to realize that

$$\lambda_k(\mathbf{A}_1^H \mathbf{A}_1) \leq 1, \qquad k = 1, ..., K. \qquad (2.117)$$

In fact, $\mathbf{A}$ is a unitary matrix such that $\mathbf{A}^H \mathbf{A} = \mathbf{I}_K$. It implies that

$$\mathbf{A}_1^H \mathbf{A}_1 + \mathbf{A}_3^H \mathbf{A}_3 = \mathbf{I}_K. \qquad (2.118)$$

with the following eigenvalue decomposition $\mathbf{A}_1^H \mathbf{A}_1 = \mathbf{S}\boldsymbol{\Psi}\mathbf{S}^H$, (2.118) can be rewritten

as

$$\boldsymbol{\Psi} = \mathbf{S}^H \mathbf{I}_K \mathbf{S} - \mathbf{S}^H \mathbf{A}_3^H \mathbf{A}_3 \mathbf{S} \qquad (2.119)$$

where $\boldsymbol{\Psi} = diag\left(\lambda_1(\mathbf{A}_1^H \mathbf{A}_1), ..., \lambda_K(\mathbf{A}_1^H \mathbf{A}_1)\right)$.

It is clear that $\mathbf{S}^H \mathbf{A}_3^H \mathbf{A}_3 \mathbf{S}$ has to be diagonal. Moreover, since $\mathbf{A}_3^H \mathbf{A}_3$ is semi positive

definite, it has to have positive elements on the diagonal which proves (2.117). Even-

tually, due to (2.116) follows from (2.117), the inequality in (2.112) is also justified and

concludes the proof.

2.5.6   Proof of inequality 2.68

This Appendix deals finding the following inequality

$$\text{trace}\left(\mathbf{B}\left(\mathbf{B}^H \mathbf{R}\mathbf{B}\right)^{-1}\mathbf{B}^H\right) \leq \text{trace}\left(\mathbf{B}\left(\mathbf{B}^H \breve{\mathbf{R}}\mathbf{B}\right)^{-1}\mathbf{B}^H\right) \qquad (2.120)$$

With the channel decomposition in (2.24), $\mathbf{R}$ can be defined again as follows

$$\mathbf{R} = \mathbf{H}^H \mathbf{H} \triangleq \mathbf{R}_H + \mathbf{R}_\Delta \qquad (2.121)$$

where

$$\mathbf{R}_H \triangleq \bar{\mathbf{H}}^H \bar{\mathbf{H}}$$

$$\mathbf{R}_\Delta \triangleq \bar{\mathbf{H}}^H \boldsymbol{\Delta} + \boldsymbol{\Delta}^H \bar{\mathbf{H}} + \boldsymbol{\Delta}^H \boldsymbol{\Delta} \qquad (2.122)$$

By employing (2.80) and (2.81), $\mathbf{R}_\Delta$ is bounded as

$$|\lambda_i(\mathbf{R}_\Delta)| \leq 2\alpha\sigma_{\max}(\bar{\mathbf{H}}_u) + \alpha \qquad (2.123)$$

where $\lambda_i(.)$ represents the i-th eigen value of respective matrix. In fact, when $\alpha \leq \sigma_{\max}(\bar{\mathbf{H}})$, (2.123) can be rewritten as

$$|\lambda_i(\mathbf{R}_\Delta)| \leq \epsilon_H \qquad (2.124)$$

where $\epsilon_H \triangleq 2\alpha\sigma_{\max}(\bar{\mathbf{H}})$. By using the following eigen value decomposition $\mathbf{R}_H = \mathbf{U}_H \boldsymbol{\Sigma}_H \mathbf{U}_H^H$, the eigen values of $\mathbf{R}$ in (2.121) can be lower bounded as

$$\lambda_i(\mathbf{R}_H + \mathbf{R}_\Delta) \leq \lambda(\mathbf{R}_H - \epsilon_H)^+ \qquad \forall \ i = 1, ..., K_m \qquad (2.125)$$

Thus, (2.125) implies that

$$\text{trace}(\mathbf{R}) \leq \breve{\mathbf{R}} \triangleq \text{trace}\left(\mathbf{U}_H(\boldsymbol{\Sigma}_H - \epsilon_H \mathbf{I}_N)^+ \mathbf{U}_H^H\right) \qquad (2.126)$$

Therefore, by assuming the same effect of $\mathbf{B}$ in both side of inequality (2.120), the lower

bound of $\mathbf{R}$ in (2.126) implies the following upper bound (i.e. worst case)

$$\text{trace}\left(\mathbf{B}\left(\mathbf{B}^H\mathbf{R}\mathbf{B}\right)^{-1}\mathbf{B}^H\right) \leq \text{trace}\left(\mathbf{B}\left(\mathbf{B}^H\breve{\mathbf{R}}\mathbf{B}\right)^{-1}\mathbf{B}^H\right) \qquad (2.127)$$

Indeed, a worst case (upper bound) can be obtained in practice by using the lower bound $\breve{\mathbf{R}}$ in lieu $\mathbf{R}$.

2.5.7   Simulation parameters, DVB-RCS2 and DVB-S2 MODCOD parameters tables

Table 2.1: Simulation parameters

Link	Title	Description
Both link common parameters	Satellite height	35786 km (GEO)
	Satellite longitude, latitude	$10°East, 0°$
	Earth radius	6378.137 Km
	Feed radiation pattern	Provided by ESA
	Number of feeds N	155
	beamforming matrix $\mathbf{B}$	Provided by ESA
	Number of cells/beams	100
	Total bandwidth	500 MHz
	Number of carriers M	12
	Roll-off factor	0.25
	Atmospheric fading	Just rain fading
Return link	Frequency	30×10^9Hz
	Receiver noise temperature	517 K
Forward link	Frequency	20×10^9Hz
	user antenna gain	41.7 dBi
	clear sky gain	17.68 dB/K

Table 2.2: DVB-RCS2 MODCOD parameters

ModCod mode	Efficiency Info bit / symbol	Required SINR [dB] (with approx. impl. losses)
QPSK_13	0.563	1.7
QPSK_12	0.874	4
QPSK_23	1.259	5.9
QPSK_34	1.422	7
QPSK_56	1.600	8.3
8PSK_23	1.704	9.9
8PSK_34	1.926	11.5
8PSK_56	2.197	13.1
16QAM_34	2.593	13.7
16QAM_56	2.874	15.2

Table 2.3: DVB-S2 MODCOD parameters

ModCod mode	Efficiency Info bit / symbol	Required SINR [dB] (with approx. impl. losses)
QPSK_14	0.5	-2.72
QPSK_13	2/3	-1.52
QPSK_12	1	0.73
QPSK_35	1.2	1.93
QPSK_23	4/3	2.83
QPSK_34	1.5	3.78
QPSK_56	5/3	4.83
8PSK_35	1.8	5.33
8PSK_23	2	6.43
8PSK_34	2.25	7.63
16APSK_23	8/3	9.95
16APSK_34	3	11.20
16APSK_45	3.2	12.05
16APSK_56	10/3	12.60
32APSK_34	3.75	14.58
32APSK_45	4	15.08
32APSK_56	25/6	16.18

Chapter 3

Precoding in multiple gateway transmission

This chapter investigates the forward link of a multigateway multibeam satellite system with multiple feeds per beam. In these systems, each gateway serves a set of beams (cluster) so that the overall data traffic is generated at different geographical areas. Full frequency reuse among beams is considered so that interference mitigation techniques are mandatory.

3.1 System overview

Bearing in mind the results of the previous chapter where it is evident that the fixed payload processing decreases the achievable rates, this chapter focuses on the multiple gateway architecture. With this scheme, each gateway can get benefited from reusing the available feeder link bandwidth which offers a more robust communication.

Some additional benefits of multiple gateway architecture include:

- Each gateway handles a smaller number of beams which implies to reduce signal processing complexity.

- In case of failing one gateway, traffic can be rerouted through other gateways to avoid service outage. Thus, this architecture leads to drastically increase the performance in terms of efficiently and reliability.

- Redundancy in case of failure and shorter distribution network loops.

- Content distributors (e.g. media companies, data centers) can be geographically distributed and thus multiple gateways could reduce the amount of backhauling to a single gateway.

It is also important to remark that in a conventional coloring scheme (i.e. using different frequency band among adjacent beams), multiple gateways do not seriously affect the transmission techniques since each beam is still individually processed, but under full frequency reuse multiple gateways create intra-system interference and limit the potential of multibeam processing [5]. Under this context, the multibeam precoding techniques (in the forward link) and multiuser detector (in the return link) shall be reconsidered since the data is separated among the gateways. The following points are necessary to consider in multiple gateway architectures:

First, since the data traffic is independently generated at each gateway, every gateway must precode the signal in a decentralized fashion and transmit through their corresponding feeder link. In other words, the overall precoding matrix is distributively computed at each gateway so that each gateway can only use certain feed elements. In fact, it implies reducing signal processing complexity and increasing the reliability of the transmission mechanism.

Second, since precoding is sensitive to channel CSI quality, computing the precoding matrix in each gateway requires CSI from other gateways which leads to to large system resources overhead.

Let us focus on the forward link of a multiple gateway multibeam satellite system. In contrast to previous works, this work studies the case where the collaboration between

the different gateways is reduced. The authors in [5] propose conventional LMMSE precoding with a power optimization scheme so that a single feed per beam is optimized. Whereas, our proposal does not consider any power allocation and it considers the multiple feed per beam structure. In addition, [38] presents a first approach to this problem where the precoding was able to block completely the inter-cluster interference which is not feasible in general satellite communication systems. Using the same argument, the authors in [39] proposed a modification of the precoding technique in [38] under per feed power constraints.

Among this chapter some unexplored aspects of multiple gateway multibeam precoding are also investigated. First, the tentative impact of the interference among different feeder links is considered. Concretely, the effect on the MSE is investigated and it results that whenever there is interference, the sum of MSE is increased. Then, aiming at decreasing the amount of information which must be necessarly exchanged, the limited cooperation among gateways is considered and a matrix compression is provided which shows a good throughput performance.

Finally, the impact of imperfect CSI is evaluated considering the current standard DVB-S2x.

To summarize, the contribution of this chapter are:

- A precoding technique for multiple gateway architecture where the transmit data and CSI is distributed among gateways. We consider two scenarios in order to design precoder

  - Full CSI is available at each gateway

  - Partial CSI exchanging among gateways via employing an optic line connection.

- The feeder link interference is studied and the MSE is characterized under this effect. It is shown both numerically and analytically that the system performance is

reduced severally whenever this interference occurs even though precoding reverts this additional interference.

- A proposal for reducing the communication overhead between gateways is presented.

- The effect of limited feedback from the users and among gateways is evaluated assuming the latest standard for broadband satellite communications.

3.1.1   Signal model

Consider the forward link of multibeam system which is detailed in section 2.2.1.2. Basically, for individual on ground processing this signal model can be easily obtained by setting $\mathbf{B}$ in (2.4) to be identical (i.e. aiming to employing non on board and only on ground processing) such that

$$\mathbf{y}_{\text{FL}} = \mathbf{HTc} + \mathbf{n} \tag{3.1}$$

where $\mathbf{y}_{FL}$ is $K \times 1$ vector contains the symbols received by each user. $K \times 1$ vector $\mathbf{c}$ denotes the stack of the transmitted signals at all feeds. The $K \times 1$ vector $\mathbf{n}$ contains the stack of zero mean unit variance AWGN such that $\mathrm{E}\{\mathbf{nn}^H\} = \mathbf{I}_K$. The vector $\mathbf{c}$ is the transmit symbol vector such that the k-th entry of $\mathbf{c}$ is the constellation symbol destined to the k-th user with $\mathrm{E}\{\mathbf{cc}^H\} = \mathbf{I}_K$. $\mathbf{T}$ denotes a $N \times K$ block linear precoding matrix at gateways. The precoding matrix is computed at the gateways and it shall be transmitted through the feeder links. Thus, in the feeder link transmission the precoding matrix shall be separated in blocks and simultaneously transmitted by the gateways. This will be presented in the following sections.

In the sequel, $\mathbf{H}$ is the overall $K \times N$ user link channel matrix whose element h_{ij} presents the gain of the link between the i-th user (in the i-th beam) and the j-th satellite feed. Remind that the channel model is detailed in (1.6).

The typical performance metric involves the received SINR for k-th user, which is expressed as

$$\mathrm{SINR}_k = \frac{|(\mathbf{HT})_{kk}|^2}{\sum_{j \neq k}^{K} |(\mathbf{HT})_{kj}|^2 + 1} \quad k = 1, \ldots, K. \tag{3.2}$$

Similar to power loading in (2.6), we assume the following average available power constraint:

$$\mathrm{E}\{||\mathbf{x}||^2\} = \mathrm{trace}(\mathbf{TT}^H) \leq P_{FL}, \tag{3.3}$$

where P_{FL} denotes the total transmit power at the satellite for the forward link.

This chapter is devoted to the study of multiple gateway precoding transmission so that in the following we will assume that beams are divided into clusters and each cluster is served by a certain gateway. There is the same number of gateways and clusters as Figure 3.1 depicts. As we remarked previously, each feed signal can only be generated by a single gateway, otherwise signal overlapping might occur. Considering that there are G gateways, we will denote N_g the number of feeds associated to the g-th gateway for $g = 1, \ldots, G$. Note that

$$N = \sum_{g=1}^{G} N_g. \tag{3.4}$$

In addition, the number of served beams by the g-th gateway is defined as K_g for $g = 1, \ldots, G$ where

$$K = \sum_{g=1}^{G} K_g. \tag{3.5}$$

In addition, we will consider that

$$K_g \leq N_g \quad g = 1, \ldots, G. \tag{3.6}$$

It is important to remark that the optimization of K_g and N_g for $g = 1, \ldots G$ is out of the scope of this study and we will assume beforehand a certain feed and beam allocation per gateway. Consequently, each gateway must compute a precoding matrix $\mathbf{T}_g$ of size
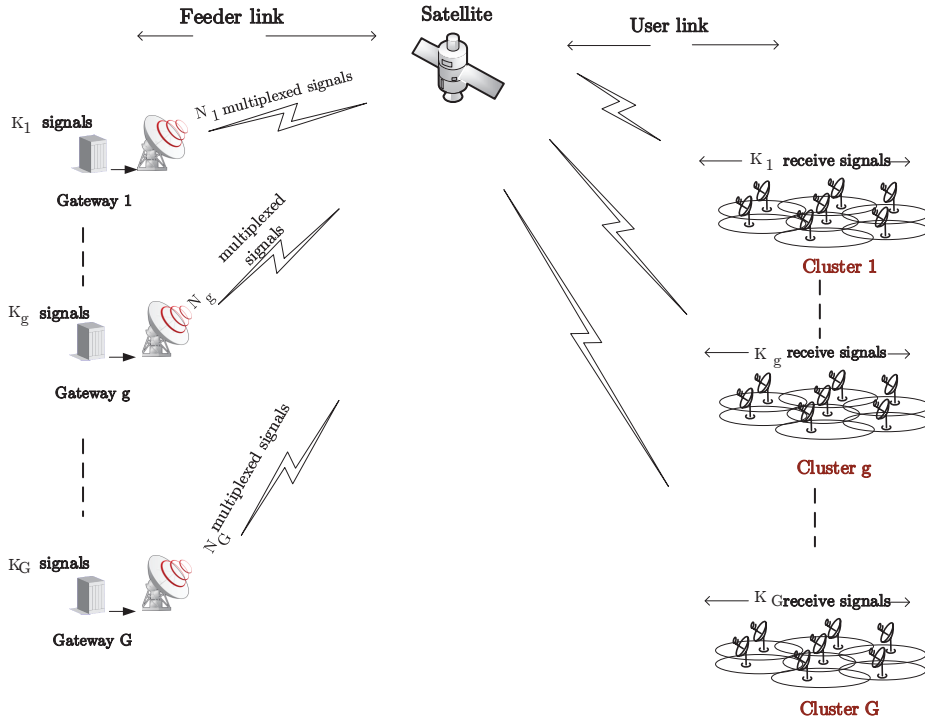
Figure 3.1: Multiple gateway structure. The transmitted symbols are produced in geographically separated areas and they are transmitted separately through the feed signals. The satellite is equipped with an array fed reflector antenna where those $N = \sum_{g=1}^{G} N_g$ feed signals are transformed into K transmitted user signals. Interference is created not only by the signals within each cluster but also within the different clusters. The number of beams (users) per cluster is equal to K_g.

$N_g \times K_g$. In other words, each gateway must compute the linear processing for serving K_g users with N_g feeds. Figure 3.1 shows the overall system architecture.

Prior to designing the precoding matrix, let us define the following division of the channel matrix

$$\mathbf{H} = (\mathbf{H}_1, \ldots, \mathbf{H}_G) \,, \tag{3.7}$$

where $\mathbf{H}_g$ of size $K \times N_g$ is the channel sub-matrix containing the contribution of the feeds assigned to the g-th gateway. Note that we will assume that the allocated feed
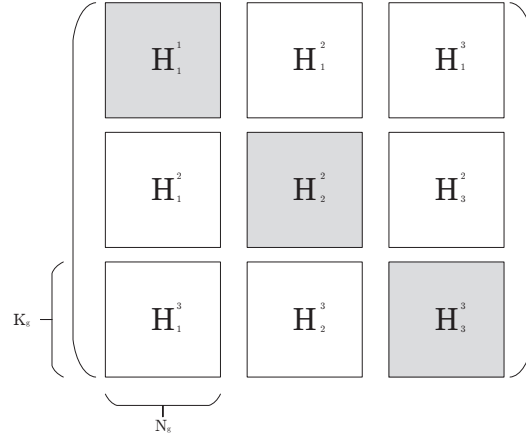
Figure 3.2: Representation an example of the channel matrix of a multibeam multigateway satellite system with three gateways. The grey sub-matrices represent the channel effect of the feed signals assigned to a certain gateway to the users assigned to the gateway. The white sub-matrices represent the impact of the feed signals to the non-intended clusters. The role of the precoding matrix is not only to revert the interference of the users within the same cluster (grey sub-matrix) but also to mitigate the interference generated to the rest (white sub-matrices).

elements for each gateway are consecutive in the channel matrix. Moreover, each sub-matrix can be decomposed into clusters as

$$\mathbf{H}_g = \left(\mathbf{H}_g^{1,H}, \ldots, \mathbf{H}_g^{G,H}\right)^H, \tag{3.8}$$

where $\mathbf{H}_g^c$ of size $K_c \times N_g$ for $c = 1, \ldots, G$ is the channel sub-matrix corresponding to the effect of the N_g feeds to the c-th cluster. An illustrative example of this sub-matrix decomposition is represented in figure 3.2.

Next sections are devoted to the design of $\mathbf{T}_g$ for $g = 1, \ldots, G$ in order not only to mitigate the interference between clusters but also the interference created within each cluster. Posteriorly, limitations of this precoding technique are studied.

3.2   Multigateway multibeam precoding

As it is described in the previous section, the multiple gateway precoding does not only have to reject the intra-cluster interference but also the inter-cluster one. For the latter, it is proposed a block regularized SVD precoding. Considering the g-th gateway channel submatrix, let us construct its regularized version

$$\mathbf{H}_g^{(R)} = \mathbf{H}_g \mathbf{H}_g^H + \frac{G}{P_{\mathrm{FL}}} \mathbf{I}_K, \tag{3.9}$$

where $\mathbf{H}_g^{(R)}$ is of size $K \times K$ and is used to construct the precoder instead of using $\mathbf{H}_g$. The reason is that the null space has zero dimension and, as a result, it is impossible to block the inter-cluster interference. Nevertheless, as it will be shown in the simulation section, the out-of-cluster interference is mitigated severally if the regularized version is used instead. This technique was also applied in [40] for the multigroup multicast scenario. To understand how, let us decompose $\mathbf{H}_g^{(R)}$, in the following sub-matrices

$$\mathbf{H}_g^{(R)} = \left(\mathbf{H}_g^{(1,R),H}, \dots, \mathbf{H}_g^{(g,R),H}, \dots, \mathbf{H}_g^{(G,R)} \right)^H, \tag{3.10}$$

where $\mathbf{H}_g^{(g,R),H}$ of size $K_g \times K$ is the sub-channel matrix of the g-th cluster in the regularized matrix. In addition, the following matrix can be constructed with the out-of-cluster sub-matrices

$$\widetilde{\mathbf{H}_g^{(g,R)}} = \left(\mathbf{H}_g^{(1,R),H}, \dots, \mathbf{H}_g^{(g-1,R),H}, \mathbf{H}_g^{(g+1,R),H}, \dots, \mathbf{H}_g^{(G,R),H} \right)^H. \tag{3.11}$$

Considering the singular value decomposition of this last matrix,

$$\widetilde{\mathbf{H}_g^{(g,R)}} = \mathbf{U}_g \mathbf{\Lambda}_g \mathbf{V}_g^H, \tag{3.12}$$

where $\mathbf{V}_g$ can be written as

$$\mathbf{V}_g = \left(\mathbf{V}_g^1 \mathbf{V}_g^0\right)^H, \tag{3.13}$$

where $\mathbf{V}_g^1$ of size $K \times (K - K_g)$ are the left singular eigenvectors of $\widetilde{\mathbf{H}_g^{(g,R)}}$ associated to the non-zero singular eigenvalues, whereas $\mathbf{V}_g^0$ of size $K \times (K_g)$ are the left singular eigenvectors associated to the zero singular eigenvalues. In this context, the gateway can use $\mathbf{V}_g^0$ as a pre-processing in order to mitigate the interference created by its feeds to the users outside its corresponding cluster.

Now it is time to design the precoding matrix in order to mitigate the intra-cluster interference. Considering that each gateway employs the aforementioned pre-processing matrix, the gateway observes a virtual channel matrix

$$\mathbf{H}_g^{\text{eq}} = \mathbf{H}_g^{(g,R)} \mathbf{V}_g^0. \tag{3.14}$$

where $\mathbf{H}_g^{\text{eq}}$ is of size $K_g \times K_g$. With this, the system designer can resort to the common designs such as ZF precoding,

$$\mathbf{W}_{g,\text{ZF}} = \mathbf{H}_g^{\text{eq},H} \left(\mathbf{H}_g^{\text{eq}} \mathbf{H}_g^{\text{eq},H}\right)^{-1}. \tag{3.15}$$

Moreover, an additional gain can be obtained by means of employing the regularized ZF or LMMSE precodings

$$\mathbf{W}_{g,\text{LMMSE}} = \mathbf{H}_g^{\text{eq},H} \left(\mathbf{H}_g^{\text{eq}} \mathbf{H}_g^{\text{eq},H} + \frac{P_{\text{FL}}}{G} \mathbf{I}_{K_g}\right)^{-1}. \tag{3.16}$$

The final precoder is computed so that

$$\mathbf{T}_g = \beta \mathbf{H}_g^{c,H} \mathbf{V}_g^0 \mathbf{W}_g, \tag{3.17}$$

for both the ZF and MMSE case and where β is set so that

$$\text{trace}\left(\mathbf{T}_g^H \mathbf{T}_g\right) = \frac{P_{\text{FL}}}{G} \quad g = 1, \ldots, G, \tag{3.18}$$

where $\mathbf{T}_g$ is of size $N_g \times K_g$. It has been assumed that the total power is equally divided for each gateway and the power constraints are fulfilled with equality. Finally, constructing the overall precoding matrix is done via

$$\mathbf{T} = \text{block-diagonal}\{\mathbf{T}_g\}_{g=1}^G, \tag{3.19}$$

where the block-diagonal operator constructs a matrix formed by the inputs matrices in the main diagonal and zero otherwise.

To sum up, the multigateway design consists of two stages. First, a pre-processing matrix that minimizes the inter-cluster interference is presented based on a regularized SVD decomposition. Second, for the resulting virtual cluster channel, two precoding techniques are considered: ZF and LMMSE. These latter techniques will mitigate the intra-cluster multiuser interference. Remarkably, the computation of the second precoding matrices can be done separately at each gateway where the first crucial pre-processing stage requires cooperation among gateways.

In the next section precoding limitations are presented. Note that the multigateway precoding relays on the assumption that gateways know the overall channel matrix and; in addition, this CSI has no errors. These two assumptions are generally unrealistic. The impact of limited CSI so as a possible reduction on the cooperation among gateways is studied in the next section. Finally, an analysis of the feeder link calibration errors is shown.

3.3   Multigateway precoding limitations

3.3.1   Reduced cooperation among gateways

The regularized block SVD multiple gateway precoding presented in the previous section assumes that each gateway knows $\mathbf{H}_g$. This assumption entails that each gateway is able to receive information by its feeder link from not only the users of its cluster but also from the rest. Unfortunately, this architecture will require complex data routing mechanisms at the payload which entails an unaffordable satellite hardware complexity. Assuming that the gateways are connected by a high speed fibre optic and assuming that satellite channel variations are minimal, full CSI sharing among gateways is implementable at expenses of a large communication overhead among gateways. In any case, the system designer might not decide to allocate such an overhead of resources for gateway cooperation and he/she can decide to keep them low. In that case, limited cooperation techniques are required.

Concretely, the g-th gateway knowns

$$\{\mathbf{H}_i^g\}_{i=1}^G, \quad g = 1, \ldots, G. \tag{3.20}$$

However, each gateway needs to know

$$\mathbf{H}_g, \quad g = 1, \ldots, G. \tag{3.21}$$

As a result, each gateway should share

$$\{\mathbf{H}_i^g\}_{i \neq g}^G, \quad g = 1, \ldots, G, \tag{3.22}$$

which is a total amount of $N_g(K - K_g)G$ complex numbers to be transmitted through the connection between gateways. In order to reduce this communication overhead, the

following approximation is presented.

Considering the operation at the g-th gateway, the CSI information to be transmitted to the i-th gateway is

$$\mathbf{H}_i^g \in \mathbb{C}^{K_g \times N_g} \quad i \neq g. \tag{3.23}$$

The best rank-one approximation of the aforementioned matrix is given by the right singular eigenvector associated to largest singular eigenvalue: $\sigma_i \mathbf{v}_{g,i}$ of size $N_g \times 1$. In this way, the g-th gateway can construct a matrix which approximates the inter-cluster interference as

$$\mathbf{G}_g = \left(\sigma_1 \mathbf{v}_{g,1}^H, \ldots, \sigma_{g-1} \mathbf{v}_{g,g-1}^H, \sigma_{g+1} \mathbf{v}_{g,g+1}^H, \ldots, \sigma_G \mathbf{v}_{g,G}^H \right)^H. \tag{3.24}$$

Under this context, each gateway only needs to transmit $N_g(G-1)$ complex numbers instead of the $N_g(K - K_g)G$ when full cooperation is considered. Matrix $\mathbf{G}_g$ of size $(G-1) \times N_g$ is an approximation of $\mathbf{H}_g$. Similar to the previous method, the null space project of $\mathbf{G}_g$ can be used as a pre-processing matrix following the scheme presented in the previous section. This development is not included in this study for the sake of brevity.

Apart from the presented reduction in terms of the singular value decomposition of $\mathbf{H}_i^g$, the system designer can limit the cooperation overhead by means of reducing the communication between gateways. With this, only a subset of gateways interchange CSI data leading to a large reduction of the communication overhead. In the simulation section this is carefully evaluated.

3.3.2 Feeder link interference

So far we have considered that the gateways are able to transmit the feed signals within several feeder links (i.e. one feeder link per gateway) in an interference-free and noiseless channel. Indeed, the satellite is equipped with G feeder link receivers so that the signals

are demultiplexed and routed through the array fed reflector.

Unfortunately, although very directive antennas are used on ground for transmitting the feed signals, pointing errors might occur and; in addition, hardware might become uncalibrated under certain conditions. Consequently, an additional interference among beams might be created due to this.

Mathematically, the channel matrix becomes

$$\mathbf{H} \leftarrow \mathbf{H}_u \mathbf{H}_f, \tag{3.25}$$

where $\mathbf{H}_f$ of size $N \times N$ models the interference generated by the different gateways and $\mathbf{H}_u$ is the channel matrix described in the previous section 3.1.1. It is assumed that the interference equally impacts all the feed signals of each gateway.

In the following we provide a tentative description of $\mathbf{H}_f$ matrix. Assuming that $\mathbf{H}_f$ is formed by block matrices, $\mathbf{H}_f^{i,j}$ of dimension $N_g \times N_g$ which model the each gateway interference, the feeder link interference impact can be described as

$$\mathbf{H}_f^{i,i} = \mathbf{I}_{N_g}, \tag{3.26}$$

$$\mathbf{H}_f^{i,j} = \rho^{|i-j|} \mathbf{E}_{N_g} \quad i \neq j, \tag{3.27}$$

for $i = 1, \ldots, G$ and where $\mathbf{E}_{N_g}$ is a $N_g \times N_g$ whose entries are equal to one. Moreover, $\rho \in [0, 1]$ is a parameter that models the overall interference signals. The larger ρ the larger feeder link interference is considered.

Intuitively, whenever the systems presents larger interference prior the precoding effect, the lower achievable rates will be obtained. This reasoning is mathematically proved in the following by means of considering an upper bound of the SMSE.

Let us consider that the inter-cluster interference is completely suppressed and each gateway performs LMMSE precoding. This scenario is an upper-bound of the overall

multibeam multigateway system performance since in general the inter-cluster interference cannot be neglected. Under this context, the forward link system achievable rates under linear precoding considering an arbitrary g cluster can be described by the SMSE which is described in the previous chapter, so that

$$\text{SMSE} = \text{trace}\Big(\mathbf{MSE}\Big). \tag{3.28}$$

where $\mathbf{MSE} = \text{diag}\Big(\text{MSE}_1, ..., \text{MSE}_i, ..., \text{MSE}_K\Big)$ and where MSE_i refers to the MSE received by i-th user. Obviously, the lower SMSE, the larger achievable rates can be obtained. It can be shown that the SMSE can be written as

$$\text{SMSE} = \frac{K}{P_{\text{FL}}}\text{trace}\left(\left(\mathbf{I}\frac{K}{P_{\text{FL}}} + \mathbf{H}_u\mathbf{H}_u^H\right)^{-1}\right), \tag{3.29}$$

where the g superscript has been omitted for the sake of clarity. With this last equation, the impact of the feeder link multigateway interference can be analytically studied. Consequently, it is possible to define

$$\text{SMSE}_{\text{no-interference}} = \frac{K}{G}\text{trace}\left(\left(\frac{G}{P_{\text{FL}}}\mathbf{I} + \mathbf{H}_u\mathbf{H}_u^H\right)^{-1}\right), \tag{3.30}$$

$$\text{SMSE}_{\text{interference}} = \frac{K}{G}\text{trace}\left(\left(\frac{G}{P_{\text{FL}}}\mathbf{I} + \mathbf{H}_u\mathbf{H}_f\mathbf{H}_f^H\mathbf{H}_u^H\right)^{-1}\right), \tag{3.31}$$

where we did not include the superscript in $\mathbf{H}_f$ for the sake of clarity but it is important to remark that its dimensions are $N_g \times N$. Prior to establishing the relation between the SMSE of these two cases, the following lemma is introduced.

Lemma 3.3.1. *Consider* $\mathbf{D} = [d_1, ..., d_k]$ *be any tall matrix and* $\mathbf{D}_r = [d_1, ..., d_r]$, *for all* $r = 1, \ldots, k-1$ *it holds that*

$$\sigma_1(\mathbf{D}_{r+1}) \geq \sigma_1(\mathbf{D}_r) \geq \sigma_2(\mathbf{D}_{r+1}) \geq ... \geq \sigma_r(\mathbf{D}_{r+1}) \geq \sigma_r(\mathbf{D}_r) \geq \sigma_{r+1}(\mathbf{D}_{r+1}) \qquad (3.32)$$

Proof. See Theorem 1 in [42].   □

With this result, the following theorem can be established.

Theorem 3.1. *For any semidefinite positive matrix* $\mathbf{H}_f$*, it results that*

$$SMSE_{interference} \geq SMSE_{no\text{-}interference}. \qquad (3.33)$$

Proof. see Appendix 3.5.1.   □

From this last result it is evident that whenever the multigateway feeder link structure is not perfectly calibrated, the system achievable rates decrease even though precoding is used. Thus, the multigateway feeder link hardware architecture shall be carefully designed in order to preclude the possible interference effect. In any case, as long as precoding is employed, the inter-feeder link interference can be reverted at the transmit side but; however, certain performance loss occurs with respect to the ideal interference-free feeder link system.

3.4   Simulation results

3.4.1   Simulation setup

In order to further compare the performance of the proposed interference mitigation techniques and payload processing scheme, this section presents the simulation results Monte Carlo simulations have been carried out. We employ the the forward link of multibeam satellite system which is detailed in section 2.4 and the simulation parameters that are collected in Table 2.1. Here, we compute the following performance metrics:

- Total average throughput (bits/symbol) according to the upgraded DVB-S2x standard which is shown in Table 3.2,

- CDF of SINR based on DVB-S2x and is detailed in (2.70).

3.4.2   Ideal feeder link system architecture

This section presents the simulation results related to the scenarios described in sections 3.2 and 3.3.

The user link in the downlink is assumed to operate at 20 GHz Ka-band. A total of $G = 14$ gateways are considered so that each gateway is serving a cluster of 7 or 8 beams. Fig. 3.3 depicts the overall system architecture. It can be observed that the g-th gateway is serving a set of 7 beams $K_g = 7$. Several collaborative schemes are presented in the following for the sake of completeness:

- **Scenario 1** : The individual cluster multibeam processing without gateway coordination so that each gateway processes its beams independently. In this context, the ZF precoding in m-th gateway can be expressed as

$$\mathbf{T}_g = \beta_{\mathrm{ICM}} \mathbf{H}_g^H (\mathbf{H}_g \mathbf{H}_g^H)^{-1}, \tag{3.34}$$

where β_{ICM} is set to preserve the gateway power constraint assumed to be $\frac{P_{\mathrm{FL}}}{G}$ for all of them. This is referred to Individual Cluster Multibeam processing (ICM).

- **Scenario 2** : 4 gateways interchange their CSI so that each gateway only has access to 3 interfering matrices. This is referred to 4 Gateways Collaboration (4GC). See Fig. 3.4.

- **Scenario 3** : 7 gateways interchange their CSI so that each gateway only has access to 3 interfering matrices. This is referred to 7 Gateways Collaboration (7GC).

- **Scenario 4** : Gateway g (respectively for all the gateways) collaborates with all gateways. This is referred to Gateway Collaboration Multibeam processing (GCM).

- **Scenario 5** : Single gateway scenario where all data and CSI is located at the same transmitter. This scenario is the Reference scenario (Ref).

- **Scenario 6** : Gateway g (respectively for all the gateways) collaborates with all the gateways that serve clusters that are directly adjacent to cluster g by means of transmitting the rank one approximation of their channels as we discussed in section 3.3.1. This is referred to Limited Multi-gateway Collaboration processing (LMC).

Table 3.1 describes the communication overhead associated to each cooperative scheme. As we anticipated in the previous section, the LMC scheme offers a large reduction of the communication overhead.

Table 3.1: Cooperation Overhead Comparison

Cooperation Scheme	Total Number of Complex Numbers to be Shared
4GC	57288
7GC	100254
GMC	200508
LMC	143

Figure 3.5 and 3.6 present the spectral efficiency when either MMSE or ZF is used as precoding matrix for mitigating the intra-cluster interference respectively. For both cases it is shown that the ICM scheme has the lowest achievable rate due to lack of interference mitigation among clusters. 4GC and 7GC achieve reasonable performance and the proposed multiple gateway scheme with CSI sharing among adjacent clusters (i.e. GCM) shows better performance. Consequently, the higher the coordination among gateways is, the higher the achievable rates are . Note that MMSE delivers higher
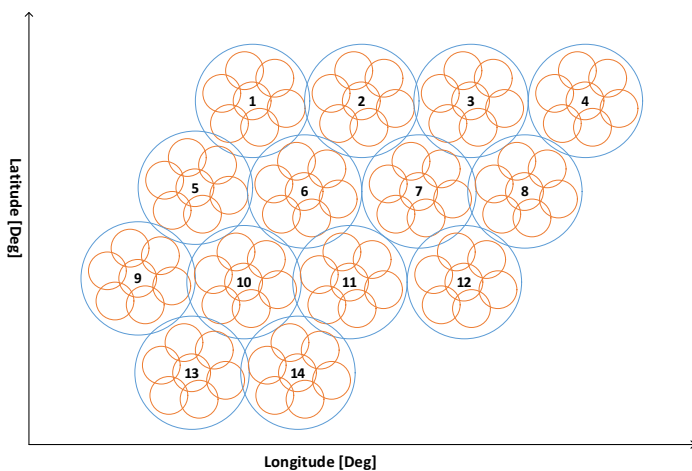
Figure 3.3: A set of 14 cluster composed by 7 beams is depicted in the figure. This will be the reference architecture assuming that all beams operate in the same frequency band. Remarkably, the precoder not only has to mitigate the inter-cluster interference but the intra-cluster one.
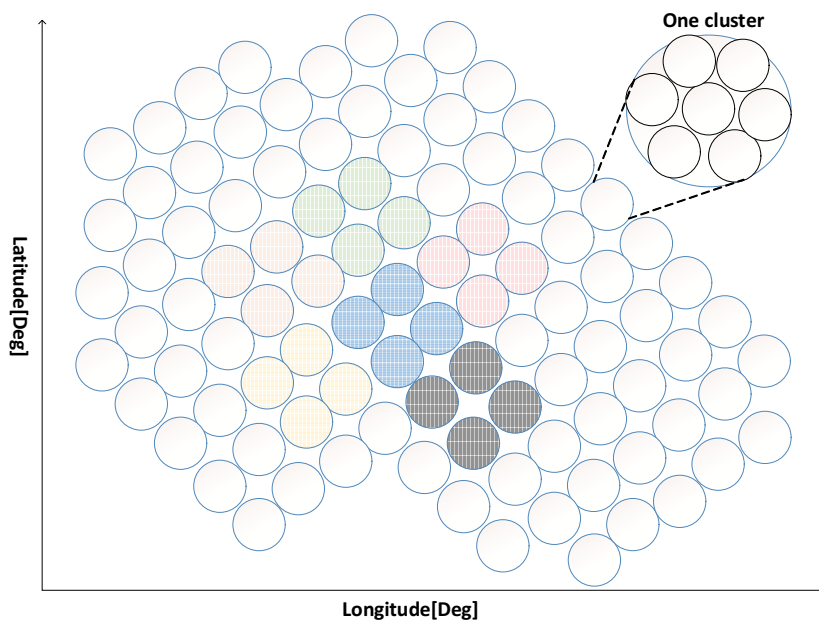
Figure 3.4: Cooperation architecture between 4 adjacent clusters: it is assumed that each gateway can cooperate with only 3 gateways whose beams are adjacent to them. The cooperative clusters are depicted with the same colour.

spectral efficiencies than ZF.
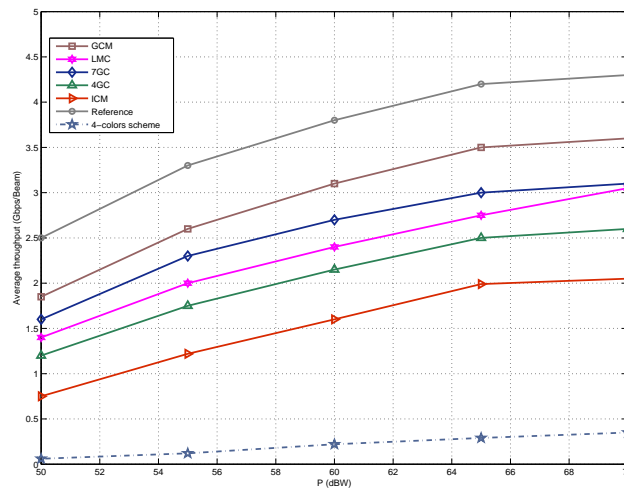
Figure 3.5: Spectral efficiency considering multigateway block regularized precoding and different collaborative architectures. The intra-cluster interference is mitigated via MMSE precoding
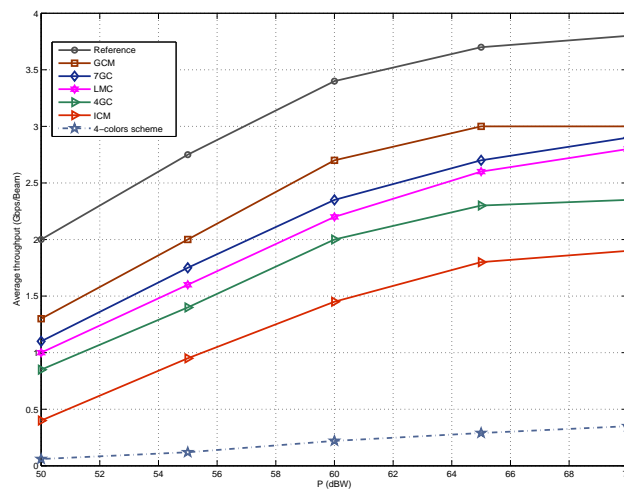
Figure 3.6: Spectral efficiency considering multigateway block regularized precoding and different collaborative architectures. The intra-cluster interference is mitigated via ZF precoding

Note that the proposed LMC offers a good trade-off between gateway cooperation overhead and overall system performance.

3.4.3   Non-ideal feeder link system architecture

In this section we analyse the scenario presented in the section 3.3.2. We consider $\rho = 1$, which is a worst-case scenario. Again, simulation results use the average total throughput as performance measurement. Figure 3.7 compares the results related to all scenarios described above considering that for each gateway receives interference from 1 to 14 gateways. The transmit power is set to $P_{FL} = 30$ dBW and MMSE precoding is used for mitigating the intra-cluster interference.

From Figure 3.7 it is evident the dramatical effect of feeder links mismatches in multi-gateway multibeam architecture even though precoding is performed. This effect appears for any cooperative architecture. It is important to remark that even if only one interfering gateway is considered, the average spectral efficiency decreases up to the 54% with respect to the ideal feeder-link scenario.
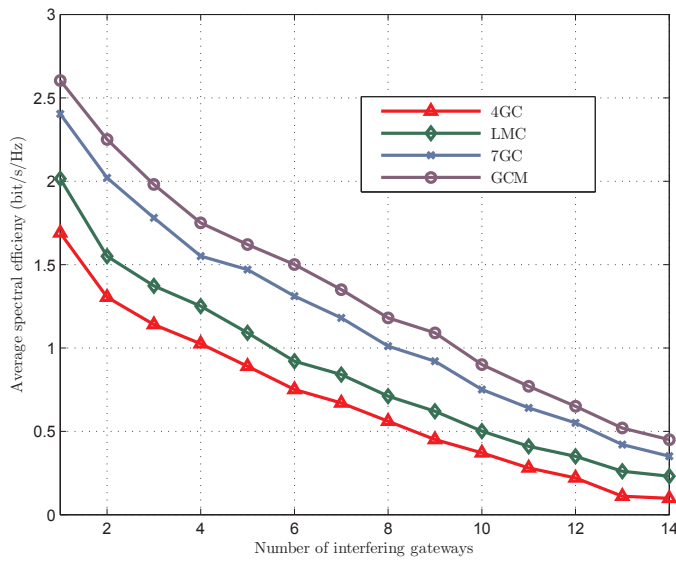
Figure 3.7: Spectral efficiency versus number of interfering gateways. The interfering parameter is set to 1 ($\rho = 1$). The feeder links uncalibrations decrease the system capacity severally.

3.4.4   Limited feedback

Let us consider the case where the CSI is not perfect but it is obtained via DVB-S2X feedback mechanisms as we described in section 1.3.0.3.

Figure 3.8 depicts the performance degradation whenever quantized feedback is used
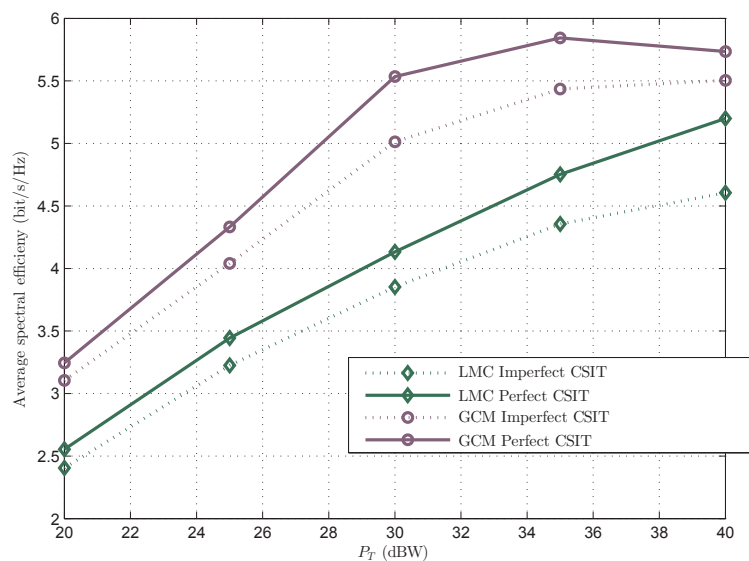
Figure 3.8: Spectral efficiency versus transmit power considering GMC and LMC processing with CSI errors. The performance decrease is high whenever the available CSI is not perfect.

instead of the perfect one. Both for the LMC and GMC case, the spectral efficiency decrease is notorious.

3.5   Appendix

3.5.1   Proof of inequality (3.33)

The SMSEs can be rewritten so that

$$\text{SMSE}_{\text{interference}} = \sum_{i=1}^{K} \frac{1}{\frac{G}{P} + \lambda_i(\mathbf{H}_u \mathbf{H}_f \mathbf{H}_f^H \mathbf{H}_u^H)}, \tag{3.35}$$

$$\text{SMSE}_{\text{no-interference}} = \sum_{i=1}^{K} \frac{1}{\frac{G}{P} + \lambda_i(\mathbf{H}_u \mathbf{H}_u^H)}. \tag{3.36}$$

Under this context and manipulating the previous equations, the theorem 1 holds as long as

$$\lambda_i(\mathbf{H}_f \mathbf{H}_f^H \mathbf{H}_u \mathbf{H}_u^H) \le \lambda_i(\mathbf{H}_u^H \mathbf{H}_u), \tag{3.37}$$

for $i = 1, \dots, K$. Bearing in mind that,

$$\lambda i(\mathbf{H}_u \mathbf{H}_f \mathbf{H}_f^H \mathbf{H}_u^f) = \sigma_i^2(\mathbf{H}_u \mathbf{H}_f \mathbf{H}_f^H \mathbf{H}_u^H), \tag{3.38}$$

$$\lambda i(\mathbf{H}_u \mathbf{H}_u^H) = \sigma_i^2(\mathbf{H}_u \mathbf{H}_u^H), \tag{3.39}$$

and considering that $\mathbf{H}_f$ has the following SVD decomposition $\mathbf{H}_f = \mathbf{U}_f \mathbf{\Sigma}_f \mathbf{V}_f^H$, we have that

$$\mathbf{H}_f \mathbf{H}_f^H = \mathbf{U}_f \mathbf{\Sigma}_f \mathbf{\Sigma}_f^H \mathbf{V}_f^H. \tag{3.40}$$

Writing $\mathbf{\Sigma}_f \mathbf{\Sigma}_f^H = \mathbf{S}_f$ it is easy to observe

$$\mathbf{S}_f = \begin{pmatrix} \mathbf{z}_{N_g \times N_g} & \mathbf{0}_{N \times (N-N_g)} \\ \mathbf{0}_{(N-N_g) \times N_g} & \mathbf{0}_{(N-N_g) \times (N-N_g)} \end{pmatrix}, \tag{3.41}$$

where $(\mathbf{\Sigma}_f \mathbf{\Sigma}_f^H)$ has only N_g non-zero singular values (i.e. $\mathbf{z}$), as $\mathbf{S}_g$ has rank equal to N_g.

Since $\mathbf{U}$ is a unitary matrix, for any matrix (same as $\mathbf{H}_u^H$ in this study) it holds that

$$\sigma_i \left(\mathbf{U}\mathbf{H}_u^H \mathbf{H}_u \right) = \sigma_i \left(\mathbf{H}_u^H \mathbf{H}_u \right). \tag{3.42}$$

Then, the right hand side of (3.37) can be worked out as

$$\sigma_i \left(\mathbf{U}_f \mathbf{S}_f \mathbf{U}_f^H \mathbf{H}_u^H \mathbf{H}_u \right) = \sigma_i \left(\mathbf{S}_f \mathbf{U}_f^H \mathbf{H}_u^H \mathbf{H}_u \right). \tag{3.43}$$

By the following definition $\mathbf{G}_f \triangleq \mathbf{U}_f^H \mathbf{H}_u^H \mathbf{H}_u$ and considering (3.42), proving (3.37) is equivalent to checking

$$\sigma_i(\mathbf{G}_f) \geq \sigma_i(\mathbf{S}_f \mathbf{G}_f), \tag{3.44}$$

for $i = 1, \ldots, N_g$. Now, remind that $\mathbf{G}_f$ is of size $N \times N$ as follows

$$\mathbf{G}_f = \begin{pmatrix} \mathbf{G}_1 \\ \mathbf{G}_2 \end{pmatrix} \tag{3.45}$$

where both sub-matrices of $\mathbf{G}_f$ are of size $N_g \times N$. Then, we have that

$$\mathbf{S}_f \mathbf{G}_f = \begin{pmatrix} \mathbf{G}_1 \\ \mathbf{0} \end{pmatrix} \tag{3.46}$$

It is clear that

$$\mathbf{G}_g^H = \begin{pmatrix} \mathbf{G}_1^H & \mathbf{G}_2^H \\ 0 & 0 \end{pmatrix}, \tag{3.47}$$

where $\mathbf{G}^H$ is matrix of size $N \times N$ whose singular values are

$$\boldsymbol{\sigma}(\mathbf{G}_f^H) = \left(\sigma_1(\mathbf{G}_f), \sigma_2(\mathbf{G}_f), \ldots, \sigma_{N_g}(\mathbf{G}_f), \mathbf{0}_{N-N_g} \right), \tag{3.48}$$

where $\mathbf{0}_{N-N_g}$ is a vector of dimension $N - N_g$ whose entries are equal to zero. By the interlacing property in Lemma 3.3.1 tells that

$$\sigma_i(\mathbf{G}_f) \geq \sigma_i(\mathbf{S}_f \mathbf{G}_f). \tag{3.49}$$

3.5.2   DVBS2x table

Table 3.2: DVB-S2x MODCOD parameters

ModCod mode	Efficiency Info bit / symbol	Required SINR [dB] (with approx. impl. losses)
QPSK_2/9	0.434	-2.85
QPSK_13/45	0.567	-2.03
QPSK_9/20	0.889	0.22
QPSK_11/20	1.088	1.45
8APSK_5/9-L	1.647	4.73
8APSK_26/45-L	1.713	5.13
8PSK_23/36	1.896	6.12
8PSK_25/36	2.062	7.02
8PSK_13/18	2.145	7.49
16APSK_1/2-L	1.972	5.97
16APSK_8/15-L	2.104	6.55
16APSK_5/9-L	2.193	6.84
16APSK_26/45	2.281	7.51
16APSK_3/5	2.370	7.80
16APSK_3/5-L	2.370	7.41
16APSK_28/45	2.458	8.10
16APSK_23/36	2.524	8.38
16APSK_2/3-L	2.635	8.43
16APSK_25/36	2.745	9.27
16APSK_13/18	2.856	9.71
16APSK_7/9	3.077	10.65
16APSK_77/90	3.386	11.99
32APSK_2/3-L	3.289	11.10
32APSK_32/45	3.510	11.75
32APSK_7/9	3.841	13.05
64APSK_32/45-L	4.206	13.98
64APSK_11/15	4.338	14.81
64APSK_7/9	4.603	15.47
64APSK_4/5	4.735	15.87
64APSK_5/6	4.933	16.55
128APSK_3/4	5.163	17.73

Chapter 4

Multicast multibeam precoding technique

This chapter investigates the forward link of an individual on-ground processing since a multicast transmitting scheme is employed in full frequency reuse pattern. In this context, we formulate the problem of multicast multibeam precoding and provide unexplored different low complex precoding strategies that would be eventually used in next generation high throughput satellite systems. These precoding techniques can be characterized as

- *Precoding design based on available full CSI at the gateway*

- *Precoding design based on available imperfect CSI at the gateway*

4.1   System overview

Apart from the disadvantages that are typical in aforementioned multiple gateway and hybrid space-ground architectures (i.e. quality of the CSI, antenna impairments, precoding/detecting computational complexity), there is an important phenomena that needs to be treated: the fact that in a single codeword is embedded the information for multiple

users which are located within each beam. This is referred to as multicast distribution. It is a matter of fact that current satellite standards aggregate different users in the same codeword in order to increase the coding gain since these systems generally need to work under a very low SNR. For instance, for the forward link, since the same message includes common information (i.e. the parity check bits), the precoding must consider the spatial signatures of the intended users. With this, the techniques to be applied are not longer the ones from the MISO broadcast channel but from the MISO multi-group broadcast channel. The precoding design of this scenario is known to be difficult in contrast to the MISO broadcast channel [27], [43]. Indeed, the main challenge is that the achievable rate is dictated by the worst user, whose optimal design always leads to iterative and complex designs.

These architectures also suffer from the following additional difficulties:

- the satellite communications embed more than one user in each single codeword in order to increase the channel coding gain.

- when the data traffic is generated by several gateways, the precoding matrix must be distributively computed and attain additional payload restrictions.

- since the feedback channel is adverse (large delay and quantization errors), the precodng must be able to deal with such uncertainties.

In order to solve the aforementioned problems, first we propose a two-stage precoding design in order to both limit the multibeam interference and to enhance the intra-beam minimum user signal power (i.e. the one that dictates the rate allocation per beam). It is important to remark that we prioritize low complex one-shot design in front of iterative grandient-based schemes [40].

Second, considering that the CSI will be corrupted at the gateway, a robust scheme is presented based on the first order perturbation theory of the eigenvectors and eigenvalues [33]. This robust design is novel and it has not been applied before. The resulting

precoding design remains low complex so that it can be implemented even if a very large number of feeds are considered.

Third, since the achievable rates decrease whenever the user channel vectors within one beam are not collinear, we propose a user grouping technique based on the spatial signature. With this, over all possible users to be served for each beam we select the most adequate set of users to be served using a variation of the k-means algorithm. This algorithm differs than the one presented in [44] as not only the channel magnitudes, but the phase effects are considered. Additionally, a novel robust user grouping scheme is proposed in order to deal with the possible channel uncertainties.

Forth, in case the data traffic is generated by multiple gateways, a precoding mechanism is presented to deal with the main challenges: CSI sharing and the distributed precoding matrix computation. Both a reduced inter-gateway communication for CSI sharing and a precoding matrix division among gateways are presented. Even though the achievable rates are decreased when the multiple gateway architecture is considered, the proposed scheme offers a good trade-off between communication overhead, payload complexity and overall throughput.

4.2   Problem formulation

Consider again the forward link of a multibeam satellite system, which is described in section 2.2.1.2.

Towards a spectrally efficient communication we use DVB-S2x modcod to transmit symbols. Moreover, all beams share the frequency band and; in a given time instant, the k-th beam serves a total amount of Q_k users. This implies each beam serves with a single DVB-S2x frame so that a multiplexed users in each frame is served. Without loss of generally, we will assume that each beam serves the same number of users simultaneously and it is equal to Q (i.e. $Q_k = Q \ k = 1, ..., K$).

It is important to remark that similar to payload architecture in chapter 2, the array fed reflector can have a single-feed-per-beam architecture whenever N = K or a multiple-feed-per-beam when N ¿ K. Remind that, this latter payload architecture presents lower beamforming scan losses and larger antenna gains. For the sake of generality will consider the a multiple-feed-per-beam structure for the rest of this chapter.

Under this context, the overall signal model in (2.4) can be rewritten as

$$\mathbf{y}_{\text{FL}} = \mathbf{H}\mathbf{x} + \mathbf{n} \tag{4.1}$$

where $\mathbf{y}$ of size $KQ \times 1$ is a vector containing the received signals at each user terminal. Vector $\mathbf{n}$ of size $KQ \times 1$ contains the noise terms of each user terminal and we will assume that they are Gaussian distributed with zero mean, unit variance and uncorrelated with both the desired signal and the other users noise terms (i.e. $E\left[\mathbf{n}\mathbf{n}^H\right] = \mathbf{I}_{KQ}$). In order to minimize the multiuser interference resulting from the full frequency reuse, linear precoding is considered. Under this context, the transmitted symbol can be modeled as

$$\mathbf{x} = \mathbf{W}\mathbf{s} \tag{4.2}$$

where $\mathbf{s}$ of size $K \times 1$ is a vector that contains the transmitted symbols which we assume uncorrelated and unit norm $\left(E\left[\mathbf{s}\mathbf{s}^H\right] = \mathbf{I}_K\right)$. Matrix $\mathbf{W}$ of size $N \times K$ is the linear precoding matrix to be designed.

4.2.1 Precoding design

Let us formulate the precoding design of a multicast multibeam satellite system. The overall system performance can be optimized considering the maximum sum rate:

$$
\underset{\mathbf{W}}{\text{maximize}} \quad \sum_{k=1}^{K} \underset{q=1,...Q}{\text{minimum}} \quad r_{k,q}
$$

subject to

$$
\text{Tr}\left(\mathbf{W}\mathbf{W}^H\right) \leq P_T
$$

$$
(4.3)
$$

where $r_{q,k}$ denotes the achievable rate of the q-th user at the k-th beam,

$$
r_{k,q} = \log_2\left(1 + \frac{|\mathbf{h}_{q,k}^H \mathbf{w}_k|^2}{\sum_{j\neq k}^{K} |\mathbf{h}_{q,k}^H \mathbf{w}_j|^2 + \sigma^2}\right), \qquad (4.4)
$$

P_T denotes the available power at the satellite and $\mathbf{w}_k$ corresponds to the k-th column of matrix $\mathbf{W}$.

Problem (4.3) is a difficult non-convex problem whose convex relaxations even require computationally demanding operations [45]. For multibeam satellite systems the computational complexity of the precoding design is an essential feature since these systems usually operate with hundreds of beams. Consequently, in contrast to other works, the target of this work is to design a low computationally complex precoding scheme able to achieve high throughput values. This is presented in the next section.

4.3 Generalized multicast multibeam precoding

The precoding design in multicast multibeam satellite systems has two main roles. First, the inter-beam interference shall be minimized and; second, the precoding shall increase the lowest SINR within each beam. Under this context, the precoding design can be

divided into two sub-matrices such as

$$\mathbf{W} = \alpha\mathbf{W}_a\mathbf{W}_b, \tag{4.5}$$

where

$$\mathbf{W}_a = [\mathbf{W}_{a_1}, \ldots, \mathbf{W}_{a_K}], \tag{4.6}$$

with $\mathbf{W}_a$ of size $N \times KQ$ and

$$\mathbf{W}_b = \begin{bmatrix} \mathbf{w}_{b_1} & \mathbf{0} & \cdots & \mathbf{0} \\ \mathbf{0} & \mathbf{w}_{b_2} & \cdots & \mathbf{0} \\ \vdots & \vdots & \ddots & \vdots \\ \mathbf{0} & \mathbf{0} & \cdots & \mathbf{w}_{b_K} \end{bmatrix} \in \mathbb{C}^{KQ\times K}, \tag{4.7}$$

with $\mathbf{W}_b$ is of size $KQ \times K$. Moreover, $\mathbf{W}_{a_k}$ and $\mathbf{w}_{b_k}$ are of size $N \times Q$ and $Q \times 1$, respectively. The matrix $\mathbf{W}_a$ is used to mitigate the inter-beam interference first and then the matrix $\mathbf{W}_b$ is used to optimize the intra-beam data rate so that $\mathbf{w}_{b_k}$ and $\mathbf{W}_{a_k}$ denotes the precoding for optimizing interference in k-th beam. Note that both matrices are essential because of twofold: the interference is the communication bottleneck and the user with lowest SINR within each beam determines the rate of the beam. Finally, the parameter α is chosen to set the total transmit power to P.

In the following subsections, two different designs for both $\mathbf{W}_a$ and $\mathbf{W}_b$ are presented.

4.3.1 Inter-beam interference mitigation precoding

4.3.1.1 MBIM scheme

Let us define $\widetilde{\mathbf{H}}_k$ as

$$\widetilde{\mathbf{H}}_k = \begin{bmatrix} \mathbf{H}_1 \\ \vdots \\ \mathbf{H}_{k-1} \\ \mathbf{H}_{k+1} \\ \vdots \\ \mathbf{H}_K \end{bmatrix} \tag{4.8}$$

where $\widetilde{\mathbf{H}}_k$ is of size $(K-1)Q \times N$ First we observe the interference impact of the precoding matrix $\mathbf{W}_a$. This can be done by means of constructing the equivalent combined channel matrix after the precoding effect:

$$\mathbf{HW}_a = \begin{bmatrix} \mathbf{H}_1\mathbf{W}_{a_1} & \mathbf{H}_1\mathbf{W}_{a_2} & \cdots & \mathbf{H}_1\mathbf{W}_{a_K} \\ \mathbf{H}_2\mathbf{W}_{a_1} & \mathbf{H}_2\mathbf{W}_{a_2} & \cdots & \mathbf{H}_2\mathbf{W}_{a_K} \\ \vdots & \vdots & \ddots & \vdots \\ \mathbf{H}_K\mathbf{W}_{a_1} & \mathbf{H}_K\mathbf{W}_{a_2} & \cdots & \mathbf{H}_K\mathbf{W}_{a_K} \end{bmatrix}, \tag{4.9}$$

where the k-th beam effective channel is given by $\mathbf{H}_k\mathbf{W}_{a_k}$ and the interference generated to the other users is determined by $\widetilde{\mathbf{H}}_k\mathbf{W}_{a_k}$.

As described in [46] an efficient design of $\mathbf{W}_a$ is given by the optimal matrix of the following modified MMSE objective function

$$\underset{\mathbf{W}_a}{\text{minimize}} \quad \mathrm{E}\left[\sum_{k=1}^K \|\widetilde{\mathbf{H}}_k\mathbf{W}_{a_k}\|^2 + \frac{1}{\alpha^2}\|\mathbf{n}\|^2\right]. \tag{4.10}$$

It is important to remark that the optimization problem in (4.10) is relaxed the non-convex SINR optimization problem in (4.3). The solution of this optimization problem is given by

$$\mathbf{W}_{a_k}^{\mathrm{MBIM}} = \mathbf{M}_{a_k}\mathbf{D}_{a_k}, \tag{4.11}$$

where

$$\mathbf{M}_{a_k} = \widetilde{\mathbf{V}}_k, \tag{4.12}$$

and

$$\mathbf{D}_{a_k} = \left(\widetilde{\mathbf{\Sigma}}_k + \frac{KQ}{P}\mathbf{I}\right)^{-1/2}. \tag{4.13}$$

Note that it has been considered the singular value decomposition of $\widetilde{\mathbf{H}}_k^H\widetilde{\mathbf{H}}_k = \widetilde{\mathbf{V}}_k\widetilde{\mathbf{\Sigma}}_k\widetilde{\mathbf{V}}_k^H$.

4.3.1.2   Regularized zero-forcing

Let $\mathbf{H}^{(R)}$ of size $KQ \times KQ$ denote the regularized channel defined as

$$\mathbf{H}^{(R)} = \mathbf{H}\mathbf{H}^H + \frac{K}{P}\mathbf{I}, \tag{4.14}$$

where the same regularization factor as that of the multicast-aware regularized zero-forcing [47] is considered. Let us define $\widetilde{\mathbf{H}}_k^{(R)}$ as

$$\widetilde{\mathbf{H}}_k^{(R)} = \begin{bmatrix} \widetilde{\mathbf{H}}_1^{(R)} \\ \vdots \\ \widetilde{\mathbf{H}}_{k-1}^{(R)} \\ \widetilde{\mathbf{H}}_{k+1}^{(R)} \\ \vdots \\ \widetilde{\mathbf{H}}_K^{(R)} \end{bmatrix} \tag{4.15}$$

where $\widetilde{\mathbf{H}}_k^{(R)}$ is of size $K(Q-1) \times KQ$.

The SVD decomposition of matrix can be described as

$$\widetilde{\mathbf{H}}_k^{(R)} = \widetilde{\mathbf{U}}_k^{(R)} \widetilde{\boldsymbol{\Sigma}}_k^{(R)} \left[\widetilde{\mathbf{V}}_k^{(R),1}, \widetilde{\mathbf{V}}_k^{(R),0} \right]^H, \tag{4.16}$$

where it is emphasized that there is always a null space of dimension Q spanned by $\widetilde{\mathbf{V}}_k^{(R),0}$. This matrix is used for this scheme such as

$$\mathbf{W}_{a_k}^{\text{R-ZF}} = \mathbf{H}^H \widetilde{\mathbf{V}}_k^{(R),0}. \tag{4.17}$$

where $\mathbf{W}_{a_k}^{\text{R-ZF}}$ is of size $N \times Q$.

4.3.2 Intra-beam Precoding

After the first precoding scheme $\mathbf{W}_a$ the k-th observes an equivalent channel $\mathbf{Z}_k = \mathbf{H}_k \mathbf{W}_{a_k}$ of size $Q \times N$. Based on $\mathbf{Z}_k$ the system designer shall construct $\mathbf{w}_{b_k}$. In the following, two different schemes are proposed. First, let us mention that the equivalent channel for the q-th user located at the k-th beam is denoted by $\mathbf{z}_{k_q}$ of size $N \times 1$ so that

$$\mathbf{Z}_k = \left[\mathbf{z}_{k_1}, \ldots, \mathbf{z}_{k_Q} \right]. \tag{4.18}$$

4.3.2.1 Max-min optimization

Since the achievable rate is dictated by the user with lowest SNR, $\mathbf{w}_{b_k}$ shall optimize

$$\begin{aligned}
&\underset{\mathbf{w}_{b_k}}{\text{maximize}} \quad \underset{q=1,\ldots Q}{\text{minimum}} \quad |\mathbf{z}_{k_q}^H \mathbf{w}_{b_k}|^2 \\
&\text{subject to} \\
&\|\mathbf{w}_{b_k}\|^2 \le 1.
\end{aligned} \tag{4.19}$$

Problem (4.19) is a non-convex problem which can be relaxed by the semidefinite relaxation technique as follows

$$
\begin{aligned}
&\underset{\mathbf{W}_{b_k}}{\text{maximize}} \quad t \\
&\text{subject to} \\
&\text{Trace}\left(\mathbf{Z}_{k_q}\mathbf{W}_{b_k}\right) \geq t \quad q = 1, \ldots, Q \\
&\text{Trace}\left(\mathbf{W}_{b_k}\right) \leq 1,
\end{aligned}
\tag{4.20}
$$

where $\mathbf{W}_{b_k} = \mathbf{w}_{b_k}\mathbf{w}_{b_k}^H$ and $\mathbf{Z}_{k_q} = \mathbf{z}_{k_q}\mathbf{z}_{k_q}^H$. Whenever $Q \leq 2$ this problem (4.20) leads to a tight solution of (4.19). Otherwise, in case $Q > 2$ rank reduction techniques such as randomization methods shall be employed which dramatically increase the computational complexity. Thus, this method is only convenient when $Q \leq 2$. Due to its large computational complexity, we will not consider this method for performance evaluation.

4.3.2.2 Average optimization

A suboptimal yet efficient approach is to maximize the average SNR considering the equivalent channel matrix. This is done with the following optimization problem

$$
\begin{aligned}
&\underset{\mathbf{w}_{b_k}}{\text{maximize}} \quad \sum_{q=1}^{Q} |\mathbf{z}_{k_q}^H \mathbf{w}_{b_k}|^2 \\
&\text{subject to} \\
&\|\mathbf{w}_{b_k}\|^2 \leq 1.
\end{aligned}
\tag{4.21}
$$

Since the objective function in (4.21) can be re-written as $\|\mathbf{Z}_k\mathbf{w}_{b_k}\|^2$, the optimal solution of (4.21) is given by the eigenvector associated to the largest eigenvalue of matrix $\mathbf{Z}_k$. Note that this precoding design offers a lower computational complexity than the previous one since only the eigenvector associated to the largest eigenvalue needs to be computed.

4.4   Robust multicast multibeam precoding

As it will be shown in the simulation section, the MBIM schemes offers larger achievable rates than the R-ZF. Consequently, we will consider this design so as the average optimization intra-beam proceding due to its lower computational complexity than the Max-min approach. We will proceed to design the worst-case robust versions of this precoding combination. Indeed, precoding performance relays on an accurate CSI fed back by the receiver. However, this CSI suffers from certain degradation due to quantization and transmission delay. Due to that, it is convenient to reformulate the optimization problem in order to take into account this possible variations [49]. This is done in the following subsections for both the inter-beam and intra-beam precoding.

First, let us introduce the perturbation where the transmitter do not longer have access to $\mathbf{H}$ but to a degraded version such as

$$\widehat{\mathbf{H}} = \mathbf{H} + \boldsymbol{\Delta}, \tag{4.22}$$

where $\boldsymbol{\Delta}$ of size $K \times N$ is the perturbation matrix where it is assumed to be constrained so that

$$\|\boldsymbol{\Delta}\|^2 \leq \gamma. \tag{4.23}$$

For notational convenience, it is important to define the following sub-matrices

$$\boldsymbol{\Delta} = \left[\boldsymbol{\Delta}_1^T, \boldsymbol{\Delta}_2^T, \ldots, \boldsymbol{\Delta}_K^T \right]^T, \tag{4.24}$$

$$\boldsymbol{\Delta}_k = \left[\boldsymbol{\delta}_{k,1}^T, \boldsymbol{\delta}_{k,2}^T, \ldots, \boldsymbol{\delta}_{k,Q}^T \right]^T, \tag{4.25}$$

$$\widetilde{\boldsymbol{\Delta}}_k = \begin{bmatrix} \boldsymbol{\Delta}_1 \\ \vdots \\ \boldsymbol{\Delta}_{k-1} \\ \boldsymbol{\Delta}_{k+1} \\ \vdots \\ \boldsymbol{\Delta}_K \end{bmatrix}, \tag{4.26}$$

where $\widetilde{\boldsymbol{\Delta}}_k$ of size $(K-1)Q \times N$. Moreover, $\boldsymbol{\Delta}_k$ of size $Q \times N$ is the perturbation associated to the k-th beam, $\boldsymbol{\delta}_{k,q}$ of size $N \times 1$ is the perturbation associated to the q-th user located at the k-th beam. Under this context, the perturbation sub-matrices can be constrained as follows

$$\|\boldsymbol{\Delta}_k\|^2 \leq \gamma_k, \tag{4.27}$$

$$\|\widetilde{\boldsymbol{\Delta}}_k\|^2 \leq \widetilde{\gamma}_k, \tag{4.28}$$

for $k = 1 \ldots, K$ and where

$$\widetilde{\gamma}_k = \sum_{l \neq k}^{K} \gamma_l. \tag{4.29}$$

Additionally, a definition of a lower bound of the perturbation matrices $\boldsymbol{\Delta}_k$ is convenient

$$\|\boldsymbol{\Delta}_k\|^2 \geq \underline{\gamma_k}. \tag{4.30}$$

Remarkably, finding the adequate γ bounds for all different perturbation matrices is not an easy task. Indeed, the computation of the different bounds shall be done on a empirical basis considering the different error sources and their final value on the perturbation matrix. This study is out of the scope of this work and we will only provide a sensitivity analysis in the simulation section.

4.4.1   Robust inter-beam precoding

Considering the modified MMSE scheme presented in the previous section, whenever the robust worst-case optimization problem (4.10) is targeted, the following new optimization problem shall be considered

$$
\underset{\mathbf{W}_a}{\text{minimize}} \quad \underset{\{\widetilde{\boldsymbol{\Delta}}_k\}_{k=1}^{K}}{\text{maximize}} \quad \mathrm{E}\left[\sum_{k=1}^{K} \|\widehat{\widetilde{\mathbf{H}}}_k \mathbf{W}_{a_k}\|^2 + \frac{1}{\alpha^2}\|\mathbf{n}\|^2\right]
$$

$$
\text{subject to}
$$

$$
\|\widetilde{\boldsymbol{\Delta}}_k\|^2 \leq \widetilde{\gamma_k} \quad k = 1, \ldots, K, \tag{4.31}
$$

where $\widehat{\widetilde{\mathbf{H}}}_k = \widetilde{\mathbf{H}}_k + \widetilde{\boldsymbol{\Delta}}_k$. Considering that the optimal design on (4.10) leads to the computation of an eigendecomposition, the perturbation matrix will both impact the eigenvectors and eigenvalues. Robust designs generally only consider the effect on the eigenvalues [22, Chapter 7]; however, the impact on the eigenvectors cannot be considered negligible [33]. The following theorem provides an approximate solution of the optimization problem in (4.31)

Theorem 4.1. *The optimal inter-beam precoding matrix that approximately minimizes* (4.31) *is*

$$
\widehat{\mathbf{W}}_{a_k}^{MBIM} = \widehat{\mathbf{M}_{a_k}} \widehat{\mathbf{D}_{a_k}}, \tag{4.32}
$$

where

$$
\widehat{\mathbf{M}_{a_k}} = \widetilde{\mathbf{V}}_k \left(\widehat{\mathbf{R}}_k + \mathbf{I}\right) \tag{4.33}
$$

and

$$
\widehat{\mathbf{D}_{a_k}} = \left(\widetilde{\boldsymbol{\Sigma}}_k + \epsilon_k \mathbf{I}\right)^{-1/2} \tag{4.34}
$$

where

$$
\epsilon_k = \widehat{\gamma}_k^2 + 2\widehat{\gamma}_k \sigma_{max}\left(\widetilde{\mathbf{H}}_k^H \widetilde{\mathbf{H}}_k\right). \tag{4.35}
$$

The rest of the matrices are defined in Appendix A and not included here for the sake of brevity.

Proof. See Appendix 4.8.1.   □

Remarkably, whenever ϵ_k increases, the resulting robust precoding design is more different than the original design $\mathbf{W}_{a_k}^{\mathrm{MMSE}}$. In any case, the computational complexity of the robust design remains the same.

4.4.2   Robust intra-beam precoding

Similarly to the previous robust design the intra-beam precoding shall consider tentative perturbations on their channel matrices. Considering the average optimization scheme, worst-case robust optimization for the k-th beam can be described as the following optimization problem

$$
\begin{aligned}
&\underset{\mathbf{w}_{b_k}}{\text{maximize}} \quad \underset{\boldsymbol{\Delta}_k}{\text{minimize}} \quad \|\widehat{\mathbf{Z}}_k \mathbf{w}_{b_k}\|^2 \\
&\text{subject to} \\
&\|\mathbf{w}_{b_k}\|^2 = 1, \\
&\|\boldsymbol{\Delta}_k\|^2 \geq \underline{\gamma_k},
\end{aligned}
\tag{4.36}
$$

where

$$
\widehat{\mathbf{Z}}_k = \mathbf{H}_k \mathbf{W}_{a_k} + \boldsymbol{\Delta}_k \mathbf{W}_{a_k}.
\tag{4.37}
$$

The next theorem presents an approximate solution of the aforementioned problem.

Theorem 4.2. *An approximate solution of* (4.36) *is* $\widehat{\mathbf{z}}_{k_1}$, *which is the the first column vector of matrix*

$$
\mathbf{L}_k \left(\nu_k \mathbf{N} \circ \left(\mathbf{L}_k^H \mathbf{L}_k^H \mathbf{T}_k + \mathbf{T}_k \mathbf{L}_k^H \mathbf{L}_k \right) + \mathbf{I} \right)
\tag{4.38}
$$

where

$$
\nu_k = \underline{\gamma}_k \mathbf{1}^T \left(\widetilde{\boldsymbol{\Sigma}}_k + \epsilon_k \mathbf{I} \right)^{-1/2} \mathbf{1},
\tag{4.39}
$$

and the rest of matrices are defined in Appendix refseda2.

Proof. See Appendix 4.8.2.   □

Note that whenever ν_k increases, the solutions is more different than the original solution. Again, the computational complexity remains the same as the non-robust case.

4.5 User grouping

One of the main limiting factors of multibeam multicast precoding is the spatial diversity of the users within each beam. Indeed, whenever the targeted users in each beam have orthogonal channel vectors, this is,

$$\mathbf{h}_{k,m}^H \mathbf{h}_{k,m} = 0 \tag{4.40}$$

for the k-th beam for $m, n = 1 \dots, Q$ and $m \neq n$; the intra-beam precoding is not able to deliver the intended symbols. Under this context it is beneficial that the system designer performs a user grouping before the precoding matrix is computed so that users with collinear channel vectors are simultaneously served.

4.5.1 k-user grouping

In a given time instant, the scheduler determines a set of tentative users to be served. The number of these scheduled users is considered the same for each beam, fixed and equal to $\mathcal{Q}$. For each beam, obtaining the most adequate groups of users is a cumbersome problem. Note that first, the system designer shall determine the adequate number of groups G_k per beam and, posteriorly, group them into those G_k groups [47].

It is important to remark that the issue of user grouping and how good it works depends local oscillators (whether on board or on ground, particularly the user terminal LNB) on

the density of the users within the beam. This will be justified in the simulation results section [48].

In order to solve this problem, we will consider a random pre-processing. This pre-processing consists of randomly choose a user from the beam and, posteriorly, obtain the group of users. Note that with this first processing, we are severally levering the computational complexity of the technique.

Under this context, let us consider that we have elected an arbitrary user m within the k-th beam. The user grouping scheme shall obtain the closest $Q-1$ users in terms of Euclidean norm. Mathematically,

$$
\begin{aligned}
&\underset{n \in 1,\ldots,Q}{\text{minimize}} \quad \|\mathbf{h}_{k,m} - \mathbf{h}_{k,n}\|^2 \\
&\text{subject to} \\
&n \neq m.
\end{aligned}
\tag{4.41}
$$

Since the considered Q in (4.41) is not expected to be large, this optimization only requires a set of Euclidean norm comparisons between the scheduled users. As it happens with the precoding design, the user grouping scheme suffers from degradation whenever the user channel vectors are corrupted. A method for robustly group them is presented in the next subsection.

4.5.2 Robust k-user grouping

Whenever the channel vectors are corrupted by a certain perturbation, a worst-case optimization shall be performed

$$
\begin{aligned}
&\underset{n \in 1, \dots, Q}{\text{minimize}} \quad \underset{\{\boldsymbol{\delta}_{k,q}\}_{q=1}^{Q}}{\text{maximize}} \quad \|\mathbf{h}_{k,m} + \boldsymbol{\delta}_{k,m} - \mathbf{h}_{k,n} - \boldsymbol{\delta}_{k,n}\|^2 \\
&\text{subject to} \\
&n \neq m, \\
&\|\boldsymbol{\delta}_{k,q}\|^2 \leq \gamma_{k,q}.
\end{aligned}
\tag{4.42}
$$

Next theorem provides an approximate version of the aforementioned problem.

Theorem 4.3. *An optimization problem whose solutions upper bound the original worst-case robust grouping problem* (4.42) *is*

$$
\begin{aligned}
&\underset{n \in 1, \dots, Q}{\text{minimize}} \quad \|\mathbf{h}_{k,m} - \mathbf{h}_{k,n}\|^2 + \gamma_{n,q} \\
&\text{subject to} \\
&n \neq m.
\end{aligned}
\tag{4.43}
$$

Proof. It is a simple derivation considering the Cauchy-Schwarz inequality and the fact that given a randomly chosen user m its perturbation does not influence the grouping optimization. $\square$

With this optimization it is evident that whenever uncertainty is assumed in the channel vectors, this shall be considered in the user grouping design by means of an additional scalar penalty. Remarkably, in case we consider the same uncertainty to all users, the proposed approximate solution remains the same.

4.6   Multiple gateway architecture

As a matter of fact, there might be the case where the feeder link cannot support the overall satellite data traffic. For instance, a payload equipped with $N = 155$ feeds with a user channel bandwidth of 500 MHz requires a feeder link bandwidth of 77.5 GHz which is an unaffordable requirement even if the feeder link carrier is located at the Q/V band. In order to solve this problem, the feeder link might get benefited from certain spatial reuse so that several gateways can simultaneously send the data to be transmitted over the satellite coverage area. Under this context, G gateways can reuse the available bandwidth for the feeder link leading to large increase of the user bandwidth (see Figure 4.1). However, in a multiple gateway scenario, the precoding scheme shall be reconsidered.

In order to keep the payload complexity low, each feeder link receiver at the payload

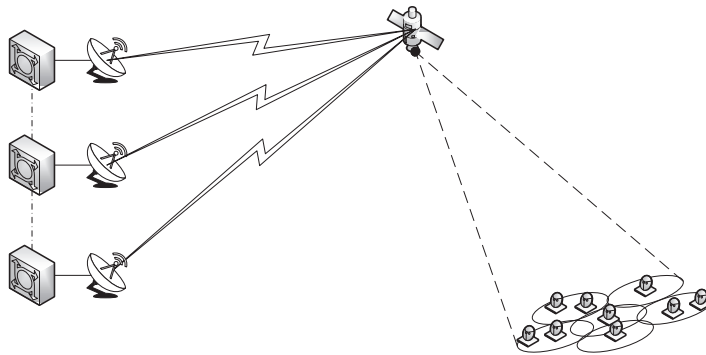Figure 4.1: The picture depicts the multiple gateway multicast multibeam satellite structure. In contrast to the single gateway architecture, several gateway transmit the data to be delivered to the coverage area. This entails two main drawbacks. First, certain inter-gateway link (dotted lines) shall exist. Second, each ground unit must compute an independent submatrix of the overall precoding matrix.

will only route signals a set of feeds N_g for $g = 1, \ldots, G$. Otherwise, a very complex ana-logical scheme shall be implemented. Considering this approach, the precoding matrix $\mathbf{W}$ must be partitioned into G sub-matrices leading to a large decrease of the achievable throughput. In the following subsections we propose some techniques in order to over-come this limitation.

In addition, considering that in order to reduce the inter-gateway communication, each gateway individually computes its precoding sub-matrix, certain cooperative scheme shall be conceived. Indeed, each gateway only have access to the feedback from its cor-responding set of feeds N_g. With this, certain CSIT cooperation among gateways shall be established so that inter-beam interference is mitigated.

4.6.1 Precoding scheme

As discussed in the previous section, the g-th gateway only has access to a set of N_g of the overall feed elements located at the payload. Additionally, the gateway serves a set of K_g beams out of the K, leading to a total amount of served users equal to $K_g Q$. We will assume a known feed allocation per gateway and fixed N_g and K_g. Precisely, we will consider that the feeds are assigned in a consecutive fashion over the channel matrix.

Let us assume that each gateway has access to the overall CSIT. With this, the matrix to be transmitted through the feeder link of the g-th gateway jointly with the user symbols is

$$\mathbf{W}^g. \tag{4.44}$$

where $\mathbf{W}^g$ is of size $N_g \times K_g$.

In other words, as each gateway only have access to a certain set of feed elements the symbols to be transmitted to the K_g beams shall be linearly transformed with $\mathbf{W}^g$ in order to increase the overall throughput. Whenever each gateway has access to the overall channel matrix $\mathbf{H}$, the precoding scheme can be computed as described in Section

4.3 and adapted to the multiple gateway scenario. This can be done by beams of setting zero entries in the precoding matrix whenever the gateway does not have access to a certain feed. This transformation leads to a block diagonal precoding matrix as follows

$$\mathbf{W}_{\text{M-GW}} = \begin{bmatrix} \mathbf{W}^1 & \mathbf{0} & \cdots & \mathbf{0} \\ \mathbf{0} & \mathbf{W}^2 & \cdots & \mathbf{0} \\ \vdots & \vdots & \ddots & \vdots \\ \mathbf{0} & \mathbf{0} & \cdots & \mathbf{W}^G \end{bmatrix}. \tag{4.45}$$

where $\mathbf{W}_{\text{M-GW}}$ is of size $N \times K$. Evidently, robust designs can be applied without any additional penalty.

4.6.2   CSIT sharing

Since the gateway only has access to certain beams, its available CSIT is reduced Under this context, the g-th receives from its feedback link the following matrix

$$\mathbf{H}^g = \mathbf{H}\left((1:N,((g-1)QK_g+1):gQK_g)\right), \tag{4.46}$$

where the Matlab notation has been used for the sake of clarity. Moreover, $\mathbf{H}^g$ is of size $QK_g \times N_g$. However, in order to compute the precoding matrix, the gateways need the channel effect between their assigned feeds to the non-intended users. With this, every gateway must transmit over the inter-gateway link (e.g. a fiber optic) the information fed back from its users corresponding the effect of the non-assigned feeds. Mathematically, the g-th gateway must share

$$\left(\mathbf{H}^{gl}\right)_{l \neq g}^G, \tag{4.47}$$

where

$$\mathbf{H}^{gl} = \mathbf{H}\left((((l-1)N_g+1):gN_g,((g-1)QK_g+1):gQK_g)\right). \tag{4.48}$$

This cooperation among gateways require a total amount of

$$(G-1)QK_gN_g \qquad (4.49)$$

complex numbers to be shared by each gateway. As a consequence, it is essential to reduce this communication overhead in order to reduce the overall system cost.

One approach is to limit the sharing between the different gateways and only consider the C closer gateways. With this, the overall data overhead reduces to

$$CQK_gN_g. \qquad (4.50)$$

In addition, there might the case where we can apply certain compression to the transmit channel submatrices. For instance, we could use the eigenvector associated to the largest eigenvalue of each matrix $\mathbf{H}^{g_l}$. This will lead to a total communication overhead of

$$(G-1)N_g. \qquad (4.51)$$

4.7   Simulations

Considering a reference scenario of a geostationary satellite with $N = K = 245$, we evaluate the proposed precoding designs considering a full frequency reuse scenario. Array fed radiation pattern has been provided by the European Space Agency and it takes into account the different user locations over the European continent. The link budget parameters are described in Table 2.1.

All results have been obtained considering 500 channel realizations and a phase effect between feeds $\chi = 10$ degrees. Moreover, throughput values are obtained by means of the user SINR and the efficiency (bit/symbol) considering DVB-S2X (see Table 3.2).

The outline of the subsequent subsections is as follows. First, we show the performance

gain of the proposed precoding schemes considering perfect CSI and single gateway architecture. Second, it is shown that larger throughputs can be obtained if user grouping techniques are applied. Third, the impact of imperfect CSI is shown and the convenience of robust designs is presented. Finally, the multiple gateway architecture is evaluated so as the proposed inter-gateway cooperation techniques.

Remarkably, for a best practice we also consider a reference scenario that consists in 4-coloring scheme. This scheme implies that adjacent beams uses the different frequency bound.

4.7.1 Generalized precoding

Figures 4.2 and 4.3 present the system throughput considering the proposed precoding schemes in section III. Both of them, R-ZF and MBIM are compared to the average MMSE design presented in [44, 50]. It can be observed that both proposals behave better than average MMSE scheme. Specially, MBIM offers larger throughputs than R-ZF over the different transmit power values. Moreover, the conventional 4-coloring scheme has the lowest achievable rate due to the lack of multibeam processing.

4.7.2 User grouping

As discussed before, whenever the users within the same beam have collinear channel vectors, large rates can be obtained. This is shown in Figures 4.4 and 4.5. Similar to the study in [48], in each beam $Q = 200$ users are uniformly distributed, resulting in an average user density of 0.023 users/km^2 inside the 3 dB coverage edge of every beam.

It results that in all cases, user grouping increases the throughput. Specifically, for $Q = 3$, the user grouping gain becomes larger than in the $Q = 2$ case. Considering these results and the associated low complexity operation, it results convenient to implement this technique in satellite systems.

Figure 4.2: Per beam average throughput with $Q = 2$ users, perfect CSI, no user grouping.
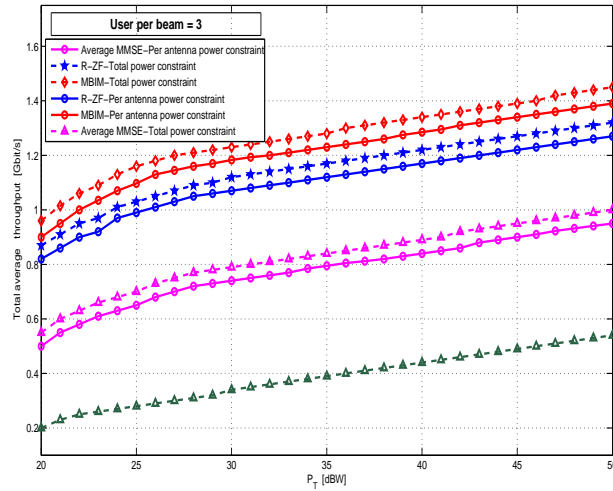
Figure 4.3: Per beam average throughput with $Q = 3$ users, perfect CSI, no user grouping.

4.7.3   Robust design

This subsection considers the effect of imperfect CSI at the transmitter. This is modelled with a additive perturbation matrix whose entries are Gaussian distributed with zero

Figure 4.4: Per beam average throughput with $Q = 2$ users, perfect CSI, user grouping.
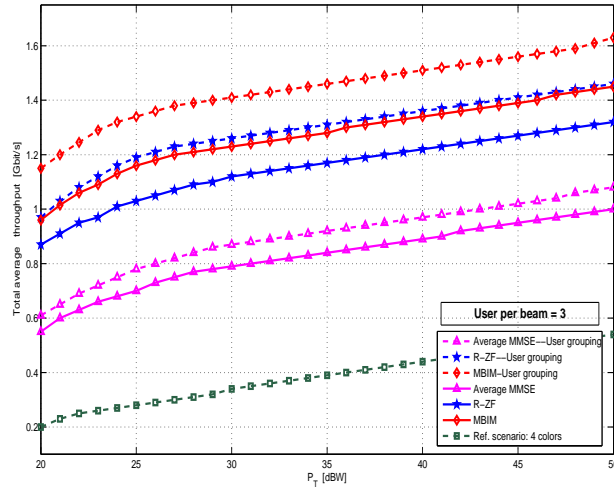
Figure 4.5: Per beam average throughput with $Q = 3$ users, perfect CSI, user grouping.

mean and variance equal to γ. The perturbation values γ_k are considered the same for all submatrices ($K = 1, \ldots, K$). Additionally, $\underline{\gamma_k}$ is set to 1.06.

Figures 4.6 and 4.7 show the performance of our proposal for different γ values represented in a ratio basis with respect to the channel matrix Frobenious norm. For the both

cases $Q = 2, 3$, the proposed technique is able to overcome the imperfect CSI values at the transmitter leading large throughputs while keep the precoding complexity low.
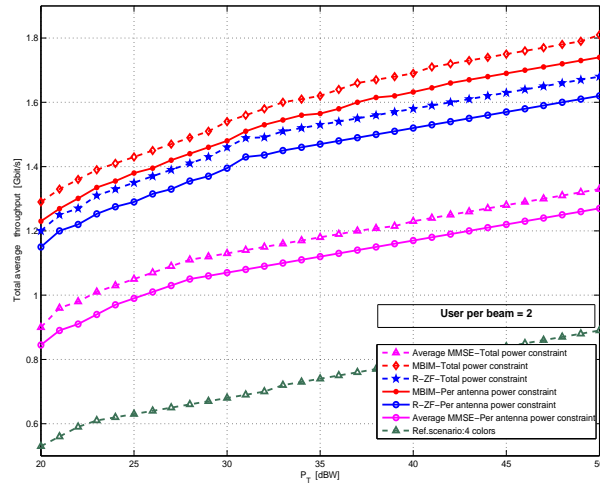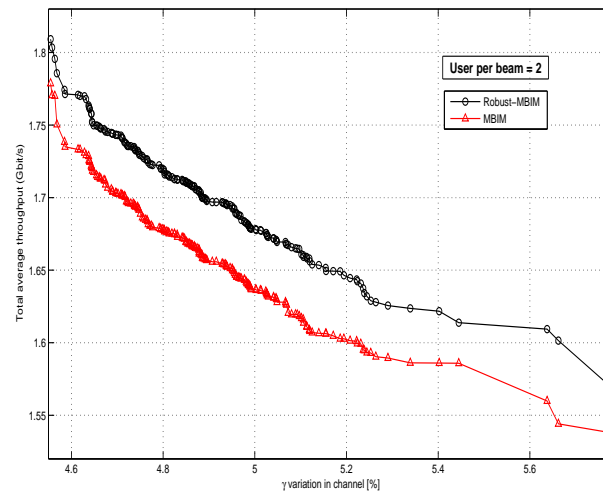

Figure 4.6: Per beam average throughput with $Q = 2$ users, imperfect CSI, no user grouping.

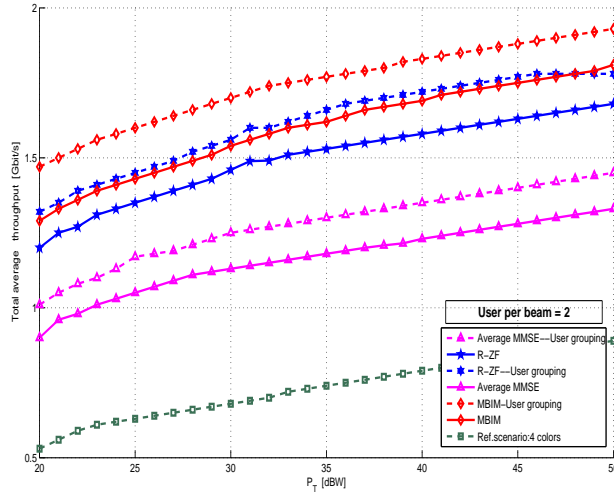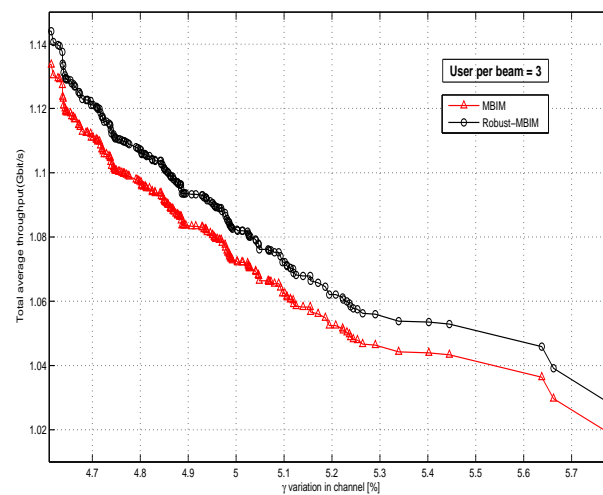Figure 4.7: Per beam average throughput with $Q = 3$ users, imperfect CSI, no user grouping.

4.7.4   Multiple gateway transmission

In order to evaluate the performance of the proposed multiple gateway schemes, we consider the following methods and inter-gateway architectures. We will consider a total number of $G = 14$ gateways each of them serving either 17 or 18 beams.

- **Scenario 1 :** Individual cluster processing. Each gateway processes its set of beams independently and only receives the CSI from its corresponding beams. With this, it is not possible to mitigate the interference of adjacent beams. This is referred to Individual Cluster Processing (ICP).

Figure 4.8: Per beam average throughput with $Q = 3$ users, perfect CSI, no user grouping and different multiple gateway architectures with MBIR precoding.

- **Scenario 2 :** Gateway g (respectively for all the gateways) collaborates with 4 gateways that serve beams directly adjacent to their beams so that g-th gateway receives prefect CSI of adjacent beams. This is referred to 4 Gateway Collaboration Processing (4GCP).

- **Senario 3 :**Gateway g (respectively for all the gateways) collaborates with 7 gateways that serve beams directly adjacent to their beams so that g-th gateway
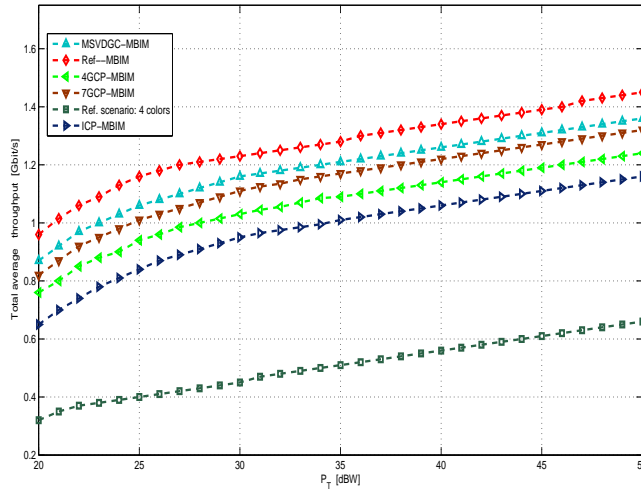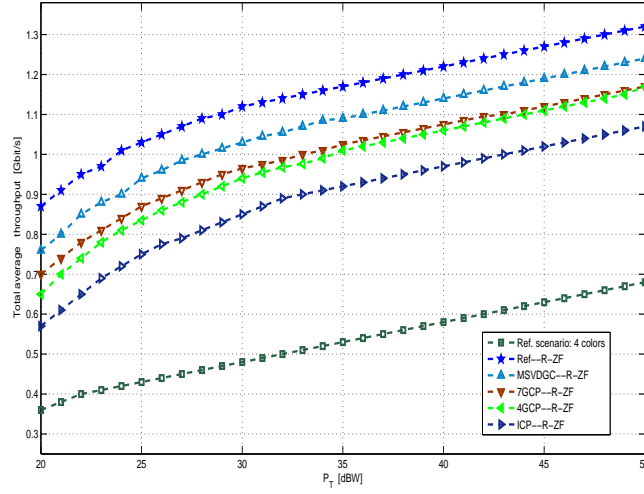
Figure 4.9: Per beam average throughput with $Q = 3$ users, perfect CSI, no user grouping and different multiple gateway architectures with R-ZF precoding

receives prefect CSI of adjacent beams. This is referred to 7 Gateway Collaboration Processing (7GCP).

- **Senario 4 :** Gateway g (respectively for all the gateways) collaborates with all gateways by means of sharing the singular left vector associated with the largest singular value of the gateway channel matrix. This is referred to Maximum SVD of Gateway Collaboration (MSVDGC).

- **Senario 5 :** Single gateway scenario so that a unique on ground processing unit is able to use all available feeds with the overall channel matrix. This scenario refers to Reference scenario (Ref).

Figure 4.8 and 4.9 show the proposed multiple gateway architectures for both the R-ZF and MBIR precoding designs. Evidently, as it happened in the single gateway scenario, MBIR provides larger overall throughputs than the R-ZF in all cases. In addition, it is observed that the larger cooperation is considered, the larger throughputs are obtained. Remarkably, MSVDGC method offers a good trade-off between overall throughput and

inter-gateway communication overhead.

4.8 Appendix

4.8.1 Proof of Theorem (4.1)

After some manipulations, the objective function can be written

$$\sum_{k=1}^{K} \text{trace} \left(\mathbf{W}_{a_k}^H \left(\widehat{\widetilde{\mathbf{H}}}_k^H \widehat{\widetilde{\mathbf{H}}}_k + \frac{KQ}{P} \mathbf{I} \right) \mathbf{W}_{a_k} \right). \tag{4.52}$$

This objective function can be re-written considering the eigendecomposition of $\widehat{\widetilde{\mathbf{H}}}_k \widehat{\widetilde{\mathbf{H}}}_k^H = \widehat{\widetilde{\mathbf{V}}}_k \widehat{\widetilde{\boldsymbol{\Sigma}}}_k \widehat{\widetilde{\mathbf{V}}}_k^H$, so that

$$\sum_{k=1}^{K} \text{trace} \left(\mathbf{W}_{a_k}^H \widehat{\widetilde{\mathbf{V}}}_k \left(\widehat{\widetilde{\boldsymbol{\Sigma}}}_k + \frac{KQ}{P} \mathbf{I} \right) \widehat{\widetilde{\mathbf{V}}}_k^H \mathbf{W}_{a_k} \right). \tag{4.53}$$

Since the objective function depends on the perturbation matrices and they are unknown by the transmitter, the following derivations aim at obtaining an upper-bound of (4.53). Concretely, an upper-bound of both $\widehat{\widetilde{\mathbf{V}}}_k$ and $\widehat{\widetilde{\boldsymbol{\Sigma}}}_k$ will be presented. The optimization problem (4.10) can yield to a tractable solution.

Proceeding with the derivation, the following equality holds

$$\widehat{\widetilde{\mathbf{H}}}_k^H \widehat{\widetilde{\mathbf{H}}}_k = \widetilde{\mathbf{H}}_k^H \widetilde{\mathbf{H}}_k + \widetilde{\boldsymbol{\Delta}}_k^H \widetilde{\mathbf{H}}_k + \widetilde{\mathbf{H}}_k^H \widetilde{\boldsymbol{\Delta}}_k + \widetilde{\boldsymbol{\Delta}}_k^H \widetilde{\boldsymbol{\Delta}}_k, \tag{4.54}$$

where it can be observed that the first term is the exact term whereas the rest are perturbation terms. In the following, we will consider the perturbation effect of

$$\Delta \mathbf{K}_k = \widetilde{\boldsymbol{\Delta}}_k^H \widetilde{\mathbf{H}}_k + \widetilde{\mathbf{H}}_k^H \widetilde{\boldsymbol{\Delta}}_k + \widetilde{\boldsymbol{\Delta}}_k^H \widetilde{\boldsymbol{\Delta}}_k, \tag{4.55}$$

in the precoding design.

Considering the first order perturbation analysis presented in [**?**], the eigenvectors of $\widehat{\widetilde{\mathbf{H}}}_k^H \widehat{\widetilde{\mathbf{H}}}_k$ can be written as

$$\widehat{\widetilde{\mathbf{V}}}_k = \widetilde{\mathbf{V}}_k \left(\mathbf{R}_k + \mathbf{I}\right), \tag{4.56}$$

where

$$\mathbf{R}_k = \mathbf{D} \circ \left(\widetilde{\mathbf{V}}_k^H \Delta\mathbf{K}\widetilde{\mathbf{V}}_k^H \widetilde{\boldsymbol{\Sigma}}_k + \widetilde{\boldsymbol{\Sigma}}_k \widetilde{\mathbf{V}}_k^H \Delta\mathbf{K}^H \widetilde{\mathbf{V}}_k\right). \tag{4.57}$$

where the g,f-entry of $\mathbf{D}$ is

$$\frac{1}{\lambda_f - \lambda_g}, \tag{4.58}$$

for $f \neq g$ and 0 whenever $f = g$. λ_f denotes the f-th eigenvalue of $\widetilde{\mathbf{H}}_k^H \widetilde{\mathbf{H}}_k$. It is important to remark that it has been considered that $\widetilde{\mathbf{H}}_k^H \widetilde{\mathbf{H}}_k$ is full rank and, therefore, its null space has 0 dimension.

From the problem definition (4.10) it is possible to bound $\Delta\mathbf{K}$ such that

$$\Delta\mathbf{K}_k \preceq \left(\widehat{\gamma}_k^2 + 2\widehat{\gamma}_k \sigma_{\max}\left(\widetilde{\mathbf{H}}_k^H \widetilde{\mathbf{H}}_k\right)\right) \mathbf{I}. \tag{4.59}$$

With this and considering the following lemma. **Lemma 1**. *For any semidefinite positive square matrices* $\mathbf{A}, \mathbf{B}, \mathbf{C}$ *and* $\mathbf{B} \preceq \mathbf{C}$ *it holds that*

$$\mathbf{A} \circ \mathbf{B} \preceq \mathbf{A} \circ \mathbf{C} \tag{4.60}$$

Proof. See Theorem 17 of [35]. □

With this lemma and with (4.59), it is possible to write the following inequality

$$\widehat{\widetilde{\mathbf{V}}}_k \preceq \widetilde{\mathbf{V}}_k \left(\widehat{\mathbf{R}}_k + \mathbf{I}\right), \tag{4.61}$$

where

$$\widehat{\mathbf{R}}_k = \epsilon_k \mathbf{D} \circ \left(\widetilde{\mathbf{V}}_k^H \widetilde{\mathbf{V}}_k^H \widetilde{\mathbf{\Sigma}}_k + \widetilde{\mathbf{\Sigma}}_k \widetilde{\mathbf{V}}_k^H \widetilde{\mathbf{V}}_k \right), \tag{4.62}$$

and

$$\epsilon = \widehat{\gamma}_k^2 + 2\widehat{\gamma}_k \sigma_{\max} \left(\widetilde{\mathbf{H}}_k^H \widetilde{\mathbf{H}}_k \right) \tag{4.63}$$

In case the perturbations of the eigenvectors are consider, the Weyl's inequality can support the approximation

Lemma 4.8.1 (Weyl's inequality). *Given two Hermitian matrices* $\mathbf{A}_1$ *and* $\mathbf{A}_2$ *with their corresponding eigenvalues collapsed in the diagonal matrices* $\mathbf{\Sigma}_1$, $\mathbf{\Sigma}_2$, *the following inequality holds*

$$\mathbf{\Sigma}_{sum} \preceq \mathbf{\Sigma}_1 + \mathbf{\Sigma}_2, \tag{4.64}$$

where $\mathbf{\Sigma}_{sum}$ *is a diagonal matrix whose diagonal entries are the eigenvalues of* $\mathbf{A}_1 + \mathbf{A}_2$.

Proof. See [51]. □

With this, the eigenvalues of $\widetilde{\mathbf{H}}_k^H \widetilde{\mathbf{H}}_k$ can be upper-bounded so that

$$\widehat{\widetilde{\mathbf{\Sigma}}}_k \preceq \widetilde{\mathbf{\Sigma}}_k + \epsilon_k \mathbf{I}. \tag{4.65}$$

With both (4.61) and (4.65), it is possible to relax the worst case maximization in (4.31).

4.8.2   Proof of Theorem (4.2)

As for the previous theorem, the main objective is to find a bound of the objective function so that the dependence with respect to $\mathbf{\Delta}_k$ variable disappears.

Considering the first order perturbation model presented in [33], the required eigendecomposition of $\mathbf{H}_k \mathbf{W}_{a_k}$ is perturbed by the following matrix

$$\Delta \mathbf{Q}_k = \mathbf{\Delta}_k \mathbf{W}_{a_k}. \tag{4.66}$$

This leads to the following approximation of the eigenvectors of $\mathbf{Z}_k$

$$\widehat{\mathbf{Z}_k} = \mathbf{L}_k \left(\mathbf{M}_k + \mathbf{I} \right), \tag{4.67}$$

where $\mathbf{L}_k$ are the eigenvectors of $\mathbf{Z}_k$ and

$$\mathbf{M}_k = \mathbf{N} \circ \left(\mathbf{L}_k^H \Delta \mathbf{Q}_k \mathbf{L}_k^H \mathbf{T}_k + \mathbf{T}_k \mathbf{L}_k^H \Delta \mathbf{Q}_k^H \mathbf{L}_k \right) \tag{4.68}$$

where $\mathbf{T}_k$ is a diagonal matrix containing the eigenvalues of $\mathbf{Z}_k$ and the g, f-th entry of $\mathbf{N}$ is

$$\frac{1}{z_{k_f} - z_{k_g}}, \tag{4.69}$$

for $f \neq g$ and 0 whenever $f = g$. z_{k_f} denotes the f-th eigenvalue of $\mathbf{Z}_k$.

After some manipulations, we can lower-bound $\Delta \mathbf{Q}_k$ so that

$$\Delta \mathbf{Q}_k \succeq \underline{\gamma}_k \mathbf{1}^T \left(\widetilde{\boldsymbol{\Sigma}}_k + \epsilon_k \mathbf{I} \right)^{-1/2} \mathbf{1I}. \tag{4.70}$$

By means of employing this last inequality and the derivation of the previous appendix, a lower bound of the eigenvalues of $\widehat{\mathbf{Z}}_k$ can be established.

Chapter 5

Thesis conclusions and future work

5.1 Conclusions

This dissertation has focused on the design of transmission (in the forward link) and detecting (in the return link) strategies to next generation multibeam satellite systems since full frequency reuse pattern among beams is considered.

In particular, the dissertation has put an special emphasis on taking into account the hybrid space-ground and individual on ground architectures in full frequency reuse pattern. As a result, the proposed transmission/detecting strategies exploit more efficiently the available multibeam resources than classical transmission/detecting strategies and improve their performance.

- **In chapter 2** A hybrid space-ground architecture with a single gateway structure is proposed, where an optimal design for on board beam generation process along with a typical advance interference mitigation technique, is used for the link pair. The on board processing is designed for both: i) to be robust to channel variations; ii) results the same for link pair. To meet all these requirements a robust MMSE optimization is conceived so that the benefits of the considered scheme are evaluated with respect to the current approaches both analytically and numerically.

In addition, this chapter developed the forward link of aforementioned hybrid space-ground architecture under per-feed power optimization. This is done in order to efficient and more realistic use of payload power resources. In this context, we reformulate the design of on board beam generation process and interference mitigation technique under per-feed power optimization strategy. We analytically show the benefit of the proposed ground and space units design respect to the current scenarios.

- **In chapter 3** We considered the forward link of a multiple gateway multibeam broadband satellite system.

  Each gateway includes a linear precoding process such that each precoding is a part of block precoding technique. Designing the precoding scheme, in contrast to single gateway scheme, entails two main challenges: i) the precoding matrix shall be separated into feed groups assigned to each gateway; ii) complete CSI is required at each gateway, leading to a large communication overhead. In order to solve these problems, a design based on a regularized singular value block decomposition of the channel matrix is presented so that both inter-cluster and intra-cluster interference is minimized. In addition, different gateway cooperative schemes are analyzed in order to keep the inter-gateway communication low.
  Furthermore, the impact of the feeder link interference is analyzed and it is shown both numerically and analytically that the system performance is reduced severally whenever this interference occurs even though precoding reverts this additional interference. Note that this effect occurs whenever the payload feeder link receiver is not properly calibrated and certain pointing errors take place.

- **In chapter 4** Proposed a two-stage low complex precoding design for multibeam multicast satellite systems. While the first stage minimizes the inter-beam interference, the second stage enhances the intra-beam signal so that the served user with

lowest SINR can decode the message. A robust version of the proposed scheme is provided based on the novel approach of the first perturbation theory. Additionally, user grouping and multiple gateway schemes are presented as essential tools for increasing the throughput in multibeam satellite systems. The conceived methods are evaluated in a continental coverage area and they result to perform better than the current approaches yet offering a very low computational complexity.

5.2   Future Works

The tentative future steps can be done are:

First Novel hybrid space-ground architecture could consider low complex channel adaptive payload architecture, where an adaptive precoding matrix is adapted with available CSI at the gateway.

Second Multiple gateway strategy presented in 3.4 is a good candidate for developing multibeam systems. It is expected that next multiple gateway strategies provide novel precoding technique so that collaboration among gateways in order to exchange CSI can be minimized

Third Another issue that needs a more deeply investigation is to apply hybrid space-ground and multiple gateway architectures to the multicast multibeam systems.

Forth Analyzing space and ground signal processing schemes for collocated satellites architecture where a collaboration between multibeam satellites is done in order to increase the coverage area.

Bibliography

[1] A.J. Paulraj, D.A. Gore, R.U. Nabar, H. Bolcskei, " An overview of MIMO communications - A key to gigabit wireless," in *Proceeding IEEE Transaction on Communication, vol. 92, no. 2, pp. 198-218, 2004.*

[2] G. Maral, M. Bousquet, "Satellite Communications Systems: Systems," in *Techniques and Technology, 4th edition, Wiley, 2002.*

[3] Mangir. T.E, "The future of public satellite communication," in *Harlow, England: Addison-Wesley, 1999.*

[4] I. Thibault, B. Devillers, E.A. Candreva, F. Lombardo, A. Vanelli-Coralli, G. E. Corazza, " Joint Feeder Link Bandwidth Compaction and Interference Mitigation based on a Hybrid Space/Ground Processing Architecture for a Broadband Multi Beam Satellite System, " in *EURASIP journal on satellite Communication Network. 2011.*

[5] G. Zheng, S. Chatzinotas and B. E. Ottersten, "Multi-Gateway Cooperation in Multibeam Satellite Systems," in *IEEE 23rd International Symposium on Personal, Indoor and Mobile Radio Communications 2012, USA.*

[6] A. Gharanjik, B. Rao, P.-D. Arapoglou, and B. Ottersten, "Gateway Switching in Q/V Band Satellite Feeder Links," in *IEEE Communications Letters, vol. 17, no. 7, pp. 13841387, July 2013.*

[7] P. Viswanath, D.N.C. Tse, V. Anantharam, "Asymptotically optimal water lling in vector multiple-access channels, " in *IEEE Transaction on Information Theory , vol. 47, no. 1, pp. 241-267, 2001.*

[8] web site:www.dvb.org, "DVB-S2x: Digital video broadcasting user guidlines for second generation system for broadcasting interactive services, newsgathering and other broadbond satellite application(DVB-S2x)," in *ETSI TR 102 376.*

[9] J. Tronc, P. Angeletti, N. Song, M. Haardt, J. Arendt, and G. Gallinaro, "Overview and comparison of on-ground and on-board beamforming techniques in mobile satellite service applications," in *International Journal of Satellite Communications and Networking, pp. n/an/a, 2013. [Online]. Available: http://dx.doi.org/10.1002/sat.1049.*

[10] L. Cottatellucci et al, "Interference mitigation techniques for broadband satellite systems, " in *Proceeding 24th AIAA International Communication Satellite Systems Conference, ICSSC, Jun. 2006.*

[11] G. Gallinaro et al, "Novel intra-system interference mitigation techniques and technologies for next generations broadband satellite systems," in *Final report of ESA/ESTEC contract No. 18070/04/NL/US, 2008.*

[12] V. Boussemart, M. Berioli, F. Rossetto, M. Joham, "On the achievable rates for the return-link of multi-beam satellite systems using successive interference cancellation, " in *IEEE Military Communications Conference (MILCOM) 07-09 Nov 2011, Baltimore MD, USA.*

[13] B. Devillers, A. Prez-Neira, C. Mosquera, " Joint Linear Precoding and Beam-forming for the Forward Link of Multi-Beam Broadband Satellite Systems, " in *Proceedings of IEEE Global Communications Conference (GLOBECOM 2011), 5-9 December 2011, Houston (Texas, USA).*

[14] J. Arnau, B. Devillers, C. Mosquera and A. Perez-Neira, " Performance study of multiuser interference mitigation schemes for hybrid broadband multibeam satellite architectures, " in *EURASIP Journal on Wireless Communications and Networking, 2012.*

[15] J. Arnau-Yanez, M. Bergmann, E.A. Candreva, G.E. Corazza, R. de Gaudenzi, B. Devillers, W. Gappmair, F. Lombardo, C. Mosquera, A. Perez-Neira, I. Thibault, A. Vanelli-Coralli, " Hybrid Space-Ground Processing for High-Capacity Multi-beam Satellite Systems, " in *Global Telecommunications Conference (GLOBECOM 2011), 2011, Houston (Texas, USA).*

[16] D.S. Komm, R. Liou, and J.W. Pyter, " Linearized TWTAs for Satellite Application, " in *Fifth IEEE International Vacuum Electronics Conference, IVEC 2004.*

[17] A. Scaglione, P. Stoica, S. Barbarossa, G. Giannakis, and H. Sampath, "Optimal designs for space-time linear precoders and decoders, " in *IEEE Transaction on Signal Processing, vol. 50, no. 5, pp. 10511064, May 2002.*

[18] N. Jaleeli, VanSlyck, D. Ewart, L. Fink, and A. Hoffmann, "Understanding automatic generation control," in *IEEE Transaction on Power System, 2006.*

[19] B. M. Hochwald, C. B. Peel, and A. L. Swindlehurst, " A vector-perturbation technique for near-capacity multiantenna multi-user communication - Part II: Perturbation," in *IEEE Transactions on Communications, vol. 53, no. 1, pp. 537544, 2005.*

[20] SM Kay, "Fundamentals os Statistical Signal processing: Estimation Theory, " in *Prentice-Hall, Inc. Upper Saddle River, NJ, USA, 1993.*

[21] J. Wang, D.P. Palomar, " Worst-Case Robust MIMO Transmission With Imperfect Channel Knowledge, " in *IEEE Transactions on Signal Processing, pp.3086-3100, volume: 57, Aug 2009.*

[22] D. P. Palomar, "A Unified framework for communications through MIMO channels", in *Ph.D. dissertation, Technical University of Catalonia (UPC), Barcelona, Spain, May 2003.*

[23] V. Joroughi, B. Devillers, M. Ángel Vaźquez and A. Ana Perez-Neira, "Design of an On-Board Beam Generation Process for the Forward Link of a Multi-Beam Broadband Satellite System, " in *IEEE Global Telecommunications Conference (GLOBECOM). Atlanta (USA), December 2013.*

[24] J Choi, "Optimal Combining and Detection: Statistical Signal Processing for Communications," in *1st edition, Cambridge University Press, 2010, New York, USA.*

[25] M. Aloisio and P. Angeletti, " Multi-Amplifiers Architectures for Power Reconfigurability, " in *Vacuum Electronics Conference, pp. 12, May 2007.*

[26] C. R. Rao and S. K. Mitra, "Generalized Inverse of Matrices and its Applications, " in *John Wiley and Sons Journals, 1971.*

[27] G. Dimic and N. D. Sidiropoulos, "On downlink beamforming with greedy user selection: Performance analysis and a simple new algorithm, " in *IEEE Transaction on Signal Processing, vol. 52, no. 10, pp. 38573868, October 2005.*

[28] T. Yoo and A. Goldsmith, "On the optimality of multi-antenna broadcast scheduling using zero-forcing beamforming, " in *IEEE Journal on Selective Areas on Commu-*

nication (Special Issue on 4G Wireless Systems), vol. 24, no. 3, pp. 528541, March 2006.

[29] A. Wiesel, Y. C. Eldar and S. Shamai (Shitz), " Zero-Forcing Precoding and Generalized Inverses, " in *IEEE Transactions on Signal Processing, September 2008.*

[30] J. Lofberg, " YALMIP A toolbox for modeling and optimization in MATLAB, " in *Proceedings of the CACSD Conference, Taipei, Taiwan, 2004, Available from http://control.ee.ethz.ch/joloef/yalmip.php.*

[31] J. H. Wilkinson, " The Algebraic Eigenvalue Problem," in *New York: Oxford University Press, 1965.*

[32] G. W. Stewart, " Perturbation theory for the singular value decomposition," in *University of Maryland , USA 1990.*

[33] J. Liu, X. Liu and X. Ma, " First-order perturbation analysis of singular vectors in singular value decomposition," in *14th IEEE workshop on Statistical Signal Processing, August 2007, Madison, USA.*

[34] Kaare Brandt Petersen, "The Matrix Cookbook, " in *ISP, IMM, Technical University of Denmark, September 2004.*

[35] C.R. Johnson, "Partitioned and Hadamard product matrix inequalities, " in *Journal of research of the National Bureau of Standards Vol . B3, No.6, November-December 1978.*

[36] web site:www.dvb.org, " DVB-S2: Digital video broadcasting user guidlines for second generation system for broadcasting interactive services, newsgathering and other broadbond satellite application(DVB-RCS), in *ETSI TR 102 37.*

[37] AW Marshall, I Olkin, "Inequalities: Theory Of Majorization and its Applications, " in *Academic Press, New York, NY, 1979.*

[38] B. Devillers and A. Perez-Neira, "Advanced interference mitigation techniques for the forward link of multi-beam broadband satellite systems, " in *Signals, Systems and Computers (ASILOMAR), pp. 18101814, 2011.*

[39] V. Joroughi, M. A. Vazquez and A. Perez-Neira, " Multiple Gateway Precoding with Per Feed Power Constraints for Multibeam Satellite Systems, " in *Proceedings of 20th European Wireless Conference, pp. 17 , May 2014.*

[40] Y. C. B. Silva and A. Klein, "Linear transmit beamforming techniques for the multigroup multicast scenario, " in *IEEE Transactions on Vehicular Technology, vol. 58, no. 8, pp. 43534367, 2009.*

[41] Q. Spencer, A. Swindlehurst, and M. Haardt, "Zero-forcing methods for downlink spatial multiplexing in multiuser MIMO channels, " in *IEEE Transactions on Signal Processing, vol. 52, no. 2, pp. 461471, 2004.*

[42] GH. Golub, CF. Van. Loan, " Matrix Computations (Johns Hopkins Studies in Mathematical Sciences, " in *3rd edition, The Johns Hopkins University Press, Baltimore, MD, 1996.*

[43] E. Karipidis, N. Sidiropoulos, and Z.-Q. Luo, "Quality of Service and Max-Min Fair Transmit Beamforming to Multiple Cochannel Multicast Groups," in *IEEE Transactions on Signal Processing, vol. 56, no. 3, 2008.*

[44] G. Taricco, "Linear Precoding Methods for Multi-Beam Broadband Satellite Systems," in *20th European Wireless Conference; Proceedings of, May 2014.*

[45] E. Karipidis, N. Sidiropoulos, and Z.-Q. Luo, "Transmit beamforming to multiple co-channel multicast groups," in *1st IEEE International Workshop on Computational Advances in Multi-Sensor Adaptive Processing, 2005.*

[46] V. Stankovic and M. Haardt, "Generalized Design of Multi-User MIMO Precoding Matrices," in *IEEE Transactions on Wireless Communications,, vol. 7, no. 3, pp. 953-961, 2008.*

[47] Y. C. B. Silva and A. Klein,"Linear transmit beamforming techniques for the multi-group multicast scenario," in *IEEE Transactions on Vehicular Technology, vol. 58, no. 8, pp. 43534367, 2009.*

[48] P. M. Arapoglou, A. Ginesi, S. Cioni, S. Erl, F. Clazzer, S. Andrenacci, and A. Vanelli-Coralli, "DVB-S2x Enabled Precoding for High Throughput Satellite Systems," in *CoRR, vol. abs/1504.03109, 2015. [Online]. Available: http://arxiv.org/abs/1504.03109.*

[49] A. Pascual-Iserte, D. Palomar, A. Perez-Neira, and M. Lagunas, "A robust maximin approach for MIMO communications with imperfect channel state information based on convex optimization," in *IEEE Transactions on Signal Processing, vol. 54, no. 1, pp. 346360, Jan 2006.*

[50] D. Christopoulos, S. Chatzinotas, and B. Ottersten, "Multicast Multigroup Precoding and User Scheduling for Frame-Based Satellite Communications," in *IEEE Transactions on wireless Communications, vol. PP, no. 99, pp. 11, 2015.*

[51] H. Weyl, "Das asymptotische Verteilungsgesetz der Eigenwerte linearer partieller Differentialgleichungen (mit einer Anwendung auf die Theorie der Hohlraumstrahlung)," in *Mathematische Annalen, vol. 71, no. 4, pp. 441479, 1912. [Online]. Available: http://dx.doi.org/10.1007/BF01456804.*